5. SITE 1041[1]

Shipboard Scientific Party[2]

HOLE 1041A

Position: 9°44.027′N, 86°06.995′W

Start hole: 2015 hr, 24 November 1996

End hole: 0915 hr, 27 November 1996

Time on hole: 61.0 hr (2.54 days)

Seafloor (drill-pipe measurement from rig floor, mbrf): 3317.1

Water depth (drill-pipe measurement from sea level, m): 3306.0

Distance between rig floor and sea level (m): 11.1

Total depth (drill-pipe measurement from rig floor, mbrf): 3472.2

Penetration (mbsf): 155.1

Coring totals:

Type: APC; No: 2; Cored: 14.3 m; Recovered: 14.30 m (100.0%)
Type: XCB; No: 16; Cored: 140.8 m; Recovered: 101.02 m (71.7%)
Total: No: 18; Cored: 155.1 m; Recovered: 115.32 m (74.4%)

Formation:

Subunit A1A (0–155.1 mbsf): Silty clay/claystone and clayey silt/siltstone (late Miocene–?Pleistocene)

HOLE 1041B

Position: 9°44.025′N, 86°06.981′W

Start hole: 0915 hr, 27 November 1996

End hole: 0345 hr, 30 November 1996

Time on hole: 66.5 hr (2.77 days)

Seafloor (drill-pipe measurement from rig floor, mbrf): 3317.1

Water depth (drill-pipe measurement from sea level, m): 3305.9

Distance between rig floor and sea level (m): 11.2

Total depth (drill-pipe measurement from rig floor, mbrf): 3712.7

Penetration (mbsf): 395.6

Drilled with center bit: 0–155.0 mbsf

Coring totals:

Type: RCB; No: 25; Cored: 240.6 m; Recovered: 133.18 m (55.4%)

Formation:

Subunit A1A (155.0–273.83 mbsf): Silty clay/claystone and clayey silt/siltstone (late Miocene–?Pleistocene)
Subunit A1B (273.83–395.6 mbsf): Clayey siltstone, sandy siltstone, and silty sandstone (late Miocene)

HOLE 1041C

Position: 9°43.989′N, 86°06.945′W

Start hole: 0345 hr, 30 November 1996

End hole: 1345 hr, 1 December 1996

Time on hole: 34.0 hr (1.42 days)

Seafloor (drill-pipe measurement from rig floor, mbrf): 3317.1

Water depth (drill-pipe measurement from sea level, m): 3305.9

Distance between rig floor and sea level (m): 11.2

Total depth (drill-pipe measurement from rig floor, mbrf): 3740.9

Penetration (mbsf): 423.8

Drilled: 0–395.0 mbsf

Coring totals:

Type: RCB; No: 3; Cored: 28.8 m; Recovered: 6.85 m (23.8%)

Formation:

Subunit A1B (395.0–423.8 mbsf): Clayey siltstone, sandy siltstone, and silty sandstone (late Miocene)

Principal results: The lithostratigraphic objectives at Site 1041 were to determine the stratigraphy of the sedimentary apron, the composition and properties of gas hydrates, and the composition of the prism material directly beneath the apron. We succeeded in determining the stratigraphy of the upper 395 m of the apron and sampling gas hydrates in a number of places downhole. Because of deteriorating hole conditions, we did not reach our target depth of 550 mbsf, thus missing the objective of determining the prism composition.

One lithologic unit is defined at Site 1041 (Fig. 1). Only the first two cores were recovered by APC. Below 14.30 mbsf (Core 2H), the cores are generally of poor quality, with incomplete recovery, extensive biscuiting because of drilling disturbance, and entire sections of rubble that is probably upper-hole infall. Beginning with Core 170-1041A-12X and extending to the bottom of Hole 1041C, the cores are extensively fractured. In the interval between Cores 170-1041A-15X through 1041B-20R, many original textures and structures are destroyed by gas-hydrate dissociation.

Apron Unit A1 consists mainly of late Miocene–Pleistocene(?) clay(stone) and silt(stone), with minor sandstone, limestone, and volcanic ash. These lithologies are dominated by terrigenous rather than biogenic material. Unit A1 is divided into two subunits, with Subunit A1B consisting of coarser grained material (siltstones and sandstones) than the claystone-dominated Subunit A1A. Gas hydrates were recovered in the interval 116–184 mbsf. Although evidence of submarine mass wasting and slumping was observed near the base of the hole, we found little evidence of tectonic deformation in the cores except for microfaults, fissility, and changes in bedding dips. Biostratigraphic markers are not abundant enough to indicate age reversals that would result from major internal faults, and age determinations are complicated by reworked middle Miocene taxa that increase near the base of the hole. However, the increase in microfaults and changes in bedding dip between 180 and 200 mbsf, and an abrupt change in bedding orientation at 275 mbsf, suggest at least two faults within the section.

[1]Kimura, G., Silver, E.A., Blum, P., et al., 1997. *Proc. ODP, Init. Repts.*, 170: College Station, TX (Ocean Drilling Program).
[2]Shipboard Scientific Party is given in the list preceding the Table of Contents.

Previous Chapter Table of Contents Next Chapter

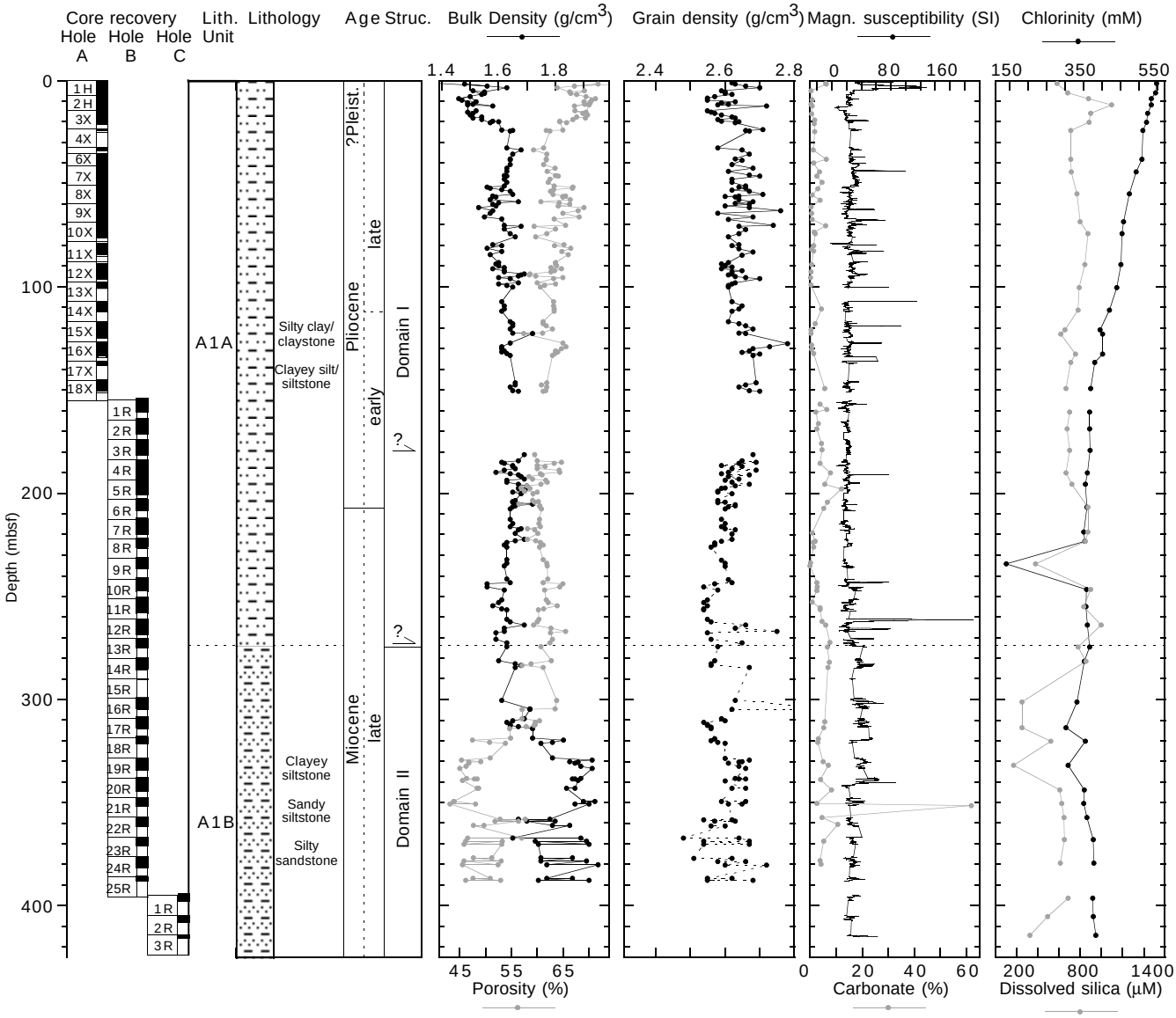

Figure 1. Graphical representation and summary plots of shipboard core and downhole measurements. Explanation of data types and their acquisition are found in the "Explanatory Notes" chapter (this volume). Shipboard descriptions of data are found in relevant sections in this chapter.

Distributions of age vs. depth in Site 1041 are not as clear as in the previous two sites because of poorer preservation and significant reworking. The general trend of age vs. depth, based largely on diatoms, suggests 55 m/m.y. in the upper 240 mbsf and 93 m/m.y. below this depth. Trends based on nannofossils are slightly higher at 62 m/m.y. above 240 mbsf.

The magnetostratigraphy of this site can be divided into two zones, an upper zone (0–160 mbsf) of apparently remagnetized, entirely normal polarity, and a zone with both normal and reversed polarity (160 mbsf–total depth [TD]). Using biostratigraphic markers, polarity intervals ranging from the onset of Chron C3n.2n (4.62 Ma) at 174 mbsf to the termination of Chron C4n.2n (7.43 Ma) at 369.5 mbsf have been identified. Age-depth relationships are 38 m/m.y. for the interval 174–222 mbsf and 99 m/m.y. for the interval 222–396 mbsf. Thermal demagnetization of multicomponent isothermal remanent magnetizations (mIRM) was performed on selected samples and indicated the presence of Fe-sulfides and magnetite.

The main geochemical scientific objectives at Site 1041 were to characterize the fluid stratigraphy and flow distribution within the slope-apron sediments, as well as in the rocks or prism sediments beneath the high-amplitude reflection at its base, and to determine the origin(s) of the fluid(s). Finally, we sought to establish the occurrence and geochemistry of the gas hydrates to deduce their mode of formation and origin. We succeeded in establishing a fluid stratigraphy in the upper 395 mbsf of the slope apron, and we established the occurrence and geochemistry of the gas hydrates. Our data have implications for the nature of the rocks beneath the apron, but we did not sample those rocks directly at Site 1041.

Below the very thin sulfate reduction zone at about 15 mbsf, methane concentrations are high in the drilled section. Gas hydrate here is concentrated between ~100 and 280 mbsf, the zone of highest total organic carbon (TOC) weight percent. Its primary mode of occurrence is disseminated, as indicated by the almost constant salinity in this depth interval, with thin sheets of gas hydrate filling microfractures. The gas hydrates analyzed within this interval also contain small amounts of the higher hydrocarbons ethane (C_2) and propane (C_3). Below about 280 mbsf, just beneath the lithologic transition from Subunit A1A to A1B, the concentrations of volatile hydrocarbons, especially of propane, are highest and then begin decreasing downhole. Across this boundary, the con-

centration depth profiles of several inorganic chemical components, particularly Cl, Ca, Si, and phosphate, and of Na/Cl and Mg/Ca values also show sharp transitions to lower or higher values, suggesting a two-tier hydrologic system having different fluid sources.

The section drilled from 1.5 to 395 mbsf has Cl concentrations and salinities lower than seawater. They decrease steadily to the depth of the main gas-hydrate zone (120–280 mbsf), are rather constant within it (~280–340 mbsf), and have slightly higher values below ~340 mbsf. The source of the fluid with low-Cl and high-Ca concentrations in the lower apron sediments is located at >3–4 km depth. Clay-mineral dehydration reactions are the most likely fluid-rock reactions responsible for freshening this fluid at the source region. The source of the low-Cl fluid in the upper apron sediments is less clear. Gas-hydrate dissociation alone would not result, for example, in Na/Cl values higher than seawater, whereas the in situ temperatures are too low for hydrous mineral dehydration reactions. Testing for the possibility of meteoric water influence requires shore-based analyses. Carbonate formation of both calcite and dolomite is pervasive throughout the apron sediments. Although the total inorganic carbonate content is not high, it ranges between 0.5 and 6.3 wt%.

The apron sediments show increasing compaction throughout the section, with porosity decreasing from nearly 75% at the seabed to less than 45% at 330 mbsf. *P*-wave velocities increase monotonically over the same interval, from 1540 to over 2000 m/s at the greater depths, reflecting increased consolidation and cementation. The widespread occurrence of (melted) gas hydrates did not significantly affect the physical properties measured on core samples, but clathrates filling pores and fractures are expected to have a major influence on velocities and resistivities in situ.

In summary, some of our objectives at Site 1041 were met, including determination of lithostratigraphy and geochemistry of the apron and sampling the distribution of gas hydrate with depth. We fell short of our total depth objective, the high-amplitude prism reflector, because of drilling problems, and therefore targeted an additional site, Site 1042, to meet that objective.

BACKGROUND AND SCIENTIFIC OBJECTIVES

Site 1041 was located on the midslope of the Costa Rica Margin, 12 km up from the toe of the slope off the Nicoya Peninsula (Fig. 11, "Introduction" chapter, this volume). The margin here consists of a prism section underlying much of the slope and a sedimentary apron, locally 500–600 m thick, which overlies the prism everywhere (Fig. 2). The prime objective of this site was to determine the nature and composition of the prism material underlying the slope apron. Additional objectives included an understanding of the fluid-flow regime of the midslope and a comparison of the apron material with that of the lower wedge above the décollement, drilled at Site 1040. An earlier objective was to penetrate an out-of-sequence fault zone, marked by a well-developed reflection at 1.4 s (two-way traveltime) beneath the seafloor. Using earlier velocities, it was estimated that the reflector depth was ~1200 mbsf. Using new seismic velocities by McIntosh and co-workers (unpubl. data), this reflection more likely lies at a depth of 1500–1600 mbsf and thus was considered to be out of range for drilling in the time available.

The seismic interpretation of the Site 1041 region is based on the study of three-dimensional (3-D) seismic data. The site is located at the intersection of 3-D in-line 177 and 3-D cross-line 450 (Fig. 11, "Introduction" chapter, this volume). The seismic stratigraphy of the sedimentary apron at Site 1041 shows little continuity of reflection events (Fig. 3). The upper 200 m of the apron is very weakly reflective and grades downward to a more highly reflective lower part, although the transition between the two is not sharply marked on the seismic record. This difference is more clear on the cross-line, showing discontinuous reflections starting at a level of about 200 mbsf and continuing to the high-amplitude reflection at 550 mbsf (Fig. 4). The high-amplitude reflection that marks the base of the apron is present throughout the Costa Rica Margin to within 5 km of the toe of the slope. It is an irregular surface, generally cut by numerous faults. The high-amplitude reflection marks the top of material with significantly greater velocity than that of the apron above it, approaching 4 km/s at Site 1041, which can be compared with values of less than 2 km/s in the apron. The reflection is broken into segments with lateral extent no greater than 1 km, and generally less than 0.5 km. Vertical displacement between segments can be from tens to a few hundred meters. The larger displacements are associated with faults that cut through the apron as well, although the latter has smaller apparent displacement. In the area of Site 1041, the faults appear to be dominantly thrust faults, because they dip upslope and cut the apron with northeast side up displacements of the high-amplitude reflection surface. There is also overlap of the reflecting surfaces across these faults, consistent with thrusting. The amount of displacement on any given fault is not large, but the array of small faults acts to disrupt reflectivity in the apron.

Heat-flow observations carried out pre-cruise (Langseth and Silver, 1996) in the region of Site 1041 were found to average 25 mW/m^2, with a span of values ranging from 17 to 34 mW/m^2. Visual observations from the submersible *Alvin* discovered a number of cold vent communities within a few kilometers of the site (Kahn et al.,

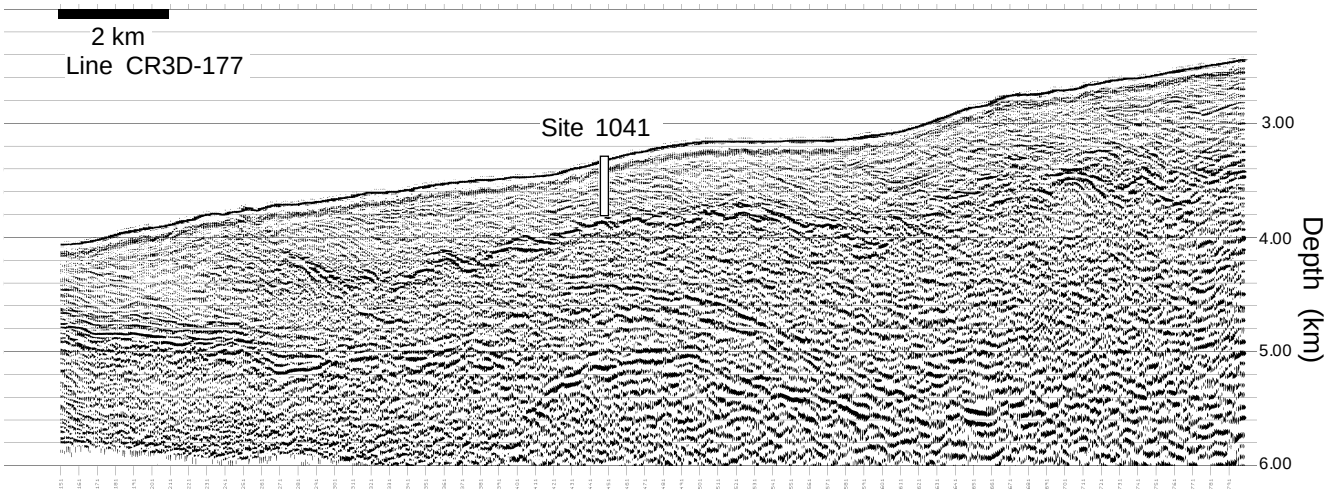

Figure 2. 3-D seismic-reflection dip Line 177, crossing the location of Site 1041 normal to the trench axis. Migrated depth profile.

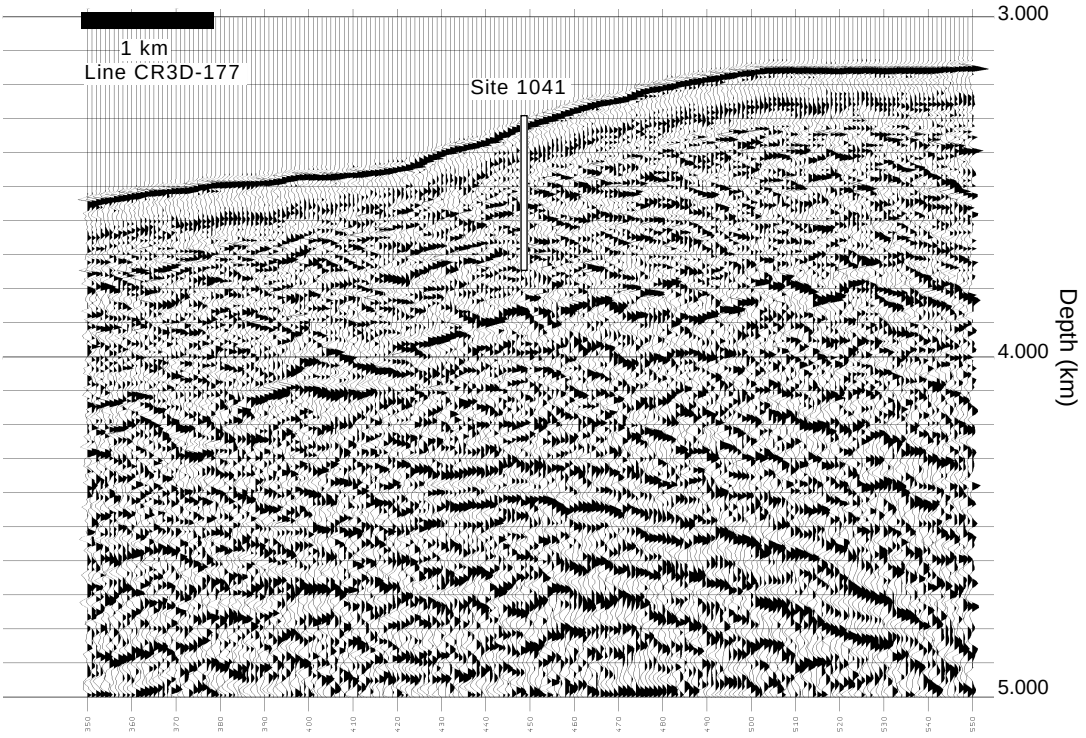

Figure 3. Detail of 3-D dip Line 177 centered on Site 1041. The section above the high-amplitude reflection that intersects Site 1041 at 3.86 km depth (measured from the sea surface) is approximately correct. The section below this reflection was migrated with too slow a velocity, so events are plotted too early. The very broken appearance of the high-amplitude reflection and most reflections in the apron section results from a number of thrust faults that dip upslope.

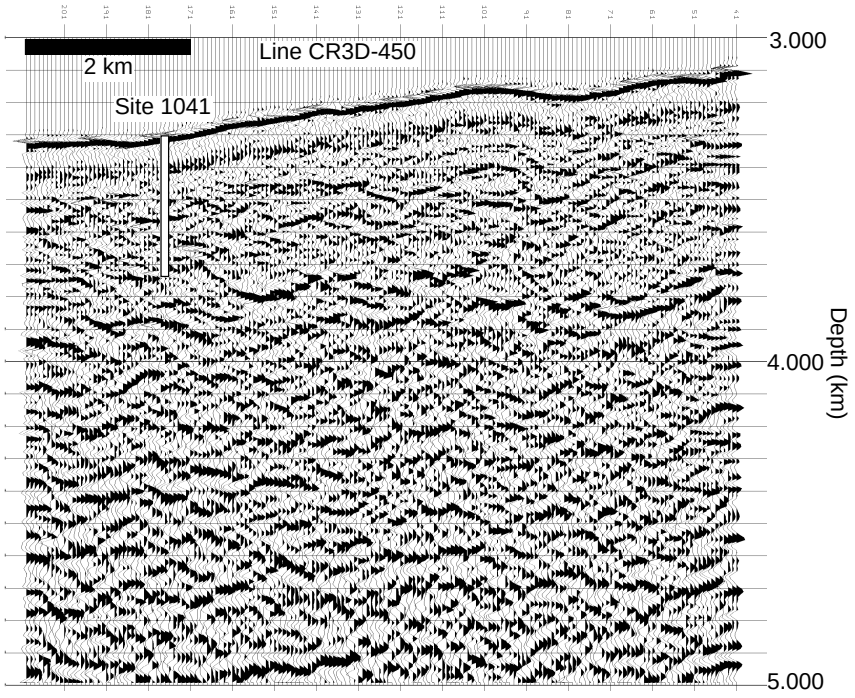

Figure 4. 3-D seismic-reflection cross-line 450, parallel to the trench axis. The fact that most of the reflections in the apron section (upper 500 m or so) are approximately horizontal means that the cross-line runs nearly parallel to the dominant structural strike.

1996). A short distance downslope were a number of small vent communities located adjacent to fault scarps (McAdoo et al., 1996). The fault scarps were located for the dives using the surface reflectivity of the 3-D seismic data set (McIntosh and Silver, 1996). Each community consisted of a few living chemosynthetic bivalves and several more articulated or disarticulated shells. Several kilometers upslope from Site 1041, the dives encountered a number of large, active communities of chemosynthetic bivalves and tube worms, as well as abundant slabs and crusts of authigenic carbonate atop a large mud diapir (Kahn et al., 1996). Analyses of the chemistry of pore waters from push cores taken with the *Alvin* show evidence of advection from greater depths in the area of the vent communities, although the

differences with seawater were small enough to suggest significant mixing during ascent (Zuleger et al., 1996).

OPERATIONS

Hole 1041A

Site 1041 is located 6.2 nmi landward of Site 1040. Hole 1041A was spudded at 0430 hr, 25 November 1996. The first advanced hydraulic piston core (APC) was shot from a depth of 3315.0 m and recovered 7.4 m of core, establishing a mudline of 3317.2 m (Tables 1, 2). APC Core 170-1041A-2H did not fully stroke and required 40 kilo-pounds (kips) overpull to extract from the stiff sediment beneath the seafloor. An extended core barrel (XCB) was dropped and XCB coring commenced with Core 3X and continued through Core 18X to a total depth of 155.1 mbsf. Coring was suspended there because of slow rate of penetration (ROP; 8.9 m/hr for last two cores), poor core quality (natural fractures in the clay/silt stone were highly disturbed by the drilling process), and steadily deteriorating hole conditions (fill, elevated pump pressure, and breakout torque after each connection). Gas hydrate nodules were recovered from Cores 15X through 18X, and fissility was observed in most cores.

The Davis-Villinger Temperature Probe (DVTP) was deployed a total of three times at depths of 45.7, 87.9, and 126.4 mbsf (see "Physical Properties" section, this chapter, for results). One run, at a depth of 78.2 m, recovered erroneous data. Hydrocarbon vacutainer analysis indicated that the hydrate-rich sediments contained 0.8–1 vol% methane. Ethane values ranged from 97 to 123 parts per million by volume (ppmv) in Core 18X. Propane values ranged from 2 to 21 ppmv. There were no higher hydrocarbons present (see "Geochemistry" section, this chapter, for results).

Two 30-bbl sepiolite mud sweeps were made in the hole at depths of 126.4 and 135.5 mbsf, respectively. The hole was displaced with 52 bbl of 10.5 lb/gal mud before retrieving the drill string. Once clear of the seafloor, 1.25 hr were taken to slip and cut the drilling line, and the drill string was recovered back to the ship.

Hole 1041B

While the rotary core barrel (RCB) bottom-hole assembly (BHA) was being made up, the vessel was offset 30 m to the east. With a center bit in place, the bit was advanced to a depth of 155.0 mbsf. No overlap between Holes 1041A and 1041B coring intervals was desired, and the objective was to advance to the high-amplitude reflector at ~500 mbsf as fast as possible. The drilled interval took a total of 6.75 hr, and an average ROP of 37.5 m/hr was achieved. RCB coring began at that depth and continued through Core 170-1041B-25R to a total depth of 395.6 mbsf. A distinct difference in formation was

Table 1. Coring summary for Site 1041.

Core	Date (Nov. 1996)	Time (UTC)	Depth (mbsf)	Length cored (m)	Length recovered (m)	Recovery (%)
170-1041A-						
1H	25	1045	0.0-7.4	7.4	7.39	99.8
2H	25	1235	7.4-14.3	6.9	6.91	100.0
3X	25	1835	14.3-23.4	9.1	6.87	75.5
4X	25	2040	23.4-32.4	9.0	1.54	17.1
5X	25	2200	32.4-35.4	3.0	1.83	61.0
6X	25	2340	35.4-41.5	6.1	5.85	95.9
7X	26	0215	41.5-50.6	9.1	9.24	101.0
8X	26	0415	50.6-59.6	9.0	9.90	110.0
9X	26	0600	59.6-8.6	9.0	9.66	107.0
10X	26	0825	68.6-78.2	9.6	7.67	79.9
11X	26	1200	78.2-87.9	9.7	6.81	70.2
12X	26	1600	87.9-97.5	9.6	8.33	86.8
13X	26	1825	97.5-107.1	9.6	3.30	34.4
14X	26	2005	107.1-116.7	9.6	5.11	53.2
15X	26	2155	116.7-126.4	9.7	8.41	86.7
16X	27	0110	126.4-135.9	9.5	7.88	82.9
17X	27	0345	135.9-145.5	9.6	1.61	16.8
18X	27	0615	145.5-155.1	9.6	6.01	62.6
Coring totals:				155.1	114.32	73.7
170-1041B-						
1R	28	0635	155.0-164.6	9.6	6.09	63.4
2R	28	0840	164.6-174.2	9.6	6.20	64.6
3R	28	1145	174.2-183.8	9.6	7.43	77.4
4R	28	1515	183.8-193.5	9.7	9.60	98.9
5R	28	1705	193.5-203.1	9.6	6.96	72.5
6R	28	1840	203.1-212.7	9.6	5.59	58.2
7R	28	2010	212.7-222.3	9.6	7.23	75.3
8R	28	2145	222.3-231.9	9.6	4.31	44.9
9R	28	2325	231.9-241.6	9.7	4.73	48.7
10R	29	0105	241.6-251.2	9.6	5.99	62.4
11R	29	0230	251.2-260.9	9.7	6.87	70.8
12R	29	0415	260.9-270.5	9.6	7.22	75.2
13R	29	0655	270.5-280.2	9.7	4.75	48.9
14R	29	0915	280.2-289.9	9.7	5.02	51.7
15R	29	1130	289.9-299.5	9.6	0.53	5.5
16R	29	1355	299.5-309.2	9.7	5.40	55.7
17R	29	1615	309.2-318.8	9.6	5.00	52.1
18R	29	1830	318.8-328.4	9.6	2.53	26.3
19R	29	2000	328.4-338.0	9.6	5.45	56.8
20R	29	2135	338.0-347.6	9.6	6.50	67.7
21R	29	2305	347.6-357.2	9.6	4.08	42.5
22R	30	0045	357.2-366.8	9.6	4.55	47.4
23R	30	0215	366.8-376.4	9.6	3.72	38.7
24R	30	0335	376.4-386.0	9.6	4.96	51.6
25R	30	0535	386.0-395.6	9.6	2.26	23.5
Coring totals:				240.6	132.97	55.3
170-1041C-						
1R	Dec. 01	1025	395.0-404.7	9.7	2.66	27.4
2R	Dec. 01	1300	404.7-414.2	9.5	2.83	29.8
3R	Dec. 01	1615	414.2-423.8	9.6	1.36	14.1
Coring totals:				28.8	6.85	23.8

Note: UTC = Universal Time Coordinated.

Table 2. Coring section summary for Site 1041.

Leg	Site	Hole	Core	Type	Top (mbsf)	Bottom (mbsf)	Advancement	Section number	Liner length (m)	Curated length (m)	Map interval top (mbsf)	Map interval bottom (mbsf)	Map type
170	1041	A	1	H	0	7.4	7.4	1	1.5	1.5	0	1.5	STD
170	1041	A	1	H	0	7.4	7.4	2	1.5	1.5	1.5	3	STD
170	1041	A	1	H	0	7.4	7.4	3	1.5	1.5	3	4.5	STD
170	1041	A	1	H	0	7.4	7.4	4	1.5	1.5	4.5	6	STD
170	1041	A	1	H	0	7.4	7.4	5	1.11	1.11	6	7.11	STD
170	1041	A	1	H	0	7.4	7.4	6	0.28	0.28	7.11	7.39	STD
170	1041	A	2	H	7.4	14.3	6.9	1	1.5	1.5	7.4	8.9	STD
170	1041	A	2	H	7.4	14.3	6.9	2	1.5	1.5	8.9	10.4	STD
170	1041	A	2	H	7.4	14.3	6.9	3	1.5	1.5	10.4	11.9	STD
170	1041	A	2	H	7.4	14.3	6.9	4	1.5	1.5	11.9	13.4	STD

Note: STD = standard.

This is a sample of the table that appears on the volume CD-ROM.

identified in Core 15R at an approximate depth of 290 mbsf. More fill was identified between connections, and higher torque was required after picking up the pipe from the dual elevator stool. Once rotation and circulation was established, however, the drilling parameters remained normal and stable. Hole conditions got progressively better during the subsequent 12 hr of coring.

After cutting Core 25R, the driller flushed the hole with a sepiolite drilling mud sweep. At this point, the pipe became seriously stuck ~12 m from the bottom. Various combinations of circulation pressure, torque, and overpull were used in attempting to work the pipe free. The pipe was worked alternately with 40 kips downward drag and 100 kips overpull, with 500 psi back pressure. After 1 hr, the pipe came free using 200 kips of overpull. No torque was in the string at the time. With the top drive still in the string, the pipe was pulled to a depth of 3565.4 mbrf (248.3 mbsf), where all back pressure was lost and drilling parameters again became normal. At that point, the hole was displaced with 74 bbl of 10.5 lb/gal mud, and the drill string was pulled to clear the mudline.

During the course of drilling and coring in this hole, eight 30-bbl sepiolite mud sweeps were pumped at depths of 203.1, 241.6, 270.5, 289.9, 309.2, 338.0, 366.8, and 395.6 mbsf, respectively.

The DVTP was deployed twice. The first run was made after Core 2R at a depth of 174.2 mbsf and did not obtain good data. A second run was made after Core 3R at a depth of 183.8 mbsf (see "Physical Properties" section, this chapter, for results).

As in Hole 1041A, gas hydrates were dispersed throughout the recovered core material beginning with Core 170-1041B-1R and continuing through Core 25R. As the formation became more indurated and the porosity decreased, the hydrates were less plentiful but were still present to some extent, primarily within naturally occurring fractures. Hydrocarbon vacutainer analysis indicated that the hydrate-rich sediments contained 0.7–1 vol% methane. Ethane values ranged from 1214 ppmv to a low of 274 ppmv. Propane values ranged from 4 to 29 ppmv. Only two cores registered higher hydrocarbons. Cores 9R and 11R identified 1 ppm *i*-C_4.

Hole 1041C

The ship was offset 100 m southeast of Hole 1041B, and Hole 1041C was spudded with a center bit in place. Drilling advanced to a depth of 395.0 mbsf in 21.0 hr, achieving a penetration rate of 28.0 m/hr. It became apparent during the course of the drilled interval that the hole was deteriorating. The pump strokes required to displace mud sweeps continually increased above the calculated amount, indicating the hole was enlarging with time. RCB coring advanced the hole from 395.0 mbsf to a depth of 423.8 mbsf (Core 170-1041C-3R). Before Core 3R could be recovered, the drill string again became stuck. A total of 30 min were taken working the pipe with 40 kips drag, 100 kips overpull, and 200–400 psi back pressure. The pipe was eventually pulled free with 225 kips of overpull. The drill string was pulled to a depth of 363.8 mbsf and the hole was displaced with 115 bbl of 10.5 lb/gal mud. The drill string was pulled clear of the seafloor, ending Hole 1041C. The total depth of the hole (423.8 mbsf) was short of the desired scientific objective estimated at ~550 mbsf. Because hole deterioration continued to present a major drilling problem, the alternate Site 1042 was picked as the next location. The geologic environment was expected to be the same as that drilled at Site 1041, although the depth of the target reflector was estimated to be only 325 mbsf.

During the course of drilling and coring this hole, sepiolite mud sweeps were pumped at depths of 280.2 (40 bbls), 309.1 (30 bbls), 337.9 (30 bbls), and 366.8 mbsf (30 bbls). There were no temperature measurements or water samples recovered from this hole.

Hydrocarbon vacutainer analysis for the three cores recovered indicated that the sediments contained 71,080–10,474 ppmv methane. Ethane values ranged from 83 ppmv to a low of 21 ppmv in Core 3R. Propane values ranged from 5 to 1 ppmv. No higher hydrocarbons were present.

LITHOSTRATIGRAPHY AND STRUCTURES

One lithologic unit is defined at Site 1041 (Table 3). Only the first two cores were recovered by APC in Hole 1041A. Below 14.30 mbsf (Core 1701041A-2H), the cores are generally of poor quality because of incomplete recovery, extensive biscuiting, and entire sections of rubble that are partially hole fill. Beginning with Core 170-1041A-12X and extending to the bottom of Hole 1041C, the cores are extensively fractured. In the interval between Cores 170-1041A-15X and 1041B-13R (120–280 mbsf), some original textures and structures are destroyed by gas hydrate sublimation.

Apron Unit A1 (late Miocene–Holocene?; 0–423 mbsf) consists mainly of clay(stone) and silt(stone), with minor sandstone, limestone, and volcanic ash (Table 4). These lithologies are dominated by terrigenous rather than biogenic material (Table 5). Unit A1 is divided into two subunits, with Subunit A1B comprising a greater proportion of coarser grained material (siltstones and sandstones) than the claystone-dominated Subunit A1A (Table 3; Fig. 1). Gas hydrates were recovered in the interval 120–280 mbsf. Although evidence of submarine mass wasting and slumping was observed near the base of the hole, we found little evidence of tectonic deformation in the cores except for microfaults, fissility, and variations in bedding dips. The increase in microfaults and changes in bedding dip between 180 and 200 mbsf, and an abrupt change in bedding orientation at 275 mbsf, suggest two possible faults within the section. A reverse or normal sense of movement on these faults cannot be established from the microfaults observed in the cores.

Description of Lithostratigraphic Units

Unit A1: Clay(stone), Silt(stone), and Sandstone

Intervals: 170-1041A-1H-1, 0 cm, to 18X-CC, 19 cm; 170-1041B-1R-1, 0 cm, to 25R-CC, 19 cm; 170-1041C-1R-1, 0 cm, to 3R-CC, 16 cm
Thickness: 423.80 m
Depth: 0–423.80 mbsf
Age: late Miocene–?Pleistocene

Table 3. Site 1041 lithostratigraphic units.

Unit	Subunit	Intervals	Thickness (m)	Depth (mbsf)	Age
A1: clay(stone), silt(stone), and sandstone (0-423.80 mbsf)	A1A: silty clay(stone) and clayey silt(stone)	1041A-1H-1, 0 cm, to 18X-CC, 19 cm	273.83	0-273.83	late Miocene to ? Pleistocene
		1041B-1R-1, 0 cm, to 13R-3, 33 cm			
	A1B: clayey siltstone, sandy siltstone, and silty sandstone	1041B-13R-3, 33 cm, to 25R-CC, 19 cm	149.97	273.83-423.80	late Miocene
		1041C-1R-1, 0 cm, to 3R-CC, 16 cm			

Table 4. Site 1041 lithologic summary.

Core	Major lithology	Color	Fossils	Diagenesis	Minor lithology	A/C/T
170-1041A-						
1H	1) Clayey silt 2) Silty clay	Medium to light olive green	C: diatoms, forams, spicules	Mn reduction	1) Glauconite sand 2) Silty clay with glauconite	T T
2H	1) Silty clay 2) Vitric ash	Olive green Light olive green	T: nannos, rads, spicules C-T: diatoms	C: pyrite concretions T: framboids T: dolomite	1) Yellowish silty clay + diatoms 2) Light greenish gray vitric ash 3) Greenish brown crystal vitric ash 4) Light gray vitric ash	T T C C+
3X	Silty clay	Dark olive green to olive green	T: nannos, diatoms, spicules, fish, pollen	C: framboids T: dolomite	1) Yellowish green silty clay 2) Light gray silty sand	T T
4X	Silty clay	Dark olive green	T: nannos, forams, diatoms, spicules	T-C: framboids T: dolomite	Dark gray vitric ash w/ framboids	T

Notes: A = abundant, C+ = very common, C = common, C- = somewhat common, T = trace. Rads = radiolarians, forams = foraminifers, nannos = nannofossils, spicules = sponge spicules, framboids = pyrite framboids, sponges = sponge spicules, and fish = fish bones/parts. Msv = massive, dissem = disseminated, w/ = with, carb = carbonate, and G.H. = gas hydrate.

This is a sample of the table that appears on the volume CD-ROM.

Subunit A1A: Silty Clay(stone) and Clayey Silt(stone)

Intervals: 170-1041A-1H-1, 0 cm, to 18X-CC, 19 cm; 170-1041B-1R-1, 0 cm, to 13R-3, 33 cm
Thickness: 273.83 m
Depth: 0–273.83 mbsf
Age: late Miocene–?Pleistocene

Subunit A1B: Clayey Siltstone, Sandy Siltstone, and Silty Sandstone

Intervals: 170-1041B-13R-3, 33 cm, to 25R-CC, 19 cm; 170-1041C-1R-1, 0 cm, to 3R-CC, 16 cm
Thickness: 149.97 m
Depth: 273.83–423.80 mbsf
Age: late Miocene

Unit A1 consists mainly of olive green clayey siltstone and silty claystone with minor layers of sandstone, sandy silty claystone, sandy clayey siltstone, claystone, and ash. The sediments are firm below 14 mbsf (Core 170-1041A-2X) and are lithified below 32 mbsf (Core 170-1041A-4X), except for ashy layers that remain unlithified to 395 mbsf (Core 170-1041C-1R). The unit is generally massive, with minor changes in proportions of clay, silt, and sand grain sizes occurring gradually over a 0.5- to 1.0-m interval. Few original sedimentary contacts or primary structures were observed. Clayey siltstone, sandy siltstone, and light gray calcareous clasts and interbeds (Fig. 5) become more common from 299 mbsf (Core 170-1041C-16R) to the bottom of the hole. Silt-sized quartz and feldspar grains are found throughout the section in trace to common amounts. Most feldspar grains are subhedral to euhedral twinned or zoned plagioclase. Euhedral to subhedral silt-sized amphibole grains are found in trace amounts from 0 to 174 mbsf (Cores 170-1041A-1H through 170-1041B-2R). Framboidal pyrite was observed in almost every smear slide (Table 5) in trace amounts and is locally common. Zeolites, probably phillipsite, were observed in smear slides around 300–304 mbsf and 350 mbsf.

Volcanic Ash

Four thick ash intervals (22–150 cm thick) were recovered (Table 6). At least two of these intervals include more than one distinct ash layer; the interval in Core 170-1041A-2H (Ash 1) has at least six layers distinguished by variations in color and composition (Table 6). These thick ash intervals probably represent major volcanic eruptions and, in some cases, multiple eruptive events. Two of the thick ash beds were gas hydrate cemented when recovered (Tables 6, 7; see also "Geochemistry" section, this chapter). Numerous smaller ash beds were also recovered (Fig. 6). Thin light gray, dark gray, and light green ash layers, small light gray ash pods, and light gray to light greenish gray reworked ash layers occur throughout the unit, but make up a relatively minor part of the total stratigraphic thickness. Rock fragments consist of pumice with plagioclase microlites, rare quartz, and, in the lower part of Subunit A1B, obsidian. Volcanic glass is mainly clear, with brown glass (obsidian) being present only in trace amounts. Most of the ashes contain trace amounts of diatoms and/or nannofossils and trace to common amounts of pyrite framboids. Many of the thinner ashes include clay, suggesting that they may have been mixed with adjoining material by bioturbation. The ashes tend to be less lithified than the adjoining lithologies.

Gas Hydrate

Gas hydrate was present in most of the cores from 120 to 280 mbsf (see also "Geochemistry" section, this chapter). Hydrate occurred in four lithologically distinct forms (Table 7): (1) small crystals <0.25 cm across, disseminated throughout the siltstone-claystone lithology; (2) massive white pieces 1–5 cm across; (3) small plates 0.1 cm thick, but 1–2 cm across, which appeared to be fracture fill veins; and 4) grain-cementing matrix in ash layers.

As the cores decompressed and warmed up upon retrieval, the gas hydrate quickly sublimated and much of the ash became soupy and lost internal structure. Massive light gray ashes cemented by gas hydrate were recovered from the intervals 234.24–235.05 mbsf (interval 170-1041B-9R-2, 84 cm, to 9R-3, 16 cm) and 257.43–257.65 mbsf (interval 170-1041B-11R-5, 128–150 cm).

Carbonate Fragments and Concretions

Hard fragments of limestone and dolomitic limestone were recovered beginning at about 69 mbsf (Sample 170-1041A-10X-1, 9 cm) and continuing to the bottom of Hole 1041C. Because most of these fragments were found in the rubble at the tops of the cores, their stratigraphic position is uncertain. Most of the calcareous fragments occur within Subunit A1B. Intact limestone concretions and calcareous claystone mudclasts were observed embedded in clayey siltstone in some cores (Fig. 5). One sandy limestone interbed may be a sand layer that was cemented by secondary carbonate (Sample 170-1041B-16R-3, 5 cm); a second such layer was also observed (Sample 170-1041B-23R-1, 5–7 cm). Most of these calcareous rocks consist of micrite plus calcite grains plus nannofossils. Many contain benthic foraminifers and sand or silt grains (e.g., quartz, feldspar, glauconite). Almost all calcareous fragments contain trace amounts of euhe-

Table 5. Site 1041 smear-slide descriptions.

Sample number							Depth	Imp.		Size				Composition																							
Leg	Site	Hole	Core	Type	Section	Interval (cm)	mbsf	Major lithology	Minor lithology	Med.-coarse sand	Fine sand	Silt size	Clay size	Quartz	Feldspar	Clay	Rock fragments	Volcanic glass	Amphibole	Glauconite	Phosphate	Dolomite	Carbonate	Micrite	Opaque	Framboid	Nannofossils	Foraminifers	Diatoms	Radiolarians	Silicoflagellates	Sponge spicules	Fish remains	Peloids/pellets	Other	Sediment or rock name	Comment
170	1041	A	1	H	1	6	0.06		X			A	C	T	C	C				C					C			T	C	C		C				Clayey silt with diatoms	
170	1041	A	1	H	1	70	0.70	X			C	C+	A	C		A		T	T	T			T			T			T	T		T				Medium olive green silty clay	
170	1041	A	1	H	3	107	4.07		X			C	A	T		A		C-	T	C	T					C-		T	T							Olive green silty clay with glauconite	
170	1041	A	1	H	3	117	4.17		X		A	C	C	C	C-	C-				A						C+										Dark gray olive green glauconite sand	
170	1041	A	1	H	5	84	6.84	X			C-	A	A	C	C-	A		T	T	C-									T			T				Light olive green clayey silt	
170	1041	A	2	H	1	101	8.41	X			T	C	A	T	C-	A	C	C-			T		T			T			C-			T				Olive green silty clay	
170	1041	A	2	H	2	40	9.30		X		T	C	A	C-	T	A	C	T	T	T			T			C-	T	T	C+	T			T		T	Yellowish olive green silty clay with diatoms	Rock fragments are tephra. Other is euhedral zircon crystal. Diatom tests filled with framboids.
170	1041	A	2	H	4	57	12.47		X		C	A	C+	C-	C-		C	A	C-	T					T	T	T		T							Greenish brown crystal-vitric ash	Rock fragments are tephra; glass is clear
170	1041	A	2	H	4	61	12.51		X		T	A	C	T	T	T	T	A					T				T		T	T						Light greenish gray vitric ash	Volcanic glass is clear, minor amount brown
170	1041	A	2	H	5	15	13.55	X		T	C-	A	C+	T	T	C-	C	A							T	T	C-		C-			T				Light olive green vitric ash	May be flow-in: looks like a mixture of ash (2H-4, 61) and olive green silty clay (2H-1, 101).
170	1041	A	3	X	1	60	14.90	X			T	C	A	C-	C-	A	C+	C-		T		T			T	C-			T			T				Dark olive green silty clay, firm	Pollen; rock fragments are tephra
170	1041	A	3	X	2	39	16.19		X		T	C	A	C-	C-	A	T	T		T	T				T	T	T		C-			T	T			Yellowish olive green silty clay, firm	Diatoms filled with framboids. Rock fragments are tephra. Glass is clear, minor glass is brown
170	1041	A	3	X	3	30	17.60	X				C	A	C-	C-	A	T	T		T					T	T			C-			T	T			Olive green silty clay, firm	Rock fragments are tephra

Note: A = Abundant, A- = somewhat abundant, C^+ = very common, C = common, C- = somewhat common, T = trace, blank box = not observed.

This is a sample of the table that appears on the volume CD-ROM.

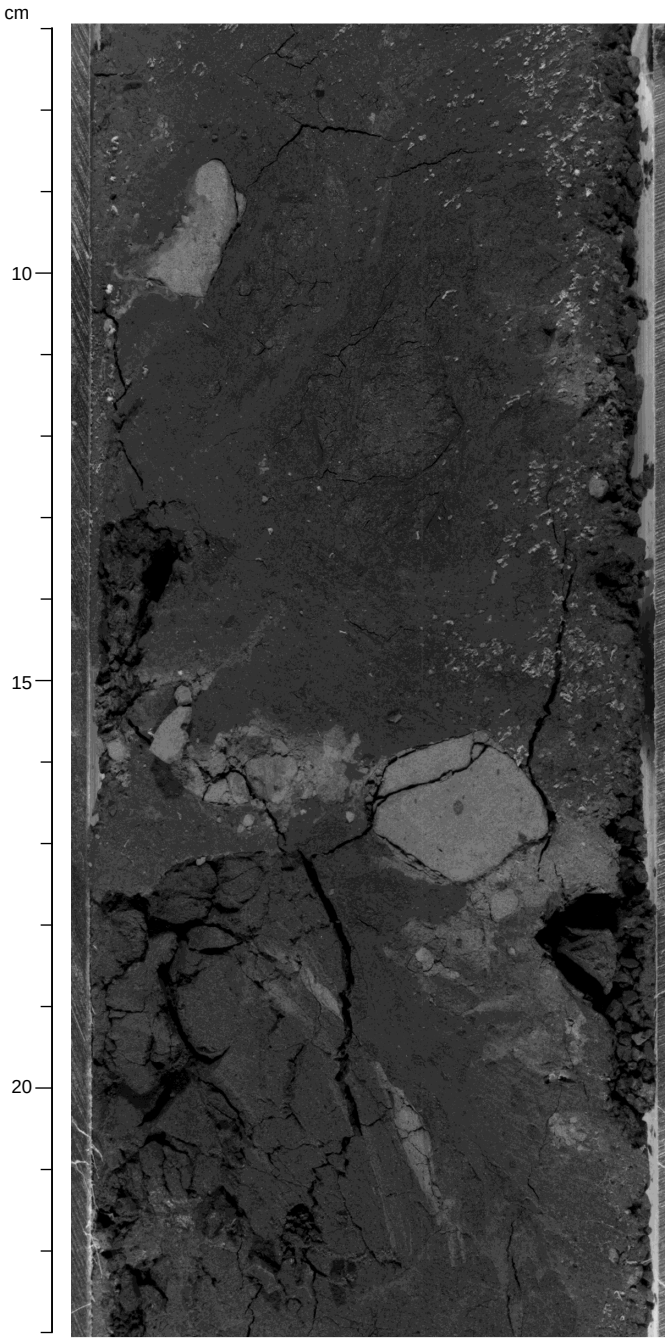

Figure 5. Calcareous, silty claystone mudclasts in siltstone of Subunit A1B (interval 170-1041B-19R-4, 7–23 cm).

dral dolomite crystals, but dolomite is more abundant than calcite below 300 mbsf. Trace amounts of dolomite rhombs are present in the claystones, siltstones, and sandstones beginning at 14.9 mbsf (Sample 170-1041A-3X-1, 60 cm) and are seen in every smear slide below 99 mbsf (Sample 170-1041A-13X-2, 27 cm; Table 5). Aragonite was identified in one smear slide (Sample 170-1041B-15R-1, 14 cm).

Subunit A1A

Subunit A1A is a clay-rich sequence that varies from dark olive green silty clay(stone) to dark olive green clayey silt(stone). Only the first two cores are truly soft sediment; Cores 170-1041A-3X through 4X are firm to very firm sediment, and Cores 5X and lower are well lithified. The general aspect of this subunit is homogeneous with thick intervals of siltstone and claystone (Fig. 7). The main sedimentary structure preserved is small burrows.

The main components of Subunit A1A are terrigenous, dominantly clay. The most common accessory grains in the siltstone and claystone include quartz, feldspar, and volcanic glass. Components present in trace amounts include amphibole, volcanic tephra in silt- to granule-sized fragments, biotite, zircon, opaque minerals, phosphate, and glauconite. Pyrite framboids are ubiquitous in trace amounts, and many diatom and foraminifer tests are filled with framboids. Biogenic components that are sparse but ubiquitous throughout the unit include nannofossils, foraminifers, diatoms, and sponge spicules. Diatoms are present in trace to common amounts throughout Subunit A1A from Cores 170-1041A-1H through 1041B-15R. Rare radiolarians and phosphatic fish remains were observed throughout the section. Pollen, spores, and wood or plant material were found in the upper portion of the subunit.

The uppermost part of the subunit contains poorly sorted thin sand layers with fine- to medium-sand–sized glauconite clasts in addition to the components described above. Patches of framboidal pyrite 1–5 mm across are common within the upper clay(stones) (Cores 170-1041A-1H through 3X). Burrows are filled with yellowish green clay(stone) that typically is richer in nannofossils and diatoms than the surrounding material.

Subunit A1B

The top of this subunit is placed at the first thick siltstone bed. Above this bed, recovery within Section 170-1041B-13R-3 is poor, but grain size is uniformly fine; this section consists of 33 cm of broken drilling rubble of dark olive green claystone. Subunit A1B consists of dark greenish gray to gray clayey siltstone with silty sandstone and sandy siltstone interbeds (Fig. 6). The coarsest layers contain claystone and siltstone granules and pebbles. Dark olive green claystone to silty claystone similar to the major lithology of Subunit A1A are locally present (Cores 170-1041C-21R through 24R).

Grains in the coarser layers are dominated by volcanic material. Volcanic glass is present in all smear slides examined, and rock fragments are mainly pumice or obsidian. Most plagioclase grains in the siltstones and sandstones are subhedral to euhedral; many are also zoned. Other dominantly euhedral to subhedral grains probably derived from nearby volcanic sources include most of the amphiboles and the sparse pyroxene, biotite, and zircon grains. Diatoms are found in trace amounts throughout the unit. Nannofossils are absent

Table 6. Thick ash layers recovered at Site 1041.

Ash layer	Depth (mbsf)	Color	Composition/character
Ash 1	12.47-14.00		
Ash 1-A	12.47-12.49	Greenish brown	Crystal vitric (plagioclase + quartz + amphibole)
Ash 1-B	12.49-12.75	Light greenish gray	Vitric; sparse crystals (quartz + plagioclase)
Ash 1-C	12.75-12.82	Light greenish gray	Altered lithic-vitric
Ash 1-D	12.82-12.97	Light gray	Crystal-vitric (plagioclase + amphibole + quartz)
Ash 1-E	12.97-13.04	Light gray	Lithic-vitric
Ash 1-F	13.04-14.00	Light olive green	Vitric
Ash 2	234.24-235.05	Light gray	Gas hydrate cement
Ash 3	257.43-257.65	Light gray	Gas hydrate cement; individual laminae 4 mm thick
Ash 4	395.00-395.50	Grayish green	Crystal-vitric (plagioclase + quartz + amphibole)

Table 7. Lithologic character of gas hydrates recovered at Site 1041.

Core	Depth to top of core (m)	Gas hydrate
170-1041A-		
15X	116.70	Massive pieces 1-5 cm across
16X	126.40	Fracture fill veins 1-2 cm by <0.05 cm; disseminated small crystals
17X	135.90	(None observed)
18X	145.50	(None observed)
170-1041B-		
1R	155.00	(None observed)
2R	164.60	Disseminated small crystals; cement in volcanic ash
3R	174.20	Scattered crystals; fracture fill veins
4R	183.80	Disseminated small crystals; fracture fill veins
5R	193.50	Abundant flakes of disseminated hydrate
6R	303.10	Disseminated crystals <0.1 cm; fracture fill veins
7R	212.70	Disseminated crystals <0.5 cm; fracture fill veins
8R	222.30	Disseminated crystals <0.1 cm and small slivers
9R	231.90	Disseminated crystals <0.1 cm; cement in ash
10R	241.60	Disseminated crystals <0.1 cm
11R	251.20	Cement in ash layers
12R	260.90	Disseminated crystals <0.1 cm
13R	270.50	Minor disseminated crystals <0.1 cm
14R	280.20	(None observed)
15R	289.90	(None observed)
16R	299.50	Cement in ash layers
17R	309.20	(None observed)
18R	318.80	(None observed)
19R	328.40	Cement in ash layer
20R	338.00	Cement in siltstone
Base of 20R	347.60	(None observed below Core 20R-CC)

to present in trace amounts as are radiolarians and sponge spicules. A few benthic foraminifers were observed. Carbonate concretions are more common than in Subunit A1A and tend to be more dolomitic. Some concretions are silty to sandy.

A poorly sorted, medium to coarse sandstone with granule- to pebble-sized clasts of claystone, shell fragments, black volcanic glass (obsidian), quartz, feldspar, and a trace of glauconite is present near the bottom of the subunit (interval 170-1041C-3R-2, 0–35 cm; Fig. 8). This sandstone layer is interpreted as a debris flow deposit. Only three ash layers were observed in Subunit A1B. One is an unusual light grayish green amphibole-rich crystal-vitric ash (interval 170-1041C-1R-1, 0–50 cm; 395.00–395.50 mbsf).

Structural Geology

We divided the cored interval at Site 1041 into two structural domains based on bedding dip (Fig. 9). Domain I extends from 0 to ~275 mbsf (Cores 170-1041A-1H through 1041B-13R) and Domain II from ~275 to 423.80 mbsf (Cores 170-1041B-16R through 1041C-3R). The boundary between Domains I and Domain II corresponds closely to the boundary between Subunits A1A and A1B.

Domain I

Domain I consists of the homogeneous, moderately bioturbated silty claystone to claystone with sparse sand layers of Subunit A1A (Fig. 1). Bedding is variable in this interval (Fig. 9; Table 8). Most dips are horizontal to steep, from 5° to 60°. Dips of bedding planes generally increase with depth, except for measurements taken between 180 and 200 mbsf (Cores 170-1041B-3R through 5R). The number of minor faults observed increases to a peak in the same interval, suggesting a possible fault at 180 mbsf (Fig. 9). Both normal and reverse senses were identified, but only for a few of the microfaults. Sense of movement on most was indeterminate.

From Cores 170-1041A-5X through 14X, the sediments exhibit weakly developed fissility. Fissility surfaces are spaced 3–5 mm apart and are polished (Fig. 7). Below Core 170-1041A-14X, fissility decreases in intensity and gradually disappears to the base of Domain I (Table 8).

Core 170-1041A-13R (270.50–280.20 mbsf) represents the transitional interval between Domains I and II. It shows an abrupt change in bedding attitude, with a difference in dip of 30° (Fig. 9). The number of observed microfaults increases in this interval, suggesting a fault at about 275 mbsf, but sense of slip is undetermined.

Domain II

Domain II is characterized by bedding that consistently dips 20°–45° (Table 8) and the lack of microfaults. Fissility and fractures gradually disappear, and the clayey siltstone and sandstone of Subunit A1B (Figs. 5, 6, and 8) do not have fissility and lack a macroscopic structural fabric. Deformation bands were observed in Core 170-1041B-23R, consisting of dark seams less than a millimeter thick and 3–4 cm long. Some are characterized by an anastomosing pattern in a single preferred orientation.

Discussion

The thick Pleistocene to late Miocene section recovered at this site differs from that of Site 1040 (sedimentary wedge) by its more proximal sedimentological character (e.g., coarse grain sizes, fresh subangular grains). Thus, it was probably deposited in its present location on the continental margin, rather than being carried to the trench by turbidity currents and then accreted to the lower slope.

The presence of volcanic glass throughout the section in amounts varying from trace to common and the presence of some ash layers 0.25–1.5 m thick suggest that the volcanic eruptions of the Middle American Arc system provided much of the terrigenous material (see also “Geochemistry” section, this chapter). This interpretation is further supported by the shapes and composition of grains interpreted as volcanic in origin (Table 5).

The ashes seen at Site 1041 are of particular interest because the thickest ash intervals probably represent major caldera-forming events in nearby Costa Rica and/or Nicaragua. Some important tuff deposits in northern Costa Rica that may correlate with Site 1041 ashes (E.M. Rojas, pers. comm., 1996) include the following:

1. Rhyodacite and pink tuff, lacking biotite, as well as andesite and dacite. Five distinct flows separated by well-developed paleosols have been recognized from Guayabo caldera, dated at 0.14–0.50 Ma.
2. Gray dacitic tuff with biotite dated at 1.8–4 Ma.

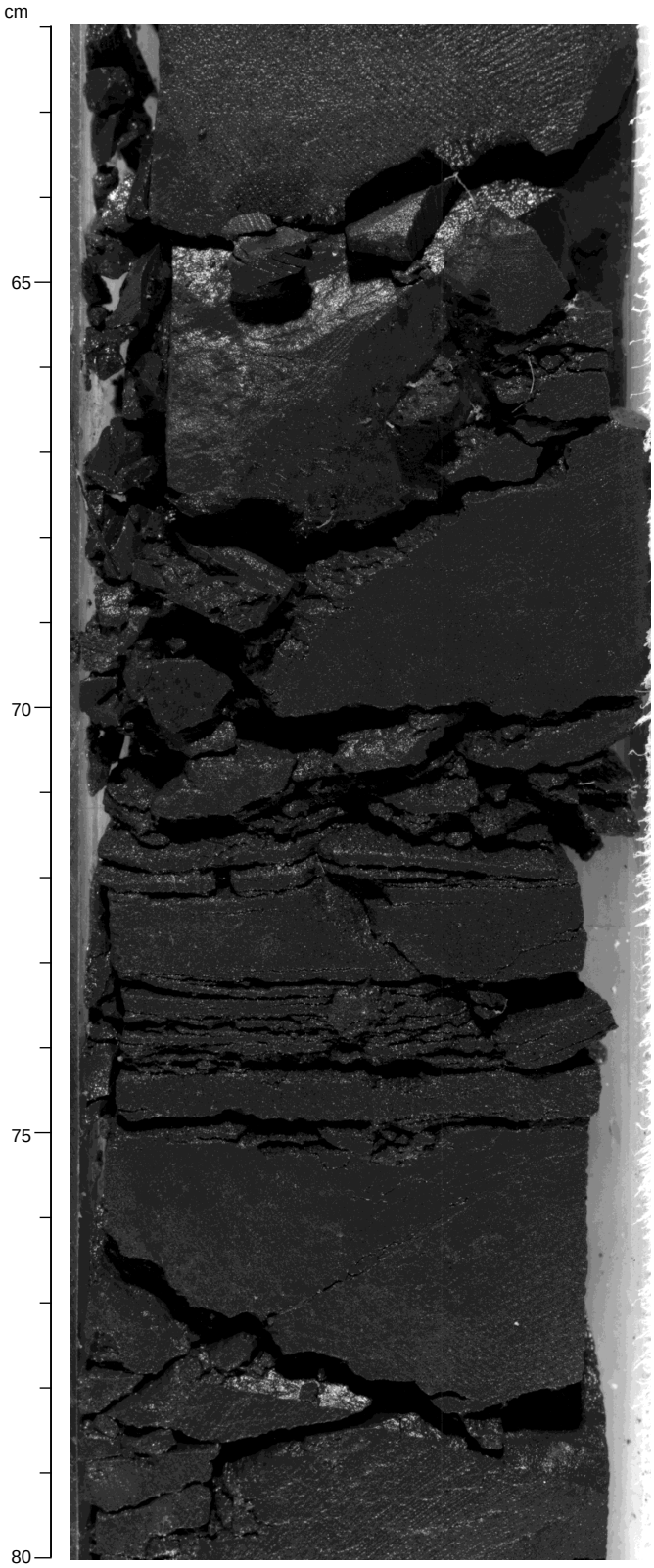

Figure 6. Interbedded siltstone and sandstone layers typical of Subunit A1B (interval 170-1041B-13R-3, 62–80 cm). Lack of fissility is typical of structural Domain II.

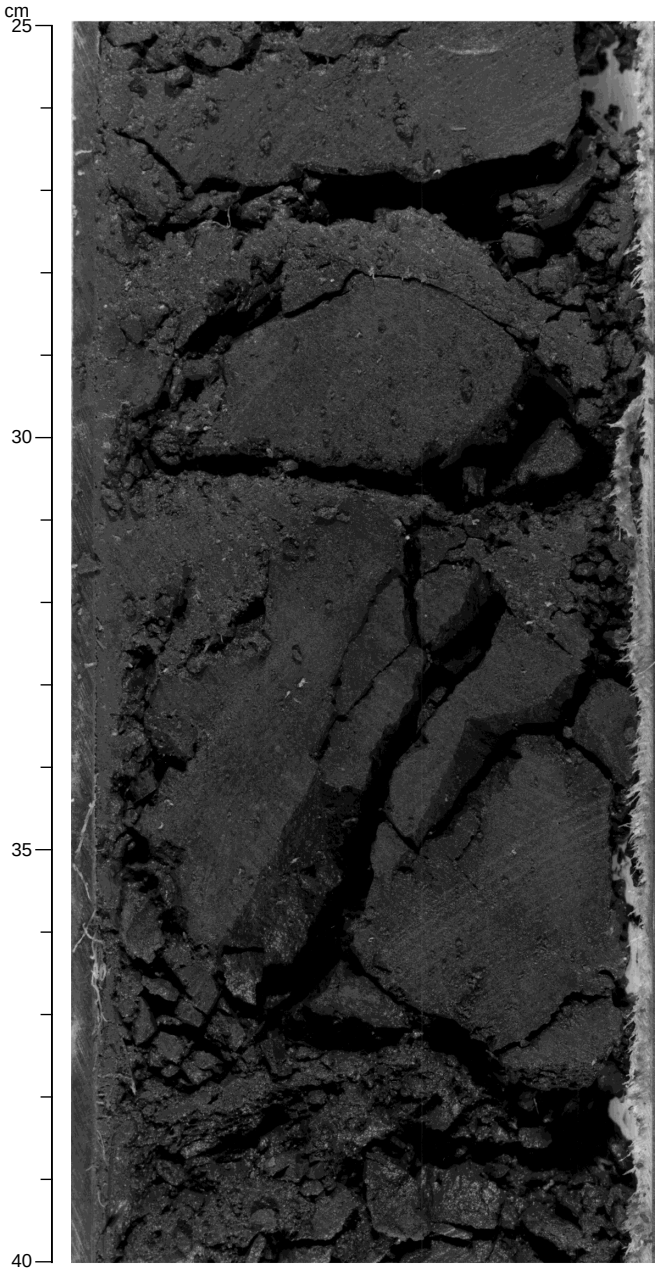

Figure 7. Homogeneous silty claystone of Subunit A1A, showing blocky disaggregation and lenticular fragments typical of structural Domain I (interval 170-1041A-12X-1, 25–40 cm).

3. Tuffs near Miravalles dated at 4.3–7.5 Ma.
4. Tuffs on the rim of Guayabo caldera dated at 0.4–1.4 Ma.

BIOSTRATIGRAPHY AND MAGNETOSTRATIGRAPHY

Biostratigraphy

Calcareous Nannofossils

Calcareous nannofossils are sufficiently numerous in all three holes drilled at Site 1041 to delineate several Pleistocene through late Miocene calcareous nannofossil zones (Fig. 10). The range, distribu-

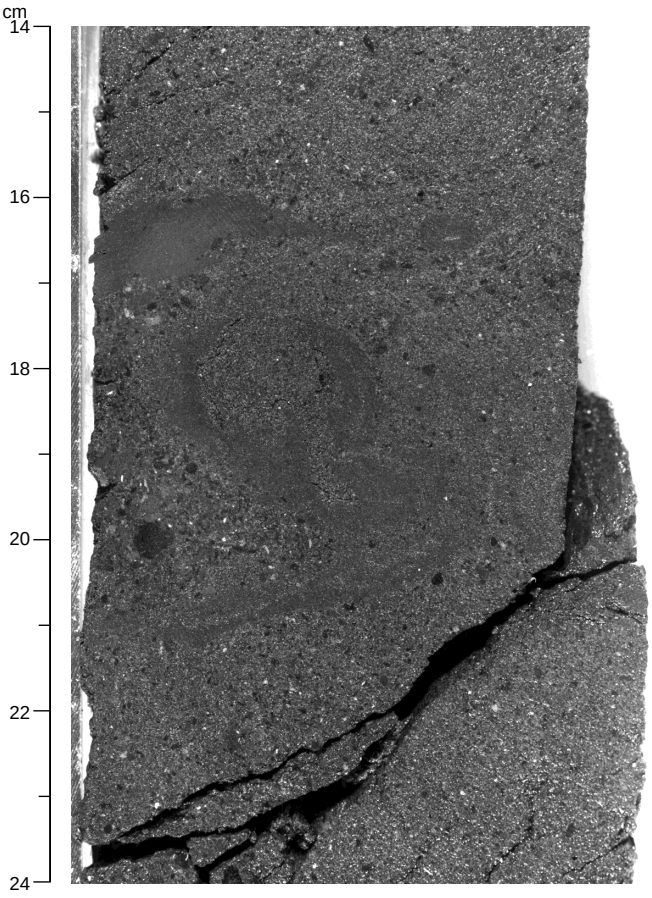

Figure 8. Sandstone with granule- and pebble-sized grains near the base of Hole 1041C, Subunit A1B (interval 170-1041C-3R-2, 14–24 cm).

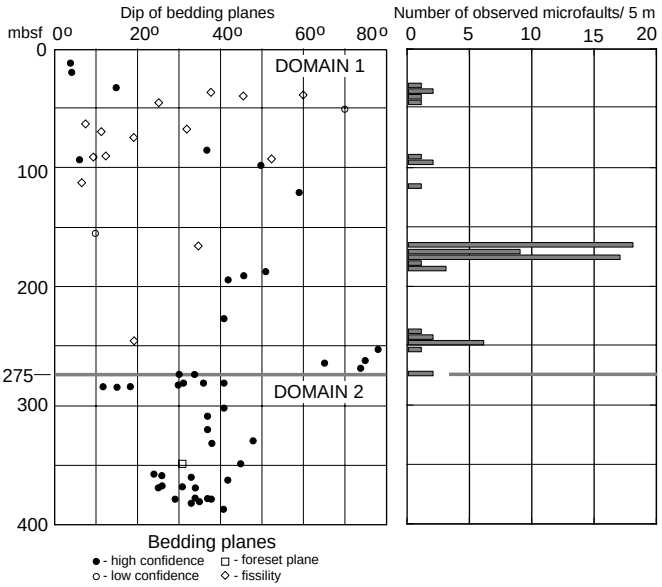

Figure 9. Summary diagram of major structural features recorded at Site 1041. Dips of bedding and number of observed microfaults per 5 m are plotted vs. depth for Site 1041.

tion, abundance, and preservation of the index calcareous nannofossil species observed in the cores taken from these holes are presented in range-distribution charts in Tables 9 and 10. Additional species observed in each sample, which were typical of the nannofossil assemblage, are also plotted in the range-distribution charts.

Hole 1041A

Samples 170-1041A-1H-CC and 2H-CC are assigned to the undifferentiated Pleistocene Zones NN21-NN19, based primarily on the absence of *Discoaster brouweri* and the rare presence of *Helicosphaera sellii* in Sample 2H-CC. Sample 1H-CC does not contain calcareous nannofossils.

Undifferentiated late Pliocene Zones NN18-NN17 are observed in Samples 170-1041A-3X-CC through 13X-CC. This determination is based primarily on the absence of *Discoaster surculus* and *Discoaster pentaradiatus*, and the presence of *D. brouweri*. It is interesting to note the occurrence of reworked *Cruciplacolithus primus*, an early to late Paleocene nannofossil, in Sample 170-1041A-4X-CC.

An assemblage of calcareous nannofossils characteristic of late Pliocene Zone NN16 is observed in Sample 170-1041A-14X-CC. In Sample 170-1041A-15X-CC small reticulofenestrids are rare, and Sample 170-1041A-16X-CC does not contain nannofossils. However, these two samples are tentatively assigned to Zone NN16 based on stratigraphic position.

Samples 170-1041A-17X-CC and 18X-CC are assigned to early Pliocene Zone NN15. The last occurrence (LO) of both the sphenoliths (3.60 Ma) and *Reticulofenestra pseudoumbilica* (3.75 Ma) is observed in Sample 17X-CC. Sample 18X-CC contains abundant sphenoliths and no amauroliths or five-rayed discoasters.

Holes 1041B and 1041C

It is not possible to place Sample 170-1041B-1R-CC (161.05 mbsf) into a zone, because the assemblage of nannofossils present could be characteristic of early Pliocene Zone NN15 through late Miocene/early Pliocene Zone NN12. This is determined partly on the assignment of Sample 170-1041B-2R-CC, immediately downsection, to Zone NN11 based on the LO of *Discoaster quinqueramus.* On the other hand, Sample 170-1041B-1R-CC does not contain any of the marker fossils that define Zones NN14 through NN12. Either this interval exists between the two core-catcher samples, or there is an unconformity. The distinction between these two possibilities will be made during shore-based analysis.

Late Miocene calcareous nannofossil Zone NN11 is assigned to Samples 170-1041B-2R-CC through 21R-CC, which has been determined by the presence of *Discoaster berggrenii* and/or *D. quinqueramus.* This zone was not divided further because of the absence of *Amaurolithus primus. Micula murus,* a nannofossil species restricted to the Maastrichtian, was observed reworked in Sample 170-1041B-19R-CC.

Samples 170-1041B-22R-CC through 24R-CC contain nannofossil assemblages that most likely belong to either Zone NN11, NN10, or NN9. These samples, however, contain none of the zonal markers necessary to make this determination.

Samples 170-1041C-1R-CC and 2R-CC (161.05–170.76 mbsf) do not contain any of the marker fossils.

The LO of *Discoaster hamatus* is observed in Sample 170-1041C-3R-CC. Thus, this sample can be assigned to middle/late Miocene Zone NN9.

Diatoms

Although diatoms show variable states of abundance and preservation in the cores recovered at Site 1041, age-diagnostic taxa are present and suggest a Pleistocene through late Miocene age for the cores (Fig. 10). Table 11 lists the stratigraphically significant diatoms and additional representative taxa that were observed at Site 1041.

Table 8. Site 1041 structural summary.

Site	Hole	Core	Type	Section	Top (cm)	Bottom (cm)	Depth (mbsf)	Cr az.	Cr dip	Cr line	Cr l.dip	Cr sense	Pm az.	Pm dip	Pm line	Pm l.dip	Sense	Conf.	Half	Tool	Identifier
1041	A	2	H	4	57	57	12.47	183	87				45	4					W	MMT	Bedd
1041	A	3	X	3	30	20	17.60	0	86				180	4					W	MMT	Bedd
1041	A	5	X	1	2	22	32.42	95	48				312	86					W	MMT	Frac (prob.bed)
1041	A	5	X	1	82	82	33.22	6	76				157	15					W	MMT	Bedd
1041	A	5	X	1	134	134	33.74	356	76				196	15					W	MMT	Bedd
1041	A	6	X	1	38	38	35.78	200	58				29	37					W	MMT	Fiss. (bedd)
1041	A	6	X	1	38	38	35.78	58	28				156	76					W	MMT	Frac
1041	A	6	X	1	38	38	35.78	313	61				233	53					W	MMT	Frac
1041	A	6	X	2	110	110	38.00	197	32				10	60					W	MMT	Fiss. (bedd)
1041	A	6	X	3	35	35	38.75	191	46				11	45					W	MMT	Fiss. (bedd)

Notes: Cr az. = core reference azimuth, Cr dip = core reference dip, Cr line = core reference lineation, Cr l.dip = core reference lineation dip, Cr sense = core reference sense, Pm az. = paleomagnetic azimuth, Pm dip = paleomagnetic dip, Pm line = paleomagnetic lineation, Pm l.dip = paleomagnetic lineation dip, Conf. = confidence, and Half = core half (W = working half, A = archive half). MMT = tool designed by Martin Mesch, and Protr. = protractor. Bedd = bedding, Frac = fracture, Fiss. = fissility.

This is a sample of the table that appears on the volume CD-ROM.

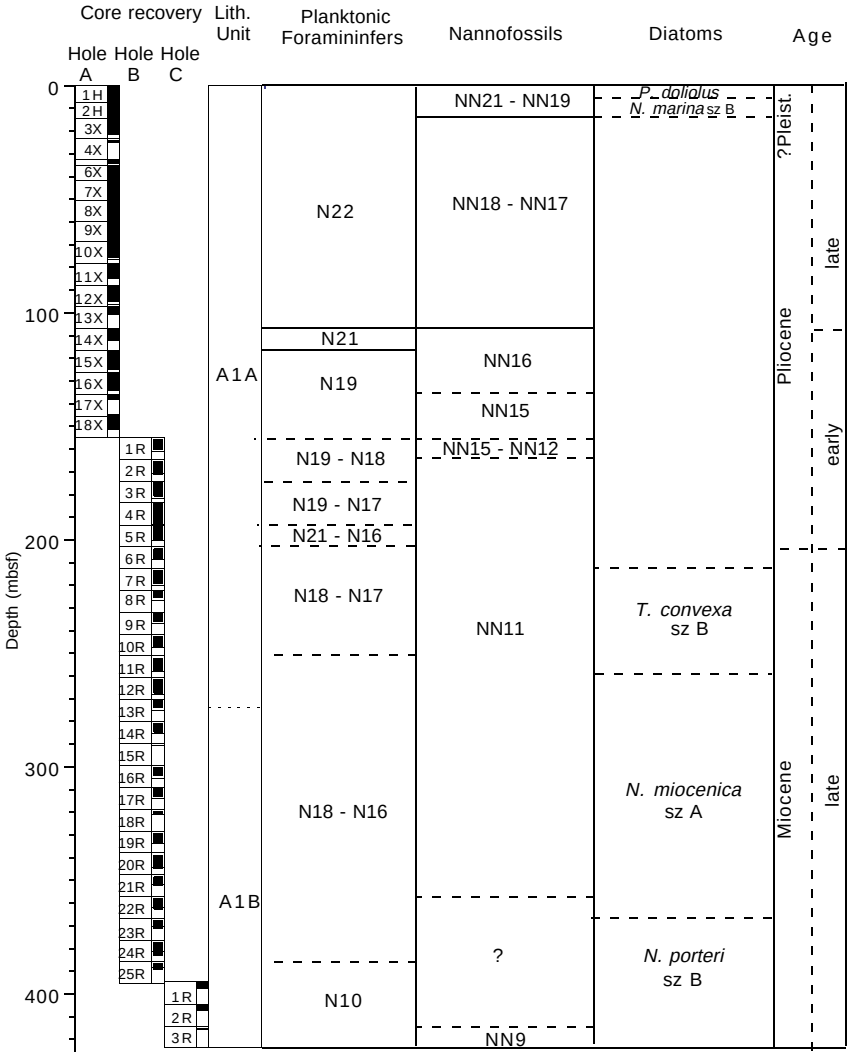

Figure 10. Correlation of planktonic foraminifer, calcareous nannofossil, and diatom zones with Site 1041 cores and sedimentary units. Dashed lines represent uncertainty in placement of the zonal boundary. Sz = subzone.

Significant reworking of middle and early Miocene diatoms is observed, particularly in Cores 170-1041B-7R through 12R, which span the Pliocene/Miocene boundary. Latest Miocene diatoms are present in sufficient abundances to recognize reworked taxa.

The late Pleistocene *Pseudoeunotia doliolus* Zone (0–0.62 Ma) is recognized in Core 170-1041A-1H by the assemblages observed in Samples 170-1041A-1H-1, 0–3 cm (mudline sample), through 1H-3, 99–101 cm (Table 11). Two additional samples examined in Core 170-1041A-1H (1H-3, 124–126 cm, and 1H-CC) are barren or contain only rare diatoms, so no age determination is possible. In interval 170-1041A-2H-1, 135–150 cm, diatoms are few and moderately preserved, and the presence of *Rhizosolenia praebergonii* (LO at 2.01 Ma), in addition to the absence of *P. doliolus* (first occurrence [FO] at 2.01 Ma), strongly suggests that the interval correlates to the late

Table 9. Calcareous nannofossil range distribution chart for Hole 1041A.

Calcareous nannofossil zone	Core, section	Depth (mbsf)	Abundance	Preservation	Small reticulofenestrids	*Calcidiscus leptoporus*	*Calcidiscus macintyrei*	*Ceratolithus telesmus*	*Coccolithus miopelagicus*	*Discoaster brouweri*	*Discoaster surculus*	*Discoaster variabilis*	*Helicosphaera carteri*	*Helicosphaera sellii*	*Pontosphaera discopora*	*Pseudoemiliania lacunosa*	*Reticulofenestra pseudoumbilicus*	*Sphenolithus abies*	*Sphenolithus heteromorphus*	*Sphenolithus verensis*	Unidentifiable placoliths	Unidentifiable 6-rayed discoasters
	170-1041A-																					
	1H-CC	7.35	B																			
NN21-NN19	2H-CC	14.03	F	P	C	F			r				F	R				r				
	3X-CC	21.12	F	P		F		R		F			R	R		F						
	4X-CC	24.92	C	M		F				F			R	R	F							
	5X-CC	34.21	C	M	C	R				F			F	F		R						
	6X-CC	41.23	A	M	C	F				F			R	F	R							
	7X-CC	50.7	C	M	C	F				F			F									
NN18-NN17	8X-CC	60.46	F	P		F		R	f	F			F									
	9X-CC	69.22	B																			
	10X-CC	76.23	A	M	A	F	R			F			F	R	R							
	11X-CC	84.99	F	P	F					R												
	12X-CC	96.19	F	P	F					R												
	13X-CC	100.78	F	M	F		R			F					R							R
	14X-CC	112.18	A	M	A		F			R	R		C		F							
NN16	15X-CC	125.09	R	P	R																R	
	16X-CC	134.25	B																			
	17X-CC	137.48	F	M	F	F				R			F		R		F	R	r			
NN15	18X-CC	151.48	F	M	F	R	R			R		R	R		R			R		R		

Notes: Abbreviations for abundances are as follows: A = abundant, C = common, F = few, R = rare, B = barren, and lowercase letters = reworked. Abbreviations for preservation are as follows: G = good, M = moderate, and P = poor. For more specific definitions refer to the "Explanatory Notes" chapter (this volume). *Cruciplacolithus primus* (early to late Paleocene) observed in Core 1041A-4X-CC.

This table also appears on the volume CD-ROM.

Pliocene *Nitzschia marina* Subzone B (2.01–2.43 Ma). Sample 170-1041A-2H-CC also contains diatoms characteristic of this zone (Table 11). Not recognized in this hole is the early Pliocene *Nitzschia reinholdii* Zone that occurs between the late Pleistocene *P. doliolus* Zone and the late Pliocene *N. marina* Subzone B.

Samples 170-1041A-3X-CC (21.12 mbsf) through 170-1041B-6R-CC (208.67 mbsf) are either barren of diatoms or contain rare to few poorly preserved assemblages (Table 11) without age-diagnostic taxa. The late Miocene *Thalassiosira convexa* Zone (Subzone B) is marked by the LO of *Thalassiosira miocenica* and occurs in Sample 170-1041B-7R-CC at an age of 5.83 Ma. Another event within this zone is the LO of *Nitzschia miocenica* at an age of 6.07 Ma, which occurs in Sample 170-1041B-8R-CC. The late Miocene *N. miocenica* Subzone A/B boundary occurs in Sample 170-1041B-12R-CC at an age of 6.69 Ma, as marked by the FO of *Thalassiosira praeconvexa.* The boundary between the *N. miocenica* and the *Nitzschia porteri* Zones occurs between Samples 170-1041B-22R-CC and 23R-CC and is marked by the last appearance of *N. miocenica.* An event within the *N. porteri* Zone is the LO of *Rossiella paleacea*, which occurs in Sample 170-1041B-23R-CC at an age of 7.37 Ma. Samples 170-1041B-24R-CC (381.32 mbsf) through 170-1041C-3R-CC (415.54) contain rare to common diatoms that are characteristic of *N. porteri* Subzone B.

Planktonic Foraminifers

Planktonic foraminifers are few to absent in all core-catcher samples at Site 1041. Preservation is moderate to poor. It was not possible to establish planktonic foraminifer zones in Holes 1041A and 1041B with precision, however, some age-diagnostic species are present (Fig. 10; Table 12).

Hole 1041A

Planktonic foraminifers from Hole 1041A are few to absent and, when present, are moderately to poorly preserved (Table 12). In Samples 170-1041A-2H-CC through 4X-CC, planktonic foraminifers are rare and include the taxa listed in Table 12. The interval is assigned to Zone N22, based on presence of *Globigerinoides trilobus* and dextrally coiled *Pulleniatina obliquiloculata.* The assemblages from Samples 170-1041A-5X-CC through 13X-CC include the LO of *Globigerinoides extremus* in Sample 5X-CC, indicating an age of 1.77 Ma. Sample 170-1041A-14R-CC is assigned to Zone N21 of the latest Pliocene, based on the presence of *Globorotalia theyeri* and sinistrally coiled *Pulleniatina* spp. Planktonic foraminifer assemblages of Samples 170-1041A-15R-CC through 18R-CC are 3.65–3.95 Ma (mid-Pliocene), based on the occurrence of dextrally coiled *Pulleniatina primalis.* Samples 170-1041A-1H-CC and 12X-CC are barren of planktonic foraminifers.

Hole 1041B

Planktonic foraminifers are rare in the upper part of Hole 1041B and, when present, are moderate to poorly preserved (Table 12). Sample 170-1041B-1R-CC (161.05 mbsf) is 3.95–6.0 Ma, based on the presence of *Globorotalia margaritae* and sinistrally coiled *Pulleniatina* spp. The interval from Samples 170-1041B-2R-CC through 4R-CC ranges in age from 3.95 to 6.4 Ma, based on the presence of sinistrally coiled *P. primalis.* Sample 170-1041B-6R-CC is younger than 8.3 Ma, based on the occurrence of *Globorotalia plesiotumida.* Planktonic foraminifer assemblages of Sample 170-1041B-12R-CC are latest Miocene, based on the occurrence of *Globorotalia conoidea.* The assemblage in Sample 170-1041B-20R-CC is older than Zone N16 of the late Miocene, based on the occurrence of *Neogloboquadrina continuosa.* Sample 170-1041B-25R-CC includes several specimens of *Globigerina druryi, Globorotalia clemenciae,* and *Globorotalia peripheroronda.* The sample is older than 14.6 Ma, based on the occurrence of *G. peripheroronda.* The age of the sample disagrees with diatom ages (Fig. 11). Samples 170-1041B-7R-CC through 10R-CC, 14R-CC through 15R-CC, 17R-CC through 19R-CC, and 21R-CC through 24R-CC are barren of planktonic foraminifers.

Table 10. Calcareous nannofossil range distribution chart for Holes 1041B and 1041C.

Calcareous nannofossil zone	Core, section	Depth (mbsf)	Abundance	Preservation	Small reticulofenestrids	*Coccolithus miopelagicus*	*Cyclicargolithus floridanus*	*Discoaster deflandrei*	*Discoaster neorectus*	*Hayaster perplexus*	*Helicosphaera ampliaperta*	*Helicosphaera carteri*	*Reticulofenestra pseudoumbilicus*	*Sphenolithus abies*	*Sphenolithus heteromorphus*	*Sphenolithus moriformis*	*Sphenolithus verensis*	*Discoaster berggrenii*	*Coccolithus pelagicus*	*Calcidiscus macintyrei*	*Discoaster intercalaris*	*Calcidiscus leptoporus*	*Discoaster surculus*	*Discoaster variabilis*	*Discoaster brouweri*	*Discoaster kugleri*	*Discoaster pentaradiatus*	*Ceratolithus armatus*	*Ceratolithus rugosus*	*Discoaster quinqueramus*	*Ceratolithus cristatus*	*Discoaster asymmetricus*	*Helicosphaera sellii*	Unidentifiable 6-ray discoasters	Unidentifiable placoliths
	170-1041B-																																		
NN15-NN12	1R-CC	161.05	C	M	A							C	C	F		F						C			R										
	2R-CC	170.76	R	P	R								R	R											R					R					
	3R-CC	181.59	R	P	R							R		R			R					R			R										
	4R-CC	193.38	A	M	A							C	C	C			F					C			F				R						
	5R-CC	200.44	A	M	C							R	C	C			F					R	R		C						T	T			
	6R-CC	208.67	A	M	C							R	F	F			F						R		F		F				R				
	7R-CC	219.91	C	M	C								F	F	r	F		R				F	R		F		R	R	R	R					
	8R-CC	226.59	F	M	R											R							R	R	R	r	R								
	9R-CC	236.61	R	M	R								R			F		R				R	R												
	10R-CC	247.56	F	P	R													R			R		R		R									T	
	11R-CC	258.03	C	M	C							R				C		C					R	R											
NN11	12R-CC	268.08	C	M	F							R	R			C		F																	
	13R-CC	275.21	C	P	R								F					R			R	R	R												
	14R-CC	285.19	R	P	R																R													T	
	15R-CC	290.39	R	P																															T
	16R-CC	304.88	R	P																															T
	17R-CC	314.18	B																																
	18R-3	320.91	R	P		r										R				R															T
	19R-CC	333.82	R	P									R				R																		
	20R-CC	344.47	F	P	F								R	R		F			R																
	21R-CC	351.65	C	P	C									R		F	R	R																	
	22R-CC	361.72	F	P	F	r						R		F			F																		F
	23R-CC	370.49	B																																
	24R-CC	381.32	R	P																															T
?	25R-CC	388.22	C	P	F	r					r	R	F	F	R	F																			
	170-1041C-																																		
	1R-CC	397.61	R	P									R																						
	2R-CC	407.51	F	P	F								F																						
NN9	3R-CC	415.54	A	P	C	r	r	r	R	R		F	C		r																				

Notes: Abbreviations for abundances are as follows: A = abundant, C = common, F = few, R = rare, B = barren, and lowercase letters = reworked. Abbreviations for preservation are as follows: G = good, M = moderate, and P = poor. For more specific definitions refer to the "Explanatory Notes" chapter (this volume). *Micula murus* (Maastrichtian) was observed in Core 170-1041B-19R-CC.

This table also appears on the volume CD-ROM.

Hole 1041C

Three cores were recovered from Hole 1041C. Planktonic foraminifers are included in Sample 170-1041C-3R-CC (415.54 mbsf) and are rare and poorly preserved (Table 12). Samples 170-1041C-1R-CC and 2R-CC are barren. Sample 170-1041C-3R-CC includes *Globigerina woodi*, *Globigerina eamsi*, *Globigerinoides immatulus*, *Dentoglobigerina altispira*, *Globorotalia clemenciae*, and *G. peripheroronda*. The sample is older than 14.6 Ma.

Paleomagnetism

Demagnetization of both split cores and discrete samples was used to characterize the remanence directions in Site 1041 sediments. Poor core quality and remagnetization in the upper portion of this site have degraded the magnetostratigraphy.

Magnetostratigraphy

The magnetostratigraphy of this site can be divided into two zones: an upper zone of apparently remagnetized, entirely normal polarity from 0 to ~160 mbsf (Fig. 12), and a zone containing both normal and reversed polarities from ~160 mbsf to TD (Fig. 13). Using biostratigraphic markers between 220 and 270 mbsf as tie points to the magnetic polarity time scale, intervals of normal and reversed polarity can be assigned to portions of the magnetic polarity time scale. Polarity intervals ranging from the onset of Chron C3n.2n (4.62 Ma) at 174 mbsf to the termination of Chron C4n.2n (7.432 Ma) at 396.5 mbsf have been identified (Fig. 14). Uncertainties in this interpretation stem from possible faults, some intervals of moderate to steep bedding dips (see "Lithostratigraphy and Structures" section, this chapter), and intervals of no core recovery.

Rock Magnetism

To evaluate the sources of remagnetization within the upper portion of this site and to define the carriers of remanence in these sediments, thermal demagnetization of multi-component isothermal remanent magnetization (mIRM; Lowrie, 1990) was performed on selected samples. Orthogonal fields of 1.0 T, 0.4 T, and 0.05 T were successively applied to each sample, and these mIRMs were then measured after sequential heating steps from room temperature to 640°C. From the remagnetized interval, the mIRM components unblocked between 200° and 300°C, indicating the presence of Fe-sulfides (either greigite or pyrrhotite), and also unblocked at about 580°C, indicating the presence of magnetite (Fig. 15).

Age-Depth Correlation

Two trends in the age-depth relationship are apparent, using biostratigraphic markers (Table 13; Fig. 11). Between ~10 and 225 mbsf, age-depth rates are 55 m/m.y. (diatoms) and 62 m/m.y. (nannofossils). Between ~225 and 400 mbsf, the age-depth rate is 93 m/m.y. (diatoms). Using the magnetostratigraphy outlined above, age-depth

Table 11. Diatom range distribution chart for Site 1041.

Diatom zone	Core, section, interval (cm)	Depth (mbsf)	Abundance	Preservation	*Actinocyclus ellipticus*	*Actinocyclus ellipticus* var. *javanica*	*Actinocyclus ellipticus* f. *lanceolata*	*Actinocyclus ingens*	*Actinocyclus moronensis*	*Actinoptychus senarius*	*Asteromphalus elegans*	*Azpeitia nodulifer*	*Cestodiscus pulchellus*	*Coscinodiscus lewisianus*	*Coscinodiscus marginatus*	*Hemidiscus cuneiformis*	*Nitzschia fossilis*	*Nitzschia marina*	*Nitzschia miocenica*	*Nitzschia porteri*	*Nitzschia reinholdii*	*Pseudoeunotia doliolus*	*Rhizosolenia praebergonii* var. *robusta*	*Rhizosolenia praebergonii*	*Rossiella paleacea*	*Thalassionema nitzschioides*	*Thalassiosira convexa* var. *aspinosa*	*Thalassiosira miocenica*	*Thalassiosira oestrupii*	*Thalassiosira praeconvexa*	*Thalassiosira tappanae*	*Thalassiosira yabei*	*Thalassiothrix longissima*	*Triceratium pileus*
	170-1041A-																																
	1H-1	0	A	G								F						F				C	r			F			A			F	
P. doliolus	1H-1, 60-62	0.62	C	M								C				F		F				F	r			R			F			R	
	1H-2, 78-80	2.3	C	M												T		F				F	r			R			C	r			
	1H-2, 140-142	2.92	C	M								R				R		C				F		r		R			C			F	r
	1H-3, 99-101	4.01	C	M								F				R		F				F				R			F			F	
?	1H-3, 124-126	4.5	B																														
	1H-CC	7.35	R	P						R																						R	
N. marina sz B	2H-1, 135-150	8.85	F	M						R	R	R				R	F	R			R			R		R			F				r
	2H-CC	14.03	F	P						R		R					F	R			R	A				R			F			R	
	3X-CC	21.12	F	P						R																						R	
	4X-CC	24.92	R	P																									R				
	5X-CC	34.21	B																														
	6X-CC	41.23	F	P						R						R	R						R			R			R				
	7X-CC	50.7	R	M													R	R					R						R				
	8X-CC	60.46	R	M												R		R								R			R				
	9X-CC	69.22	B																														
	10X-CC	76.23	R	P						R																							
	11X-CC	84.99	R	P						R																R			R				
	12X-CC	96.19	B																														
	13X-CC	100.78	B																														
?	14X-CC	112.18	R	P																													
	15X-CC	125.09	B																														
	16X-CC	134.25	B																														
	17X-CC	137.48	F	P																												F	
	18X-CC	151.48	R	P																												R	
	170-1041B-																																
	1R-CC	161.05	R	P						R				r																			
	2R-CC	170.76	R	P						R			r																R			R	
	3R-CC	181.59	R	P						R		R																	R				
	4R-CC	193.38	R	P						R																			R				
	5R-CC	200.44	R	P						R																							
	6R-CC	208.67	F	M						R		F																	F				
	7R-CC	219.91	C	M		r					R	F	r			R		R		r	F					R		R	F				r
	8R-CC	226.59	F	P			r	r	r	R		F	r					R	R		F					R	R	R	R		r		r
	9R-CC	236.61	C	M						R		F							F		F					F	F		R			F	
T. convexa sz B	10R-CC	247.56	C	M					r	R	R	R				R		R	F							R	F		R	F		R	r
	11R-CC	258.03	C	M					r	R		F				R		R	F			R				R	F		F	F	r	F	r
	12R-CC	268.08	C	P		r			r	R		R	r	r		R		R	F			R				R			R	F	r	R	r
	13R-CC	275.21	F	P						R		R	r			R		R	F										R	R		R	
	14R-CC	285.19	F	P	r							R			R				R							R						R	
	15R-CC	290.39	R	P																						R			R			R	
	16R-CC	304.88	B																														
	17R-CC	314.18	B																														
N. miocenica sz A	18R-CC	321.3	F	P						R		R			R				R							R			R			R	
	19R-CC	333.82	B																														
	20R-CC	344.47	R	P						R																R			R			R	
	21R-CC	351.65	R	P								R						R								R						R	
	22R-CC	361.72	R	P	r																					R						R	
	23R-CC	370.49	F	M		r				R		R				R		R	R						F				R	R		R	
	24R-CC	381.32	F	M														R	R		R				R	F			F			F	
	25R-CC	388.22	F	P						R			R		R											R			R				r
	170-1041C-																																
N. porteri sz B	1R-1,134-135	389.57	C	M		R				R	R	R						R		R	R				F				F			F	
	1R-CC	397.61	R	P														R											R			R	
	2R-CC	407.51	F	M		R					R							R		R	R				R	F			R			F	
	3R-CC	415.54	F	P														R		R					R				R			R	

Notes: Abbreviations for abundances are as follows: A = abundant, C = common, F = few, R = rare, B = barren, r = reworked, and Sz = subzone. Abbreviations for preservation are as follows: G = good, M = moderate, and P = poor. For more specific definitions refer to the “Explanatory Notes” chapter (this volume).

This table also appears on the volume CD-ROM.

Table 12. Planktonic foraminifer range distribution chart for Site 1041.

Planktonic foraminifer zone	Core, section	Depth (mbsf)	Abundance	Preservation	*Dentoglobigerina altispira*	*Dentoglobigerina globosa*	*Globigerina bulloides*	*Globigerina eamsi*	*Globigerinella aequilateralis*	*Globigerinoides conglobatus*	*Globigerinoides extremus*	*Globigerinoides immaturus*	*Globigerinoides obliquus*	*Globigerinoides quadrilobatus*	*Globigerinoides ruber*	*Globigerinoides sacculifer*	*Globigerinoides tenellus*	*Globigerinoides trilobus*	*Globoconella conoidea*	*Globoquadrina dehiscens*	*Globoquadrina venzuelana*	*Globorotalia inflata*	*Globorotalia juani*	*Globorotalia limbata*	*Globorotalia mararitae*	*Globorotalia menardii*	*Globorotalia multicamerata*	*Globorotalia peripheroronda*	*Globorotalia plesiotumida*	*Globorotalia scitula*	*Globorotalia theyeri*	*Globorotalia tosaensis*	*Globorotalia tumida*	*Globorotaloides hexagona*	*Neogloboquadrina acostaensis*	*Neogloboquadrina continuosa*	*Neogloboquadrina dutertrei*	*Neogloboquadrina humerosa*	*Pulleniatina obliquiloculata*	*Pulleniatina primalis*	*Sphaeroidinella dehiscens*	*Sphaeroidinellopsis seminulina*	*Tenuitella clemenciae*	*Zeaglobigerina apertura*	*Zeaglobigerina decoraperta*	*Zeaglobigerina druryi*	*Zeaglobigerina nepenthes*	*Zeaglobigerina rubescens*	*Zeaglobigerina woodi*
	170-1041A-																																														
	1H-CC	7.35	B																																											
	2H-CC	14.03	F	P														F														R			R											
	3X-CC	21.12	R	P																					R							R			R		R		R						
	4X-CC	24.92	T	P			T																										T												
	5X-CC	34.21	F	M							R	R	R					R				R			R						R	R			R	R	R								
	6X-4	40.8		P																																									
N22	6X-CC	41.23	R	P					R				R		R	R									R					R					R										
	7X-CC	50.7	R	M							R			R	R										R							R			R										
	8X-CC	60.46	R	M											R	R																			R		R								
	9X-CC	69.22	R	M							R				R			R												R			R	R		R	R								
	10X-CC	76.23	R	M							R				R	R	R	R							R						R		R	R		R	R								
	11X-CC	84.99	R	M							R		R		R	R		R							R					R			R	R		R	R								
	12X-CC	96.19	B																																										
	13X-CC	100.78	R	M											R	R									R							R	R	R		R		R						
N21	14X-CC	112.18	R	M																					R						R					R		R						
	15X-CC	125.09	F	M							R				R	R		R							R	T											R								
N19	16X-CC	134.25	R	M						R	R				R	R	R																R			R	R	R			R				
	17X-CC	137.48	R	P	R	R					R		R			R					R		T	R											R						T			
	18X-CC	151.48	R	M	R						R		R		R			R							R					R					R				R				T	R	
	170-1041B-																																													
	1R-CC	161.05	R	P	R								R								R				R	R													R		R				
N19-N18	2R-CC	170.76	R	P									R							T	R					R									R		R		R		R				
	3R-CC	181.59	R	P		R							R													R													R						
N19-N17	4R-CC	193.38	R	M		R										R										R													R						
N16-N21	5R-CC	200.44	R	M																															R										
	6R-CC	208.67	R	M	R						R		R			R		R			R								R					R							R			
	7R-CC	219.91	B																																										
N18-N17	8R-CC	226.59	B																																										
	9R-CC	236.61	B																																										
	10R-CC	247.56	B																																										
	11R-CC	258.03	T	M															R																										
	12R-CC	268.08	R	M									R						R																R										
	13R-CC	275.21	R	P								R	R													R																			
	14R-CC	285.19	B																																										
	15R-CC	290.39	B																																										
	16R-CC	304.88	T	M														R																											
N18-N16	17R-CC	314.18	B																																										
	18R-CC	321.3	B																																										
	19R-CC	333.82	B																																										
	20R-CC	344.47	R	M									R																						T										
	21R-CC	351.65	T	P								T						R																											
	22R-CC	361.72	B																																										
	23R-CC	370.49	B																																										
	24R-CC	381.32	B																																										
	25R-CC	388.22	R	P																									R																
	170-1041C-																																													
N10	1R-CC	397.61	B																																										
	2R-CC	407.51	B																																										
	3R-CC	415.54	R	P	R				R			R																R																R

Notes: Abbreviations for abundances are as follows: A = abundant, C = common, F = few, R = rare, T = trace, and B = barren. Abbreviations for preservation are as follows: M = moderate, and P = poor. For more specific definitions refer to the "Explanatory Notes" chapter (this volume).

This table also appears on the volume CD-ROM.

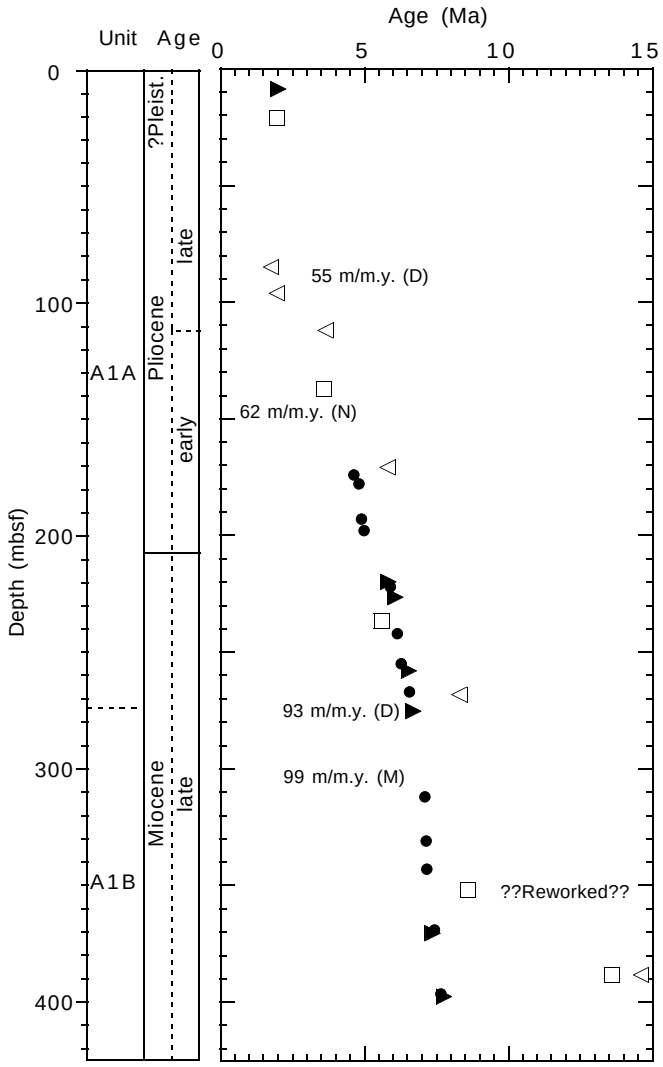

Figure 11. Age-depth relationship of key biostratigraphic datums from the composite section of Holes 1041A, 1041B, and 1041C. Calcareous nannofossils are represented by open boxes, diatoms by solid triangles, and planktonic foraminifers by open triangles. Linear rates are approximated for each major biostratigraphic segment (biostrat) of the of the age-depth curve. Paleomagnetic datums are plotted as solid circles for comparison with the biostratigraphic datums. Paleomagnetic linear age-depth rates are also approximated for each major paleomagnetic interval. D = diatoms, N = nannofossils, and M = magnetostratigraphy.

rates for Site 1041 can also be estimated. From 174 to 222 mbsf, the rate is 38 m/m.y., and from 222 to 396.5 mbsf, the rate is 99 m/m.y. Early middle Miocene nannofossil and planktonic foraminifer taxa occur in Sample 170-1041B-25R-CC (388.22 mbsf) but are most likely reworked.

GEOCHEMISTRY

The main geochemical scientific objectives at this site, located ~14 km arcward of the trench, are

1. To characterize the fluid stratigraphy and flow distribution within the slope-apron sediments, as well as in the rocks or prism sediments beneath the high-amplitude reflection at its base, and to determine the origin(s) of the fluid(s);
2. To relate the fluid chemistry and flow at this site to those associated with the wedge at and above the décollement zone at Site 1040;
3. To determine the chemistry, and thus the sources of the apron and prism sediments, and compare them with the hemipelagic sediments at Site 1039; and
4. To establish the distribution, nature, and geochemistry of gas hydrates to deduce their mode of formation and origin.

Below the very thin sulfate reduction zone of about 15 m, methane concentrations are high throughout the section drilled, which, based on the in situ temperature and pressure regime, lies within the stability zone of methane and the other important natural hydrocarbon gas hydrates (Sloan, 1990). Therefore, the occurrence of mostly methane hydrate was anticipated and indeed encountered, as it was at Deep Sea Drilling Project Site 565, located about 3 km from this site (Kvenvolden and McDonald, 1985). At this site, gas hydrate is mostly concentrated between about 120 and 280 mbsf, the zone of highest TOC content of 1–2.5 wt%. Its primary mode of occurrence is disseminated, with very thin sheets of gas hydrate filling microfractures, as indicated by the almost constant salinity and chlorinity in this depth interval. The gas hydrates analyzed within this interval also contain small amounts of the higher hydrocarbons ethane (C_2) and propane (C_3). The volumetric ratio of gas, mostly methane, to water ranged from 120 to 140. Just beneath the lithologic transition from Subunit A1A to A1B (see "Lithostratigraphy and Structures" section, this chapter), between ~280 and 320 mbsf, the concentrations of volatile hydrocarbons, especially propane, are highest and decrease below it. Across this boundary the concentration depth profiles of several inorganic chemical components, particularly Cl, Ca, Si, phosphate, Na/Cl, and Mg/Ca, also show sharp transitions to lower or higher values, suggesting a two-tier hydrologic system having different fluid sources. At this depth, porosity also decreases abruptly by 15%–20%, and bulk density values increase from ~1.6 to >1.8 g/cm^3 (see "Physical Properties" section, this chapter). A corresponding transition zone exists at Site 1040 at ~180 mbsf, which is ~100 m shallower burial depth.

Other important characteristics of the inorganic chemical data are that the entire sediment section drilled below 1.5 mbsf has Cl concentrations and salinities that are lower than seawater. Salinities decrease steadily downhole to the depth of the main gas hydrate zone (120–280 mbsf) and are rather constant within it. They are lower at about 280–340 mbsf, and slightly higher below ~340 mbsf. The source of the low-Cl and high-Ca concentration fluid in the lower apron sediments is located at >3–4 km depth, as discussed in the "Site 1040" chapter (this volume). Clay mineral dehydration is the most likely fluid-rock reaction responsible for freshening this fluid at the source region. The source of the low-Cl fluid in the upper apron sediments is yet undetermined. Gas hydrate dissociation alone cannot explain the other chemical characteristics of this fluid; for example, the elevated Na in the higher than seawater Na/Cl values must have another source. The in situ temperatures are, however, too low for hydrous mineral dehydration reactions to occur. Testing for the possibility of meteoric water influence requires shore-based analyses.

The detrital components of the apron sediments consist primarily of mixtures of terrigenous/volcaniclastic clays with arc-derived siliceous volcanic ash. The mixtures are more variable than those seen in the homogeneous wedge sediments at Site 1040. Consequently, the chemistry of the apron bulk sediments show a considerable and larger range of variations.

Carbonate formation of both calcite and dolomite is pervasive throughout the apron sediments. The total inorganic carbonate content is, however, not high, ranging between 0.5 and 6.3 wt%. Accumulation rates are not available yet.

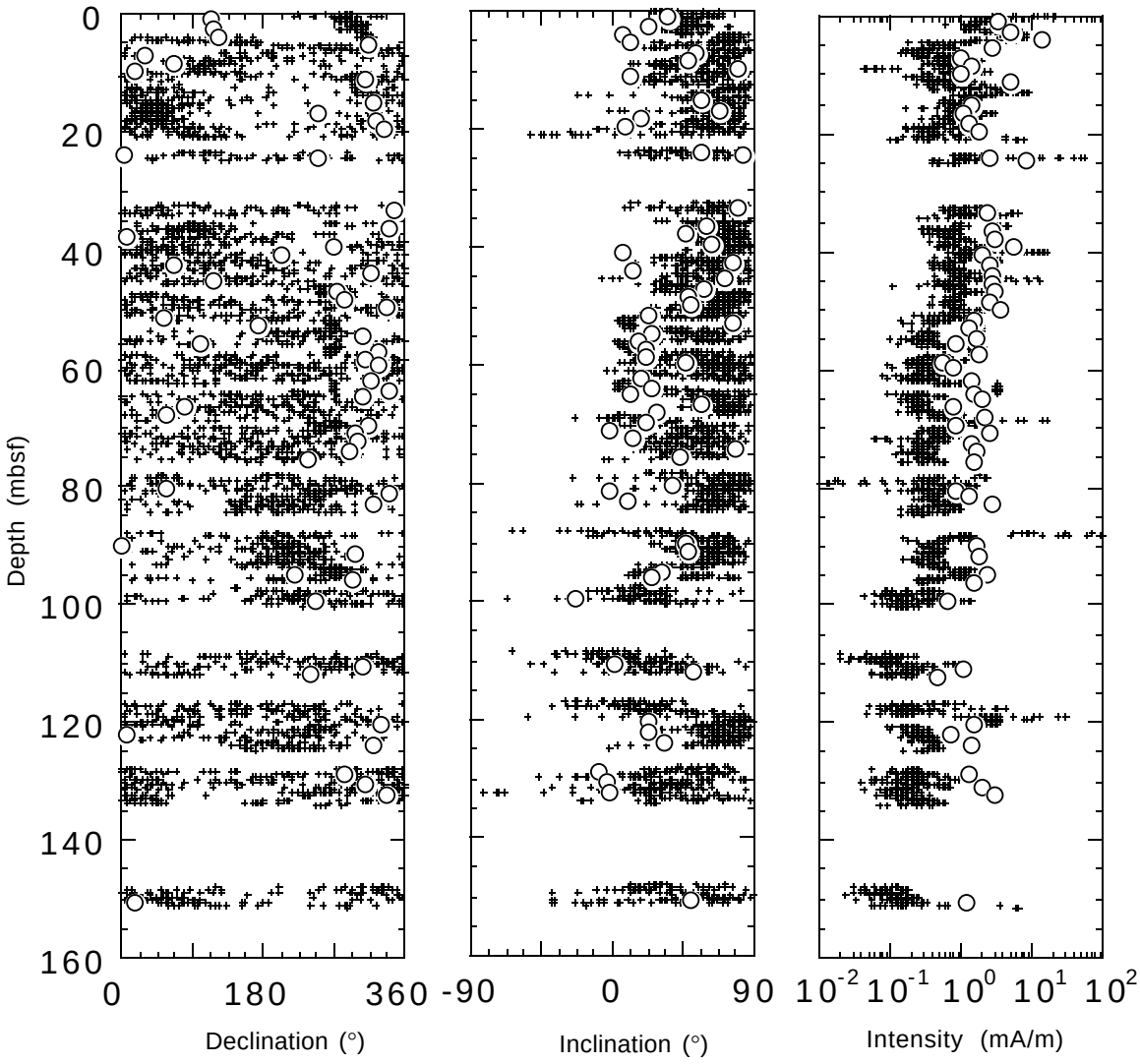

Figure 12. Paleomagnetic results from the remagnetized interval of Site 1041, showing declination, inclination, and intensity of remanence after 20-mT demagnetization of split cores from Hole 1041A. 0–160 mbsf = crosses; discrete samples = circles.

Gas Results

Volatile Hydrocarbons

Volatile hydrocarbon test results are reported in Table 14. Methane concentrations measured by the headspace technique range between 3 and 343,465 ppmv. The C_1 concentration increases sharply from 19 ppmv at 6.03 mbsf to 230,345 ppmv at 71.6 mbsf (Fig. 16A). Between 98.9 and 303.5 mbsf, continuously increasing methane contents (from 3,950 to 343,465 ppmv) were observed. Below 303.5 mbsf, methane concentration decreases irregularly to a minimum of 10,474 ppmv at 414.2 mbsf. Ethane and propane were also detected. The distribution of ethane and propane are reported in Table 14. Ethane concentrations show a first maximum at 71.6 mbsf (69 ppmv). Below this depth, significant peaks in headspace ethane were found (Fig. 16B) in the sediments cemented by gas hydrates at 234.9 mbsf (264 ppmv; see "Lithostratigraphy and Structures" section, this chapter), at 283.2 mbsf (267 ppmv), and at 358.7 mbsf (307 ppmv). Propane was absent or was detected in minor quantities at Hole 1041A (Table 14; Fig. 16C). The highest propane concentrations, which ranged from 8 to 14 ppmv, were found in an interval between 189.8 and 312.2 mbsf.

The C_1/C_2 profile for headspace gases in Holes 1041A and 1041B is shown in Figure 16D. With the exception of the two uppermost samples (6.03 and 11.93 mbsf), methane/ethane values above 205 mbsf are >2000. The ratios calculated for the samples below 205 mbsf vary between 1739 at 222.33 mbsf and 409 at 404.7 mbsf (Section 170-1041C-2R-2).

Molecular Composition of Hydrate Gas and Expansion Void Gas

The first vacutainer sample was taken at a depth of 54.3 mbsf (Section 170-1041A-8X-3). Dissociated gas of solid (visible) gas hydrates was analyzed in nine samples (between 119 and 259 mbsf). The results are displayed in Table 15. The gases were found to contain hydrocarbons in the methane (C_1) to propane (C_3) range. Only two samples (at 233.3 and 254.8 mbsf, respectively) showed traces of detectable butane (C_4). Methane and ethane concentrations released from gas hydrates show similar values to those measured in gas voids for equivalent depth intervals (Table 15). The propane concentrations in gases dissociated from gas hydrates are lower than those in the free gas samples (Fig. 17A). Hydrocarbon profiles (C_1–C_3) at Site 1041 generally show the same vertical trends as the headspace gases. The

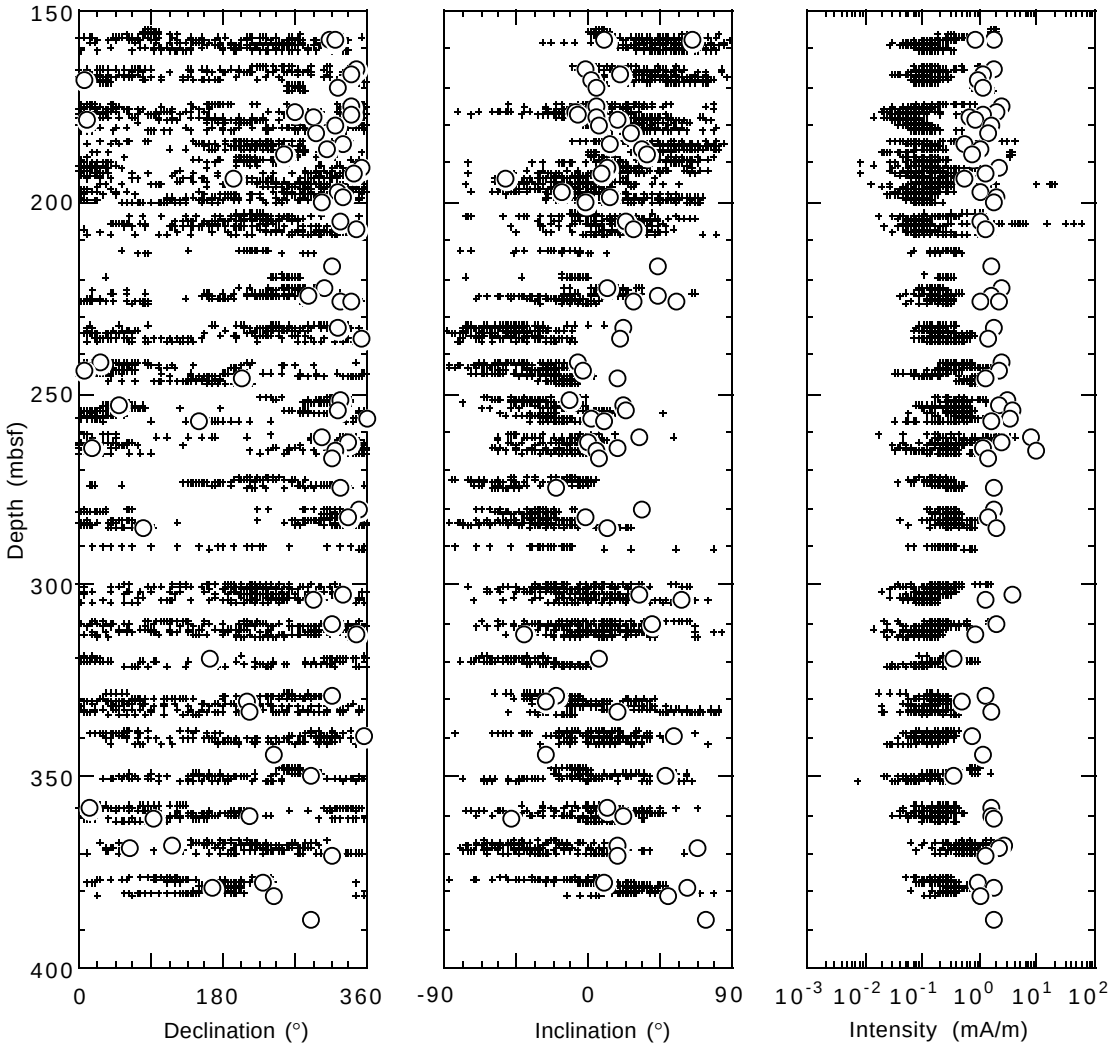

Figure 13. Paleomagnetic results from the mixed-polarity interval of Site 1041, showing declination, inclination, and intensity of remanence after 20-mT demagnetization of split cores from Hole 1041B. 150–400 mbsf = crosses; discrete samples = circles.

methane/ethane profile also displays the same pattern as the equivalent headspace profile (Figs. 16D, 17B).

Pore-Water Results

Chloride and Salinity

It would not be surprising to encounter slightly dilute pore fluids already at >50–60 mbsf because (1) the whole section drilled at this site lies within the stability field of hydrocarbon gas hydrates; (2) dissolved sulfate is being completely consumed within the uppermost ~15 m, allowing methane to rise to high concentrations at this shallow depth; and (3) the coring system used does not prevent methane hydrate from dissociating. The presence of gas hydrate was visibly detectable in all cores between ~120 and 280 mbsf, the depth interval of approximately constant chlorinity (360–370 mM, equivalent to 36%–34% seawater Cl dilution) and salinity (20–22; Fig. 18). In most of the cores, the gas hydrate was disseminated in the sediment with occasional very thin sheets of pure gas hydrate filling microfractures. The only massive nodular, primarily methane, hydrate was encountered in interval 170-1041A-15X-4, 28–43 cm, at 122 mbsf. At 235 and 256 mbsf, intervals 170-1041B-9R-2, 99–134 cm, and 11R-3, 99–134 cm, volcanic ash was completely cemented by gas hydrate. The above-mentioned nodular gas hydrate sample is conspicuous in the Cl and salinity profiles of Figure 18 as the small Cl and salinity minima at ~122 mbsf. A piece of the ash that was cemented by gas hydrate was squeezed, and the Cl concentration and salinity are shown in the same figure by the large horizontal arrows, and the corresponding actual values are given in the brackets. The lowest Cl (302–331 mM, equivalent to 46%–41% seawater Cl dilution) and salinity (15.5–17) values at 300–330 mbsf were not associated with unusual gas hydrate concentrations.

The above salinity, Cl, and gas hydrate observations, together with the fact that even in the uppermost 15 mbsf within the sulfate reduction zone, Cl concentrations and salinity are below the bottom-water Cl concentration and salinity, (the vertical arrows in Fig. 18), suggest either that the overall Cl and salinity depth profiles are largely representative of the in situ concentrations and salinities and are only slightly modified by gas hydrate dissociation, or that they are controlled by considerably more gas hydrate dissociation than indicated by what was actually observed. The apron section cored is thus permeated by either one or two low-Cl and low-salinity fluids, separated by a conduit situated at the lowest Cl and salinity zone at 290–330 mbsf. The division of the apron into two distinct parts is even more pronounced in several of the other chemical depth profiles, as for example in the Na/Cl profile in Figure 19. The source of the shallower low-Cl fluid is as yet unknown, and meteoric water may be in-

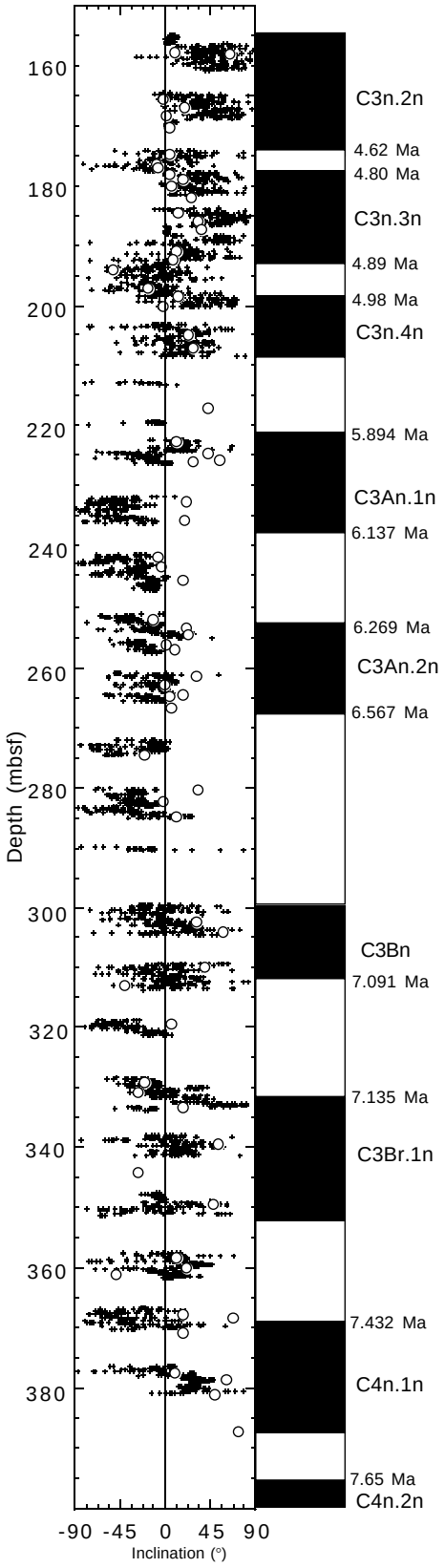

Figure 14. Remanence inclinations and the interpreted magnetostratigraphy from the mixed polarity interval of Site 1041, with the normal polarity chrons shown on the right.

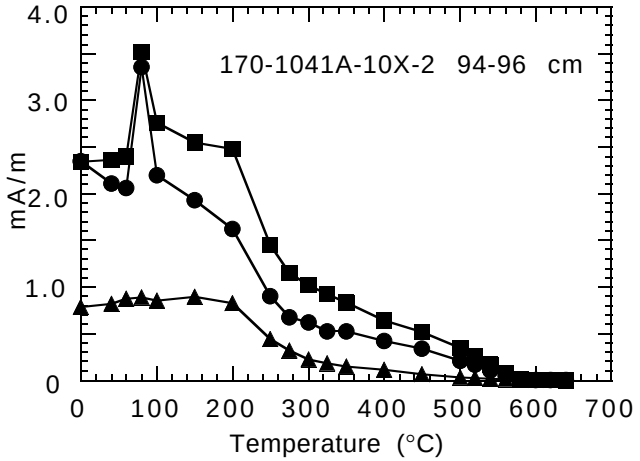

Figure 15. Results of mIRM experiments on remagnetized sediments. Circles = 0.05-T component; squares = 0.4-T component; triangles = 1.0-T component. Loss of remanence, particularly in the 1.0-T component, between 200° and 300°C indicate the presence of magnetic Fe-sulfides (either greigite or pyrrhotite).

volved. Clearly, the in situ temperatures are too low for mineral dehydration reactions to occur, which can therefore be excluded as a potential source. Shore-based isotopic analyses are needed to distinguish between gas hydrate dissociation and meteoric water as the possible freshwater source. The source of the second low-Cl conduit below the ~300 mbsf fluid is at >3–4 km depth, as discussed below.

Sodium and Potassium.

Except for the minimum ratio of 0.82 at ~12 mbsf (Fig. 19A), which is associated with the maximum intensity of carbonate diagenesis as discussed in the "Site 1040" chapter (this volume), the Na/Cl values at Site 1041 increase with depth and reach the penultimate maximum ratios of 0.89–0.90 at the 280–300 mbsf conduit situated between the upper and lower apron hydrologic regimes. Below the conduit, the ratios decrease with depth (Fig. 19A; Table 16). The lowest Na/Cl value encountered is 0.74, at >400 mbsf, and the highest is 0.92 at 235 mbsf, whereas the seawater ratio is 0.85. Above the conduit, the increase with depth in both Na concentrations and Na/Cl is caused by clay-mineral ion exchange with ammonium, which reaches extremely high concentrations of over 9 mM, and/or by mixing with a low-Cl/high-Na fluid. Below the conduit the decrease of Na/Cl with depth is most likely a result of zeolitization and albitization reactions at the source region of the deep-seated fluid.

The K concentration depth profile is not discussed in detail, because the data shown in Figure 19B are of mixed quality. The uppermost 150 m that were analyzed by atomic emission (AE), the preferred method (see "Explanatory Notes" chapter, this volume), show concentrations above seawater between 0 and 100 mbsf, which is caused by clay ion exchange with ammonium. Below this depth, because of instrumental problems, the data shown were determined by ion chromatography. The higher K concentrations below ~340 mbsf had to be corrected from AE data, as described in the "Explanatory Notes" chapter (this volume). The K concentrations will therefore be reanalyzed.

Sulfate, Alkalinity, Ammonium, and Phosphate

Dissolved sulfate is being consumed rapidly within the uppermost 15 m of the apron sediments (Fig. 20A), and below this depth the apron sediments are anaerobic. Consequently, the alkalinity and methane concentrations rise rapidly (Figs. 20B, 16A, respectively) to

Table 13. Depths of biostratigraphic and magnetostratigraphic datums observed in Site 1041 cores.

Core	Depth (mbsf)	Diatoms (Ma)	Nannofossils datums (Ma)	Foraminifers datums (Ma)	Paleomagnetic datums (Ma)	Combined biostratigraphic datums (Ma)	Combined biostrat. and paleomag. datums (Ma)
170-1041A-							
1H	0.00						
1H	1.50						
1H	7.35						
2H	8.85	2.01				2.01	2.010
2H	14.03						
3X	21.12		1.95			1.95	1.950
4X	24.92						
5X	34.21						
6X	41.23						
7X	50.70						
8X	60.46						
9X	69.22						
10X	76.23						
11X	84.99			1.77		1.77	1.770
12X	96.19			1.95		1.95	1.950
13X	100.78						
14X	112.18			3.65		3.65	3.650
15X	125.09						
16X	134.25						
17X	137.48		3.60			3.60	3.600
18X	151.48						
170-1041B-							
1R	161.05						
2R	170.76			5.80		5.80	5.800
2R	174.00				4.620		
2R	178.00				4.800		
3R	181.59						
3R	193.00				4.890		4.890
4R	193.38						
4R	198.00				4.980		4.980
5R	200.44						
6R	208.67						
7R	219.91	5.83				5.83	5.830
7R	222.00				5.894		5.894
8R	226.59	6.07				6.07	6.070
8R	236.61						
9R	236.61		5.60			5.60	5.600
9R	242.00				6.137		6.137
10R	247.56						
10R	255.00				6.269		6.269
11R	258.03	6.55				6.55	6.550
11R	267.00				6.567		6.567
11R	268.08					8.30	8.300
12R	268.08			8.30		8.60	
13R	275.21	6.69				6.90	6.900
14R	285.19						
15R	290.39						
16R	304.88						
16R	312.00				7.090		7.090
17R	314.18						
18R	321.30						
18R	331.00				7.135		7.135
19R	333.82						
19R	343.00				7.172		7.172
20R	344.47						
21R	351.65		8.60				8.600
22R	361.72						
22R	369.00				7.432		
23R	370.49	7.37				7.37	7.370
24R	381.32						
24R	388.22					13.60	13.600
25R	388.22		13.60	14.60		14.60	14.600
170-1041C-							
1R	396.50				7.650		7.650
1R	397.61	7.75				7.75	7.750
2R	407.51						
3R	415.54						

This table also appears on the volume CD-ROM.

levels favorable for diagenetic carbonate and methane hydrate formations. As a result of carbonate diagenesis, alkalinity values decrease with depth. The minimum alkalinity spike at ~235 mbsf represents the ash sample cemented by gas hydrate.

Ammonium concentrations increase with depth (Fig. 20C), as expected in sediments with high organic carbon contents, especially at elevated sedimentation rates. The concentrations reach ~9 mM. The steady increase in concentration within the gas hydrate zone, where dilution caused by gas hydrate dissociation occurs, suggests production rates that exceed the dilution caused by hydrate dissociation during recovery. At such high ammonium and alkalinity concentrations, ammonium carbonate may precipitate. Equilibrium calculations are needed to verify this possibility. The deep-seated fluid seems to be enriched in ammonium as well.

Table 14. Molecular composition of headspace gases.

Core, section, interval (cm)	Depth (mbsf)	C_1 (ppmv)	C_2 (ppmv)	C_3 (ppmv)	C_1/C_2
170-1041A-					
1H-5, 0-5	6.03	19	1	1	19
2H-4, 0-5	11.93	35	1	0	35
3X-3, 0-5	17.33	3,549	1	1	3,549
4X-1, 0-5	23.43	294	0	0	ND
5X-1, 0-5	32.43	3	0	0	ND
6X-2, 0-5	36.93	1,456	0	0	ND
7X-5, 0-5	47.53	1,939	0	0	ND
8X-5, 0-5	56.63	56,310	7	0	8,044
9X-5, 0-5	65.63	1,033	0	0	ND
10X-5, 0-5	71.63	230,345	69	1	3,338
11X-3, 0-5	81.23	82,119	23	0	3,570
12X-3, 0-5	90.23	64,484	17	0	3,793
13X-1, 145-150	98.98	3,950	1	0	3,950
14X-2, 0-5	108.63	7,368	1	0	7,368
15X-5, 0-5	122.73	20,593	2	0	10,297
16X-4, 0-5	129.43	5,107	0	0	ND
17X-1, 145-150	137.38	18,141	3	2	6,047
18X-3, 0-5	148.53	23,959	6	3	3,993
170-1041B-					
1R-3, 0-5	158.03	8,269	2		4,135
2R-2, 145-150	167.58	39,805	5	3	7,961
3R-5, 0-5	180.23	49,632	8	5	6,204
4R-5, 0-5	189.83	111,891	46	8	2,432
5R-2, 115-120	196.18	73,878	18	8	4,104
6R-2, 0-5	204.63	26,218	12	5	2,185
7R-5, 0-5	218.73	59,793	60	2	997
8R-1, 0-5	222.33	93,904	54	5	1,739
9R-3, 0-5	234.93	221,442	264	1	839
10R-3, 0-5	244.63	60,434	58	13	1,042
11R-3, 0-5	254.23	144,307	137	8	1,053
12R-2, 0-5	262.43	119,560	143	6	836
13R-2, 0-5	272.03	80,187	61	6	1,315
14R-2, 0-5	283.23	261,578	267	13	980
16R-3, 0-5	303.53	343,465	235	14	1,462
17R-3, 0-5	312.23	164,334	117	9	1,405
18R-1, 145-150	320.28	73,741	102	5	723
19R-3, 0-5	331.43	18,389	23	0	800
20R-4, 0-5	343.98	75,976	145	2	524
21R-2, 0-5	349.16	78,465	129	2	608
22R-2, 0-5	358.73	246,436	307	5	803
23R-2, 0-5	368.35	60,765	69	4	881
24R-2, 0-5	377.93	97,892	100	4	979
170-1041C-					
1R-1, 145-150	395	71,080	83	5	856
2R-2, 0-5	404.7	26,398	65	5	406
3R-2, 0-5	414.2	10,474	21	1	499

Notes: C_1, C_2, and C_3 represent methane, ethane, and propane, respectively. ppmv = parts per million by volume. ND = not determined.

This table also appears on the volume CD-ROM.

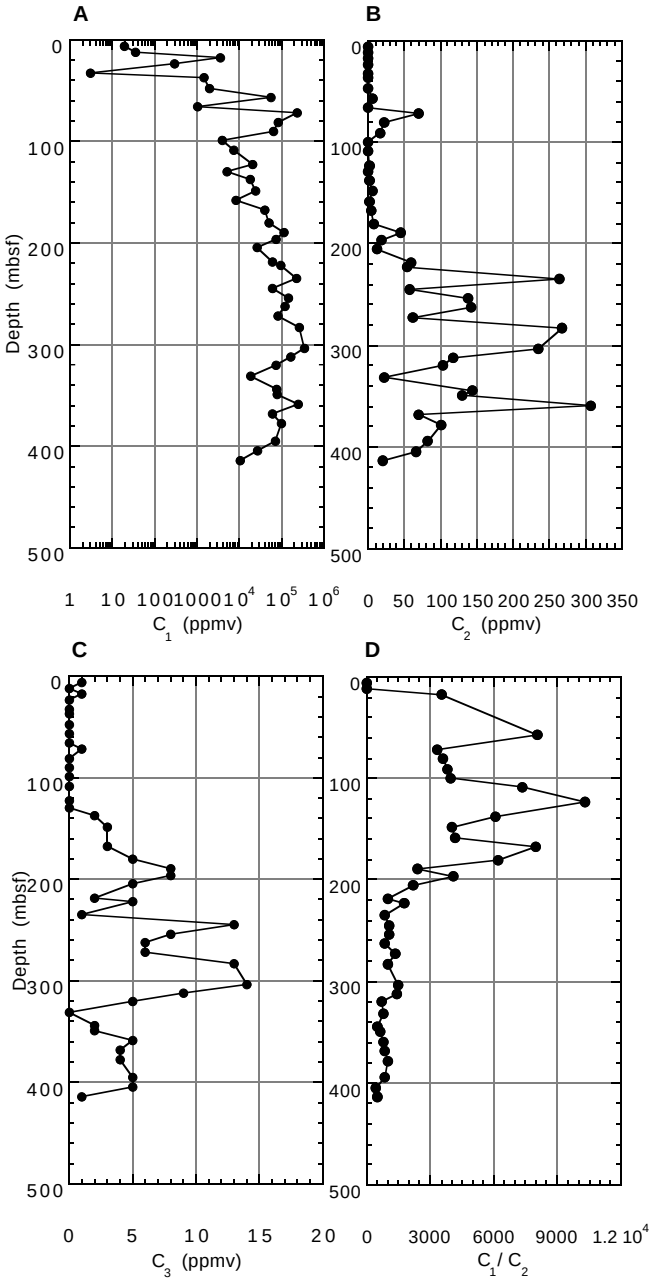

Figure 16. Results of headspace gas analyses for (**A**) methane, (**B**) ethane, (**C**) propane, and (**D**) C_1/C_2 values vs. depth. ppmv = parts per million by volume.

Phosphate concentrations peak at about the depth of maximum alkalinity and decrease with depth as alkalinity does (Fig. 20D). The maximum concentration of phosphate of 81 µM is low for such an organic matter–rich system, especially relative to the very high alkalinity and ammonium concentrations, suggesting mixed terrestrial and marine organic matter inputs. The deep-seated fluid does not contain detectable dissolved phosphate.

Calcium, Magnesium, and Silica

The two-tier hydrologic regime in the apron sediments is seen clearly in the Ca concentrations and Mg/Ca depth distribution, but not in the Mg concentrations that have been greatly depleted in the uppermost 200 m of the apron (Fig. 21). Dissolved Ca concentrations decrease rapidly from 10.5 to 4.5 mM by carbonate precipitation close to the sediment/water interface, where sulfate reduction and alkalinity production are intense. Mg is also being depleted at this depth interval, but at a lower rate; therefore the Mg/Ca values increase to a maximum of about 8. At high alkalinity, high Mg/Ca, and low sulfate concentration, dolomite formation is kinetically enhanced. Below about 20 mbsf, Ca concentrations remain almost constant, whereas Mg concentrations decrease, most likely through dolomitization. Below the conduit at ~300 mbsf, Ca concentrations increase steeply at a gradient of almost 0.3 mM/m, reducing the Mg/Ca value of the fluid to <1; dolomitization is no longer possible at the prevailing temperature. Thus the carbonate system has returned into the calcite stability field. The deep-seated fluid is highly enriched in Ca and depleted in Mg, similar to hydrothermal solutions.

In the shallower apron hydrologic regime, dissolved Si rapidly reaches a steady-state concentration of 750 ±100 µM, a concentration considerably lower than the solubility of opal-A at the pressures and temperatures at this site. This low concentration suggests that diatoms do not play an important role in controlling Si concentrations and that reactions between the fluid and Si-rich silicates control it in-

Table 15. Molecular composition of vacutainer gas analyses, including gas hydrates.

Core, section, interval (cm)	Depth (mbsf)	C_1 (ppmv)	C_2 (ppmv)	C_3 (ppmv)	C_1/C_2
170-1041A-					
8X-3, 71-72	54.31	954,832	95	12	10,051
9X-3, 102-103	63.63	964,568	98	12	9,843
10X-5, 24-25	75.63	959,692	97	12	9,894
11X-2, 100-101	82.23	916,118	268	4	3,418
15X-3, 27-30*	119.99	843,556	177	2	4,766
16X-4, 0-10*	130.95	881,380	179	2	4,924
18X-4, 80-81	150.80	987,650	123	21	8,030
170-1041B-					
1R-4, 50-51*	160.00	988,136	260	9	3,801
2R-2, 0-10	164.65	815,697	270	3	3,021
4R-5, 0-5*	189.83	991,000	427	4	2,321
5R-2, 95-120*	196.08	918,366	416	4	2,208
6R-3, 145-150*	207.58	922,264	533	4	1,730
7R-5, 0-5	218.71	981,535	732	11	1,341
7R-4, 145-150*	218.65	820,619	524	4	1,566
8R-3, 72-73	226.03	982,739	614	19	1,601
9R-1, 138-139	233.29	983,675	954	7	1,031
9R-2, 99-134*	234.50	933,827	941	5	992
10R-3, 130-131	245.91	982,903	981	15	1,002
11R-3, 66-67	254.87	977,845	785	23	1,246
11R-5, 128-150*	258.48	927,917	1,205	5	770
12R-2, 120-121	263.61	988,830	1,214	12	815
13R-2, 75-76	272.76	985,332	888	25	1,110
14R-3, 95-96	284.16	961,420	830	28	1,158
16R-3, 66-67	303.17	985,102	734	26	1,342
17R-1, 59-60	312.80	957,209	542	29	1,766
18R-1, 146-147	320.27	946,610	1,014	18	934
19R-1, 145-146	329.86	980,157	852	17	1,150
20R-4, 10-11	342.61	982,154	1,340	11	733
21R-2, 36-37	349.47	980,527	1,189	11	825
22R-3, 9-10	360.3	981,915	1,045	10	940
23R-2, 143-144	369.74	687,526	550	7	1,250
24R-3, 20-21	379.61	953,143	681	9	1,400

Notes: C_1 = methane, C_2 = ethane, C_3 = propane, and C_1/C_2 = methane/ethane ratio. ppmv = parts per million by volume. * = gas hydrates present in this interval.

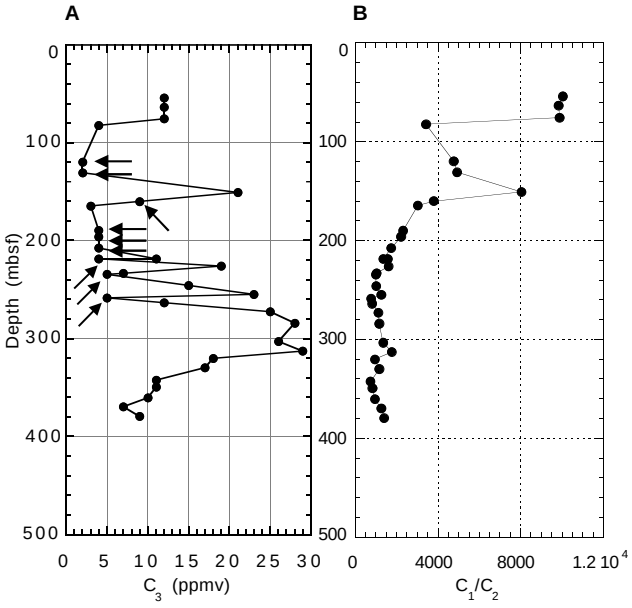

Figure 17. (**A**) Propane distribution (**B**) and C_1/C_2 values in vacutainer samples. Arrows = gas hydrates.

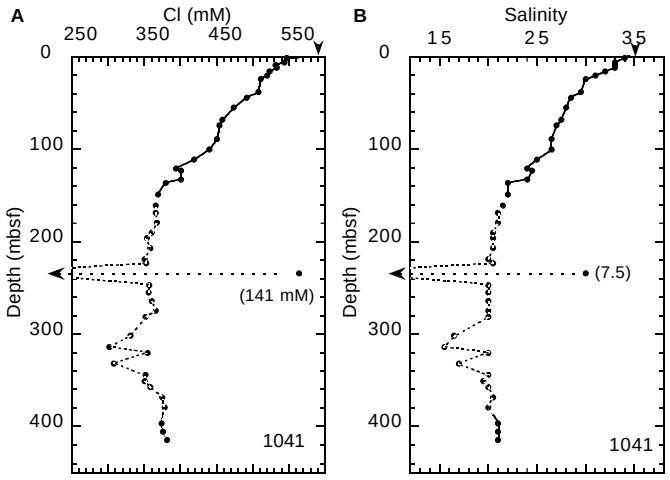

Figure 18. Concentration depth profiles of (**A**) Cl and (**B**) salinity. Vertical arrows = seawater concentration. Hole 1041A = solid line; Hole 1041B = dashed line. Horizontal arrows indicate values lower than the lowest value on the x-axis (actual values given in parentheses).

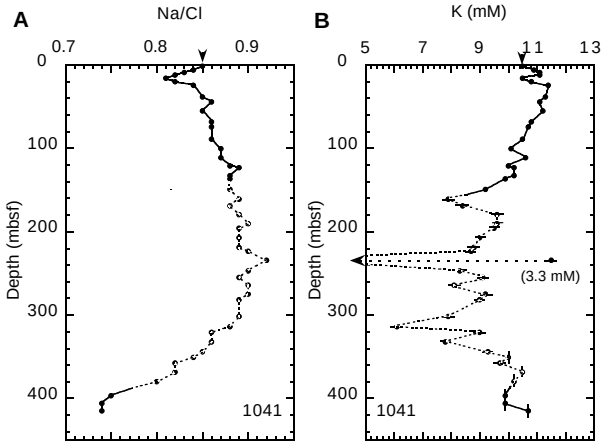

Figure 19. Depth profiles of (**A**) Na/Cl and (**B**) K concentration. Vertical arrows = seawater concentration. Horizontal arrow in (B) delineates the location of the volcanic ash cemented by methane hydrate. Hole 101A = solid line; Hole 1041B = dashed line.

stead. If present, diatoms could not survive for long in this environment. The most interesting aspect of the dissolved Si concentration profile in Figure 21D is the discontinuity in the profile at about 300 mbsf. The deep-seated fluid is characterized by a lower Si concentration, suggesting equilibration with either a lower solubility silica polymorph or with less siliceous rocks.

Sediment and Igneous Rock Results

Inorganic Carbon, Organic Carbon, and Total Sulfur

The results of inorganic carbon, organic carbon, calcium carbonate, nitrogen, and sulfur measurements in the sediments of Site 1041 are displayed in Table 17 and Figure 22. Sediments were generally analyzed at a frequency of two to three samples per core.

The weight percentage of calcium carbonate ($CaCO_3$) was calculated from the inorganic carbon concentrations, assuming that all of the carbonates are present as calcite. In Hole 1041A (0–132.4 mbsf), the $CaCO_3$ content is generally low. Concentrations range from 0.5 to 6.3 wt% (average = 2.1 wt%). Below a depth of 150 mbsf (Hole

Table 16. Pore-fluid chemical data for major and minor constituents, Site 1041.

Core, section, interval (cm)	Depth (mbsf)	Volume (cm^3)	pH	Alkalinity (mM)	Salinity	Cl (mM)	SO_4 (mM)	Mg (mM)	Ca (mM)	K (mM)	Na (mM)	Si (µM)	NH_4 (µM)	PO_4 (µM)	Na/Cl	Mg/Ca
170-1041A-																
WSTP		10	ND	ND	35.00	558	27.6	53.62	10.53	10.11	475	134	12	ND	0.85	5.09
1H-1, 145-150	1.45	50	7.88	5.34	34.00	547	22.5	50.0	9.4	10.5	463	585	264	11.4	0.85	5.33
1H-4, 140-150	5.9	36	8.09	13.23	33.00	544	14.9	44.92	6.9	10.9	459	684	1128	46.2	0.84	6.48
2H-1, 135-150	8.75	50	8.26	21.06	33.00	532	9.9	42.91	6.8	11.07	441	880	1800	54.9	0.83	6.28
2H-3, 135-150	11.75	50	8.35	24.55	33.00	533	7.6	42.46	6.6	11.09	439	1096	2052	80.9	0.82	6.47
3X-1, 135-150	15.75	39	8.30	31.32	32.00	523	0.0	39.14	5.2	10.48	424	898	2682	71.0	0.81	7.48
3X-4, 135-150	20.15	48	8.04	28.31	31.00	520	0.0	36.0	4.5	10.84	428	884	3276	59.9	0.82	8.09
4X-1, 99-105	24.39	12	ND	ND	30.00	511	0.0	30.49	4.5	11.37	430	713	4002	33.8	0.84	6.85
6X-2, 135-150	38.25	18	8.01	ND	29.50	508	0.0	27.49	4.7	11.27	432	715	4620	53.6	0.85	5.87
7X-2, 130-150	44.30	44	7.97	24.33	28.50	492	0.0	25.34	4.8	11.1	421	718	5142	36.2	0.86	5.30
8X-3, 130-150	54.90	40	7.90	27.49	28.00	474	0.0	24.11	5.0	11.24	405	772	5352	32.5	0.85	4.87
9X-6, 125-150	68.35	44	7.89	28.74	27.50	458	0.0	23.06	4.2	10.8	393	802	5232	44.9	0.86	5.48
10X-4, 125-150	74.35	44	7.82	28.58	27.00	454	0.0	22.51	4.9	10.7	389	876	5400	46.2	0.86	4.64
11X-3, 125-150	89.15	40	7.80	26.82	26.50	451	0.0	19.29	4.4	10.11	390	789	5976	35.0	0.87	4.09
14X-3, 120-150	111.15	28	7.94	28.24	25.00	419	0.0	17.51	4.2	10.63	365	783	6528	30.0	0.87	4.21
15X-4, 28-43	120.87	6	ND	ND	24.00	394	0.0	16.21	1.5	10.0	348	657	6450	18.8	0.88	10.53
15X-6, 58-78	123.10	11	8.03	25.89	24.50	401	0.0	15.58	2.3	10.21	355	619	6432	12.7	0.89	6.69
16X-6, 52-82	132.58	32	7.94	25.39	24.00	401	0.0	16.48	3.0	10.16	352	755	6542	23.8	0.88	5.57
17X-1, 73-88	136.63	13	7.96	ND	22.00	380	0.0	14.54	3.5	9.9	334	715	6414	20.1	0.88	4.20
18X-3, 125-150	149.27	30	7.98	22.74	22.00	369	0.0	13.85	3.3	9.2	325	667	6072	23.8	0.88	4.16
170-1041B-																
1R-5, 0-27	160.8	5	ND	ND	21.50	366	0.0	13.33	3.3	7.9*	325	702	ND	ND	0.89	4.06
2R-4, 31-66	168.91	40	7.95	22.19	21.00	366	0.0	14.1	4.0	8.4*	322	677	5418	21.0	0.88	3.50
3R-5, 115-150	179.17	26	7.99	21.53	21.00	368	0.0	12.1	3.5	9.6*	327	702	6414	7.2	0.89	3.42
4R-5, 83-111	190.13	15	7.96	18.62	20.50	360	0.0	11.1	2.5	9.6*	323	666	6594	15.6	0.90	4.48
5R-2, 85-120	195.85	20	7.93	18.72	20.50	354	0.0	10.4	3.7	9.5*	316	723	6840	9.6	0.89	2.84
6R-4, 77-112	207.05	42	7.85	19.79	20.50	359	0.0	11.4	4.3	9.0*	319	873	6564	8.4	0.89	2.64
7R-6, 115-150	218.93	27	7.86	19.68	20.00	351	0.0	9.6	4.6	8.8*	314	875	7284	15.0	0.89	2.07
8R-1, 103-133	223.33	50	7.95	18.48	20.50	353	0.0	9.9	3.9	8.7*	317	850	7320	4.8	0.90	2.52
9R-2, 99-134	234.39	10	8.58	5.63	7.50	141	0.0	2.5	1.3	3.3*	130	385	ND	ND	0.92	1.95
10R-5, 0-15	246.79	35	7.79	16.30	20.00	357	0.0	10.2	4.2	8.3*	320	902	7470	4.8	0.90	2.45
11R-3, 115-150	255.05	46	7.90	14.16	20.00	356	0.6	9.9	5.4	9.1*	318	835	8178	3.6	0.89	1.83
12R-3, 114-139	264.18	40	7.76	15.86	20.00	360	0.0	10.1	3.9	8.1*	324	999	7848	2.4	0.90	2.62
13R-3, 115-150	274.65	30	7.86	13.47	20.00	366	0.0	9.7	4.4	9.2*	329	784	9042	1.2	0.90	2.21
14R-1, 115-150	281.35	30	7.90	11.74	20.00	352	0.0	9.5	4.6	9.0*	315	856	8550	0.6	0.89	2.06
16R-2, 115-150	301.35	6	ND	ND	16.50	331	0.0	7.8	6.5	7.9*	294	257	ND	ND	0.89	1.20
17R-4, 0-35	313.67	5	ND	ND	15.50	302	0.0	8.5	7.2	6.1*	265	255	5928	0.0	0.88	1.18
18R-2, 0-25	320.30	7	ND	ND	20.00	355	0.0	10.6	9.0	9.0*	307	525	ND	ND	0.86	1.18
19R-3, 110-150	331.93	6	ND	ND	17.00	308	0.0	8.2	9.9	7.8*	264	177	7140	0.0	0.86	0.83
20R-5, 110-135	344.02	14	7.84	7.56	20.00	352	0.0	10.5	12.0	9.3†	298	609	ND	ND	0.85	0.87
21R-3, 0-35	350.60	14	7.82	6.64	19.50	351	0.0	10.2	13.2	10.0*	294	628	8670	0.0	0.84	0.77
22R-1, 10-38	357.30	18	7.82	6.52	20.00	359	0.0	11.4	15.8	9.7†	295	649	8982	0.0	0.82	0.72
23R-1, 125-105	368.05	26	7.79	7.36	20.50	375	0.0	11.43	18.0	10.5†	306	654	9126	0.0	0.82	0.64
24R-3, 0-25	379.40	15	ND	ND	20.00	378	0.0	11.7	20.8	10.0†	303	614	ND	ND	0.80	0.56
170-1041C-																
1R-2, 0-25	396.50	9	ND	ND	21.00	374	0.0	12.3	28.9	9.9†	282	687	ND	ND	0.75	0.43
2R-1, 65-90	405.35	12	7.76	3.64	21.00	376	0.9	12.5	33.0	9.9†	277	495	8586	0.0	0.74	0.38
3R-1, 31-47	414.51	8	ND	ND	21.00	382	0.0	12.1	32.5	10.7†	282	329	ND	ND	0.74	0.37

Notes: ND = not determined. Data without * or † were determined by spectroscopy; data with * were determined by Ionic Chromatography (ICr), and data with † were determined by ICr and corrected from AES data (–8%).

1041B), $CaCO_3$ values are slightly elevated, ranging between 0 and 12.2 wt% (average = 4.6 wt%). The lowest carbonate concentrations at Hole 1041B occur between 219.3 and 252.7 mbsf (0.0–3.0 wt%).

TOC contents in the sediments at Site 1041 range from 0.6 to 2.5 wt%. The highest concentrations (up to 2.47 wt% TOC) occur between 190 and 252 mbsf (Fig. 22B). This interval is characterized by the frequent occurrence of visible gas hydrate flakes and gas hydrate cements (see also "Lithostratigraphy and Structures" section, this chapter).

Total sulfur (TS) concentrations at Site 1041 vary between 0.1 and 2.0 wt% (Fig. 22C). The high sulfur contents probably reflect disseminated pyrite and pyrite nodules that are present in the core (see "Lithostratigraphy and Structures" section, this chapter).

Total nitrogen (TN) generally varies systematically with the organic carbon contents at Site 1041. The TN concentrations range from 0.13 to 0.29 wt%, with an average value of 0.19 wt% (Table 17). To characterize the type of organic matter in the sediments, TOC/TN values have been used. Most of the TOC/TN values range from 6 to 9 (Table 17), which indicate a predominantly marine origin of the present organic material (Bordovskiy, 1965; Emerson and Hedges, 1988). TOC/TN values of >10 occur in the uppermost sediments of Hole 1041A (0–52.4 mbsf) and probably reflect an increased input of terrigenous organic material.

X-ray Fluorescence Analyses of the Solid Phases

Major and trace element analyses for siliciclastic sediments and volcanic ashes are reported in Tables 18 and 19. The data may be used to evaluate the provenance of the detrital particles at Site 1041 and to document the chemistry of the volcanic ashes.

Figure 23 shows the variation in SiO_2, Fe_2O_3*, TiO_2, and Ba with depth. In sediments and ashes with less than 5 wt% calcium carbonate, SiO_2 shows a large range of variation between 55 and 72 wt%. Fe_2O_3*, TiO_2, and Ba also show large variations (about 3–10 wt%, 0.4–1.2 wt%, and 200–1400 ppm, respectively). Tables 18 and 19 show that most other elements have similarly large concentration variations. No systematic chemical differences are seen in the sediments from Subunit A1A (above 278.3 mbsf) vs. those from Subunit A1B. The sample density was chosen to characterize representative lithologies; it was not dense enough to sample the interval of lower porosity and higher bulk density between about 280 and 320 mbsf.

Much of the variation seen in Figure 23 is produced by the contribution of silicic ashes (68–72 wt% SiO_2) to the sedimentary section. These crystal-vitric ashes (see "Lithostratigraphy and Structures" section, this chapter) have high Zr/Nb values (19–39), elevated Ba contents, and high Ba/Ce values (35–55) indicative of their origin in the volcanic arc. The three ashes and one ashy sediment reported in

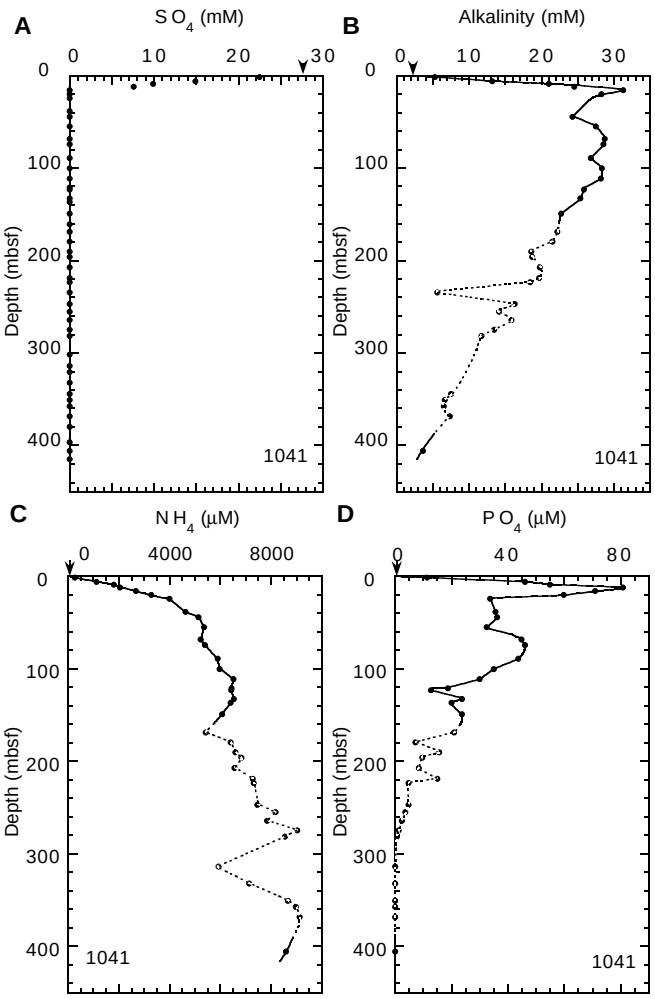

Figure 20. Concentration depth profiles of (**A**) sulfate, (**B**) alkalinity, (**C**) ammonium, and (**D**) phosphate. Arrows = seawater concentration. Hole 1041A = solid line; Hole 1041B = dashed line.

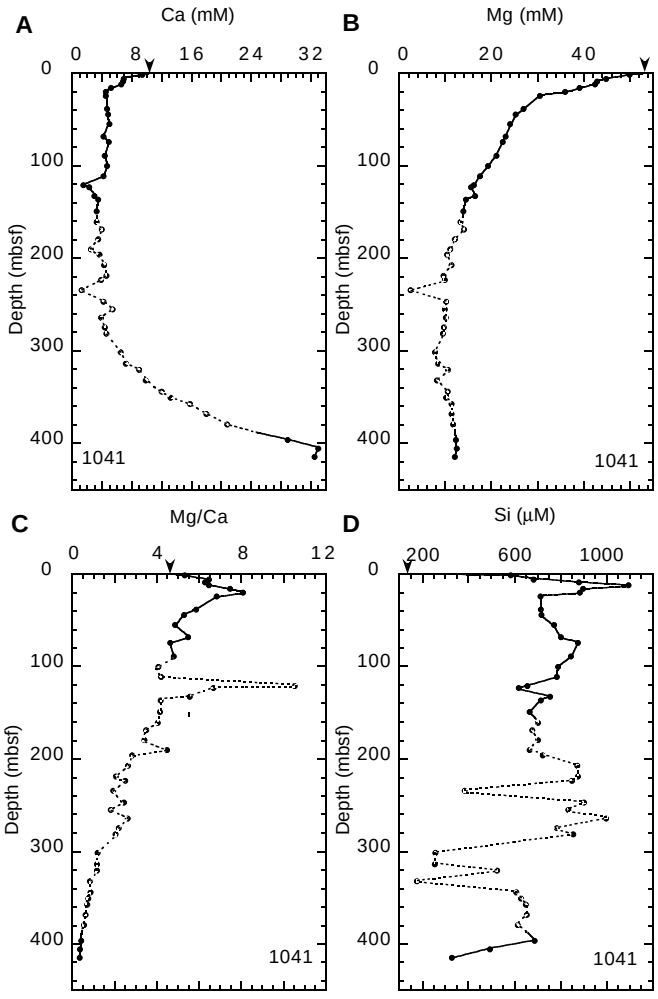

Figure 21. Concentration depth profiles of (**A**) Ca, (**B**) Mg, (**C**) Mg/Ca, and (**D**) silica. Arrows = seawater concentration. Hole 1041A = solid line; Hole 1041B = dashed line.

Tables 18 and 19 from 12.7, 13.1, 234.4, and 234.9 mbsf, respectively, all have similar compositions. The ashes are chemically very similar to the one ash sampled at Site 1040 (166.4 mbsf) and to the four ashes from above 164 mbsf at Site 1039 (see "Geochemistry" sections, "Site 1039" and "Site 1040" chapters, this volume).

The provenance of the siliciclastic sediments at Site 1041 may be seen more clearly in Figure 24. The smear slides (see "Lithostratigraphy and Structures" section, this chapter) show the sediments to be largely mixtures of clay, ash, siliceous microfossils, small amounts of carbonate, and other, very minor constituents. The concentration of Al_2O_3 in these mixtures will be determined by the clay and ash components, and diluted by the contribution of calcium carbonate and siliceous microfossils. To a first order, dividing the concentration of an element to the Al_2O_3 concentration in the sample neutralizes the effects of variable amounts of dilution and allows the chemistry of the detrital grains to be evaluated more directly. The three panels shown in Figure 24 are representative of a suite of similar mixing diagrams. In these mixing diagrams, the siliciclastic sediments from Site 1041 form an elongate array that begins within the field formed by the sedimentary wedge above the décollement at Site 1040. The data trend toward the composition of the silicic ashes, suggesting that the detrital grains within the apron at Site 1041 are a mixture of terrigenous/volcaniclastic clays that are similar to those in the wedge at Site 1040 plus siliceous volcanic ash. At Site 1041, variations in the proportion of clay and ash are clearly seen, in contrast to Site 1040 where the sediments are very homogeneous, despite the presence of both clay and ash within the wedge (see "Geochemistry" Section, "Site 1040" chapter, this volume).

PHYSICAL PROPERTIES

Density and Porosity

Physical properties measurements on extracted core specimens are considered to be reliable through most of the recovered interval despite a high level of fracturing and common drilling disturbance. Cores from the base of Hole 1041B (Cores 170-1041B-20R through 25R) and all of those from Hole 1041C (Cores 170-1041C-1R through 3R) were disturbed, and the data show considerable scatter (Fig. 1). Gamma-ray attenuation (GRA) bulk density measurements (Table 20) also show the deleterious effects of core recovery and intense drilling deformation. All values are significantly lower than those obtained from mass and volume measurements of core specimens, and are therefore not plotted in Figure 1. Some of the main trends are nevertheless defined by the high-end cut off in the GRA scatter, which indicates intervals where the cored material filled the

Table 17. Inorganic carbon, calcium carbonate, total carbon, total organic carbon, total nitrogen, total sulfur, and TOC/TN in sediments.

Core, section, interval (cm)	Depth (mbsf)	IC (wt%)	$CaCO_3$ (wt%)	TC (wt%)	TOC (wt%)	TN (wt%)	TS (wt%)	TOC/TN
170-1041A-								
1H-1, 144-145	1.44	0.74	6.2	2.71	1.97	0.18	1.09	11
1H-2, 34-35	1.84	0.76	6.3	2.57	1.81	0.19	1.35	10
1H-4, 34-35	4.84	0.06	0.5	1.39	1.33	0.15	1.28	9
2H-2, 33-34	9.23	0.12	1.0	2.00	1.88	0.20	0.73	9
2H-3, 131-132	11.71	0.06	0.5	1.28	1.22	0.15	0.75	8
2H-4, 32-33	12.22	0.12	1.0	1.65	1.53	0.17	0.60	9
3X-2, 34-35	16.14	0.10	0.8	1.66	1.56	0.16	1.33	10
3X-4, 34-35	19.14	0.23	1.9	1.38	1.15	0.15	1.41	8
3X-CC, 33-34	20.98	0.22	1.8	1.76	1.54	0.18	1.16	9
4X-CC, 32-33	24.78	0.23	1.9	1.87	1.64	0.17	0.99	10
5X-1, 111-112	33.51	0.15	1.3	1.80	1.65	0.13	1.27	13
6X-2, 130-131	38.2	0.75	6.3	2.12	1.37	0.15	1.01	9
6X-4, 8-9	39.98	0.18	1.5	2.15	1.97	0.23	0.81	9
7X-2, 129-130	44.29	0.44	3.7	2.07	1.63	0.17	1.12	10
7X-4, 33-34	46.33	0.33	2.7	1.62	1.29	0.16	1.18	8
7X-6, 32-33	49.32	0.56	4.7	2.09	1.53	0.16	1.12	10
8X-2, 33-34	52.43	0.37	3.1	1.80	1.43	0.15	0.77	10
8X-4, 33-34	55.43	0.10	0.9	1.44	1.34	0.14	0.54	10
8X-6, 35-36	58	0.47	3.9	1.40	0.93	0.15	0.77	6
9X-2, 33-34	61.43	0.06	0.5	1.12	1.06	0.16	1.24	7
9X-4, 34-35	64.44	0.08	0.7	1.28	1.20	0.14	0.54	9
9X-6, 34-35	67.44	0.11	0.9	0.90	0.79	0.14	1.17	6
10X-2, 34-35	70.44	0.73	6.1	1.90	1.17	0.16	1.54	7
10X-4, 34-35	73.44	0.22	1.8	1.88	1.66	0.17	1.00	10
10X-4, 125-126	74.35	0.25	2.1	1.51	1.26	0.16	0.66	8
11X-2, 34-35	80.04	0.16	1.4	1.16	1.00	0.15	1.05	7
11X-3, 109-110	81.76	0.08	0.7	0.87	0.79	0.14	1.13	6
11X-4, 34-35	82.51	0.18	1.5	1.30	1.12	0.15	1.09	7
12X-1, 124-125	89.14	0.09	0.8	1.20	1.11	0.13	0.39	9
12X-4, 33-34	92.73	0.07	0.5	1.04	0.97	0.16	0.34	6
12X-6, 28-29	95.68	0.05	0.4	1.23	1.18	0.16	0.71	7
13X-2, 24-25	99.06	0.06	0.5	1.19	1.13	0.16	1.74	7
14X-3, 84-85	110.79	0.55	4.6	2.07	1.52	0.18	1.45	8
15X-2, 37-38	117.96	0.26	2.2	1.42	1.16	0.16	1.35	7
15X-4, 27-28	120.86	0.07	0.6	1.25	1.18	0.15	0.60	8
15X-6, 32-33	122.84	0.07	0.6	1.26	1.19	0.16	5.93	7
16X-2, 33-34	128.23	0.08	0.7	0.78	0.70	0.14	0.53	5
16X-4, 33-34	130.34	0.09	0.7	0.90	0.81	0.15	0.86	5
16X-6, 33-34	132.36	0.16	1.4	1.03	0.87	0.16	0.86	5
18X-3, 120-121	149.22	0.68	5.7	2.02	1.34	0.19	0.80	7
170-1041B-								
1R-2, 34-35	156.84	0.46	3.8	1.47	1.01	0.16	1.52	6
1R-4, 34-35	159.62	0.78	6.5	2.58	1.80	0.22	1.59	8
1R-4, 149-150	160.77	0.29	2.4	ND	ND	ND	ND	ND
2R-2, 33-34	166.43	0.41	3.3	1.77	1.36	0.21	1.64	6
2R-4, 27-28	168.87	0.32	2.6	1.27	0.95	0.19	0.78	5
3R-2, 34-35	176.04	0.55	4.6	1.73	1.18	0.19	1.21	6
3R-5, 108-109	179.1	0.58	4.8	1.66	1.08	0.20	0.78	5
4R-2, 34-35	185.64	0.47	3.9	1.82	1.35	0.20	1.00	7
4R-5, 82-83	190.12	0.95	7.9	2.39	1.44	0.22	1.13	7
5R-2, 83-84	195.83	0.70	5.8	2.49	1.79	0.24	1.19	7
5R-4, 33-34	198.03	1.47	12.2	3.27	1.80	0.23	1.15	8
6R-2, 33-34	204.49	0.80	6.7	2.89	2.09	0.27	1.39	8
6R-5, 9-10	207.49	0.65	5.4	2.31	1.66	0.23	1.32	7
7R-7, 2-3	219.3	0.11	1.0	1.91	1.80	0.23	1.66	8
8R-1, 102-103	223.32	0.25	2.1	1.89	1.64	0.25	2.00	7
8R-2, 32-33	223.95	0.16	1.3	ND	ND	ND	ND	ND
8R-4, 33-34	226.2	0.19	1.6	1.58	1.39	0.21	1.70	7
9R-2, 33-34	233.73	0.02	0.2	2.38	2.36	0.26	1.74	9
9R-3, 34-35	235.23	0.00	0.0	2.26	2.26	0.26	1.53	9
10R-2, 33-34	243.43	0.34	2.8	2.81	2.47	0.29	1.77	9
10R-4, 33-34	245.62	0.36	3.0	2.57	2.21	0.26	1.21	9
10R-6, 33-34	247.27	0.33	2.7	2.07	1.74	0.24	1.59	7
11R-2, 35-36	252.76	0.11	0.9	1.81	1.70	0.21	1.52	8
11R-4, 29-30	255.69	0.46	3.8	ND	ND	ND	ND	ND
11R-5, 33-34	256.48	0.46	3.8	1.59	1.13	0.20	1.63	6
12R-2, 34-35	262.09	0.57	4.7	2.22	1.65	0.22	1.06	8
12R-3, 107-108	264.11	0.73	6.1	2.27	1.54	0.20	1.06	8
13R-2, 34-35	272.34	0.93	7.7	2.47	1.54	0.22	1.70	7
13R-3, 114-115	274.64	0.81	6.7	2.28	1.47	0.24	1.15	6
14R-2, 34-35	282.04	0.90	7.5	2.20	1.30	0.21	1.13	6
14R-4, 34-35	284.55	0.82	6.9	1.60	0.78	0.18	0.98	4
17R-2, 33-34	311.03	0.69	5.7	1.45	0.76	0.18	1.28	4
17R-3, 145-146	313.65	0.65	5.4	1.86	1.21	0.16	1.36	8
18R-1, 33-34	319.13	0.40	3.3	1.16	0.76	0.16	1.07	5
18R-3, 32-33	320.87	0.39	3.2	2.14	1.75	0.23	1.60	8
19R-2, 33-34	330.23	0.61	5.1	ND	ND	ND	ND	ND
19R-3, 104-105	331.87	0.87	7.2	1.60	0.73	0.16	0.68	5
20R-2, 30-31	338.72	0.48	4.0	1.10	0.62	0.15	1.02	4
20R-5, 95-96	343.87	1.01	8.4	2.81	1.80	0.23	1.95	8
21R-2, 149-150	350.59	0.32	2.7	1.38	1.06	0.18	1.73	6
21R-4, 63-64	351.58	7.40	61.7	8.09	0.69	0.08	0.29	9
22R-1, 7-8	357.27	0.57	4.7	2.11	1.54	0.21	1.71	7
22R-4, 31-32	360.53	1.28	10.7	2.35	1.07	0.19	1.33	6
23R-2, 33-34	368.63	0.62	5.2	2.03	1.41	0.22	1.13	6
24R-2, 33-34	378.23	0.45	3.8	1.80	1.35	0.23	0.12	6
24R-4, 33-34	379.98	0.51	4.3	1.93	1.42	0.23	0.61	6

Table 17 (continued).

Core, section, interval (cm)	Depth (mbsf)	IC (wt%)	$CaCO_3$ (wt%)	TC (wt%)	TOC (wt%)	TN (wt%)	TS (wt%)	TOC/TN
170-1041C-								
1R-1, 148-149	ND	0.63	5.3	ND	ND	ND	ND	ND
2R-1, 57-58	ND	0.48	4.0	ND	ND	ND	ND	ND
3R-2, 31-34	ND	1.32	11.0	ND	ND	ND	ND	ND

Notes: IC = inorganic carbon, $CaCO_3$ = calcium carbonate, TC = total carbon, TOC = total organic carbon, TN = total nitrogen, and TS = total sulfur. ND = not determined.

This table also appears on the volume CD-ROM.

Table 18. Major element (XRF) analyses of siliciclastic sediments and volcanic ashes.

Core, section, interval (cm)	Sample type	Lithology	Depth (mbsf)	SiO_2	TiO_2	Al_2O_3	Fe_2O_3*	MnO	MgO	CaO	Na_2O	K_2O	P_2O_5	Total	LOI
170-1041A-															
1H-1, 145-150	IWSJ	Sediment	1.45	55.17	1.23	16.88	9.79	0.075	4.04	5.42	2.35	2.130	0.189	97.25	10.24
2H-1, 135-150	IWSJ	Sediment	8.75	62.68	1.01	17.18	8.00	0.068	3.49	1.54	3.11	2.373	0.141	99.58	8.32
7X-2, 130-150	IWSJ	Sediment	44.30	62.89	1.05	17.11	8.29	0.068	3.25	2.52	2.80	2.413	0.163	100.52	8.26
2H-4, 83-88	XRF	Ash	12.73	69.15	0.40	15.25	3.01	0.092	1.22	2.84	5.26	3.122	0.174	100.51	6.45
2H-4, 124-130	XRF	Ash	13.14	71.75	0.41	15.51	3.09	0.103	1.22	2.58	5.03	3.330	0.118	103.13	6.51
16X-6, 55-82	IWSJ	Sediment	132.58	59.96	1.13	17.20	9.97	0.101	4.30	2.72	2.69	2.233	0.203	100.49	7.83
170-1041B-															
3R-5, 115-150	IWSJ	Sediment	179.17	61.16	1.08	17.28	9.10	0.051	3.52	2.45	2.18	2.168	0.184	99.16	9.35
9R-2, 99-134	IWSJ	Sediment	234.39	70.41	0.59	15.89	4.13	0.082	1.03	3.36	3.53	2.585	0.131	101.71	4.99
9R-3, 1-5	XRF	Ash	234.90	69.82	0.59	15.71	4.15	0.078	1.03	3.23	3.77	2.559	0.127	101.04	5.53
18R-CC, 0-2	XRF	Sediment	321.30	18.65	0.22	5.79	2.59	0.037	0.81	67.75	–0.33	0.616	0.605	96.73	35.34
21R-3, 0-35	IWSJ	Sediment	350.60	60.81	1.02	17.72	8.01	0.039	2.65	4.52	1.79	2.109	0.210	98.87	7.40
24R-3, 0-25	IWSJ	Sediment	379.40	65.16	0.95	16.72	7.92	0.075	3.06	2.86	1.42	1.733	0.247	100.13	10.19
170-1041C-															
2R-1, 65-90	IWSJ	Sediment	405.35	63.92	0.99	16.97	9.05	0.064	2.83	2.98	1.23	1.840	0.267	100.12	10.52

Notes: Fe_2O_3* = total iron as Fe_2O_3. All concentrations in weight percent. IWSJ = interstitial water squeezecake split, XRF = picks from sampling table, and LOI = loss on ignition.

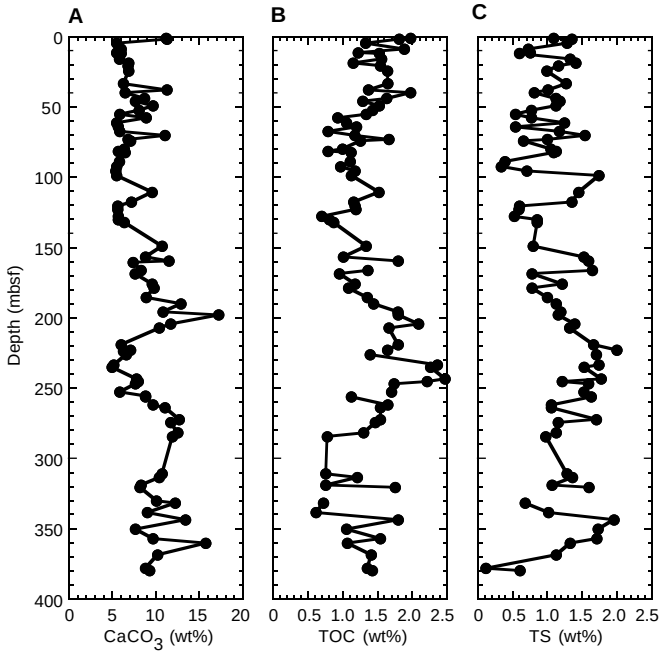

Figure 22. Depth distribution of (**A**) carbonate, (**B**) total organic carbon (TOC), and (**C**) total sulfur (TS).

liner. Discrete specimen measurements were probably not affected significantly by the presence of gas hydrates, because soupy and moussy intervals, and those consisting of comminuted chips, were avoided during sampling.

Wet bulk density measured on extracted core specimens (Fig. 1) increases rapidly from values of around 1.4 g/cm^3 at the seafloor to 1.6 g/cm^3 at 30 mbsf (Table 21). The corresponding change in porosity is from ~75% to 65%. The sediment bulk density changes little with depth, but a gradual trend of increasing consolidation occurs down to ~200 mbsf, where porosity is 60% and wet bulk density reaches 1.65 g/cm^3. A small increase in porosity and decrease in bulk density is observed between 200 and 280 mbsf. Between 300 and 330 mbsf, porosity decreases to ~45% and wet bulk density increases to around 1.85 g/cm^3. Data below this depth are scattered, but suggest a small increase in porosity and decrease in bulk density. The GRA density data show variations with depth similar to specimen-based densities, but GRA data typically provide better depth resolution. However, GRA densities are consistently about 0.05 g/cm^3 less than the specimen densities, probably because the diameter of cores extracted using the RCB method are smaller than the core liner.

Grain density measurements on core specimens remain at 2.60 ±0.15 g/cm^3 throughout the recovered interval, suggesting that no significant changes occur in the major mineral composition (e.g., clays, quartz, and feldspars) down to a depth of ~350 m. Below this depth, the data are scattered and may not be reliable. However, grain density measurements are not affected by mechanical core disturbance, and the range of values determined may be real, indicating differing amounts of carbonate cement and biogenic components in the claystone, siltstone, and sandstone of this interval.

Natural Gamma Ray

On Leg 170, natural gamma-ray measurements were made for the first time by the MST for unsplit cores from Site 1041 (Fig. 25; Table

Table 19. Trace element (XRF) analyses of siliciclastic sediments and volcanic ashes.

Core, section, interval (cm)	Sample type	Lithology	Depth (mbsf)	Nb	Zr	Y	Sr	Rb	Zn	Cu	Ni	Cr	V	Ce	Ba
170-1041A-															
1H-1, 145-150	IWSJ	Sediment	1.45	6.8	104.7	18.8	259.6	37.9	117	68	55	119	202	25	208
2H-1, 135-150	IWSJ	Sediment	8.75	6.3	116.6	16.7	222.2	44.1	124	74	43	78	166	30	401
7X-2, 130-150	IWSJ	Sediment	44.30	6.8	114.0	16.2	258.5	43.3	118	80	46	84	171	18	850
2H-4, 83-88	XRF	Ash	12.73	7.8	148.7	10.5	507.4	64.3	54	20	7	5	37	48	1395
2H-4, 124-130	XRF	Ash	13.14	7.3	153.5	10.5	469.4	66.8	54	18	8	6	41	40	1414
16X-6, 55-82	IWSJ	Sediment	132.58	6.6	112.0	20.1	212.8	42.1	141	97	77	104	203	21	650
170-1041B-															
3R-5, 115-150	IWSJ	Sediment	179.17	4.2	109.1	17.8	191.3	38.7	120	54	41	80	174	22	521
9R-2, 99-134	IWSJ	Sediment	234.39	3.8	153.8	23.1	309.3	34.5	66	44	11	2	58	23	1283
9R-3, 1-5	XRF	Ash	234.90	3.9	152.3	22.5	294.6	35.4	65	44	11	5	61	20	1268
18R-CC, 0-2	XRF	Sediment	321.30	–0.3	25.6	6.3	208.8	9.5	25	17	4	13	33	10	138
21R-3, 0-35	IWSJ	Sediment	350.60	3.9	104.5	18.5	317.0	38.0	97	52	20	55	169	21	475
24R-3, 0-25	IWSJ	Sediment	379.40	4.3	100.8	16.0	229.5	34.5	109	61	26	59	155	22	432
170-1041C-															
2R-1, 65-90	IWSJ	Sediment	405.35	3.8	106.4	15.7	214.0	34.9	114	46	27	72	157	21	451

Notes: All concentrations in parts per million. IWSJ = interstitial water squeezecake split. XRF = picks from sampling table.

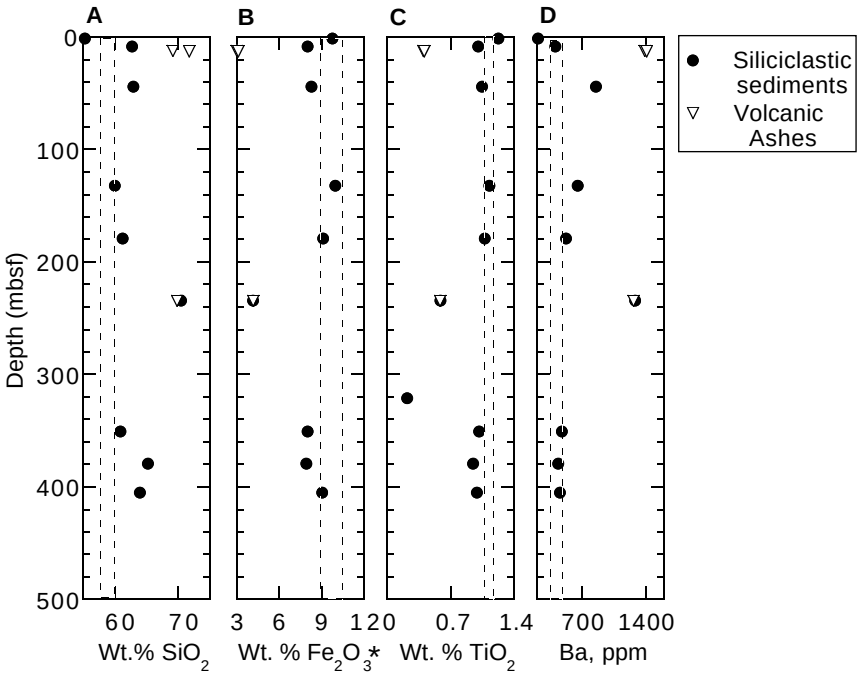

Figure 23. Concentrations of (**A**) SiO_2, (**B**) Fe_2O_3*, (**C**) TiO_2, and (**D**) Ba in siliciclastic sediments and volcanic ashes vs. depth. Narrow dashed box indicates composition of sedimentary wedge from Site 1040 (mean ±1σ).

22). General trends can be identified easily, but considerable scatter in the data is attributable to voids in the core or the material not filling the liner completely. Both effects tend to reduce measured values, so values near the maximum of the recorded range are more representative of in situ conditions.

An overall decrease in total counts was recorded from an average of 38 counts per second (cps) at 30 mbsf to 32 cps at 135 mbsf. Below this depth, values fluctuate until 274 mbsf at the Subunit A1A/A1B boundary. Within Subunit A1B, the total count increases to a maximum of about 35 cps at 320 mbsf, below which the count slowly decreases.

P-wave Velocity

Drilling disturbance precluded the use of the *P*-wave logger on the MST track, except at the top of Hole 1041A. Sonic velocity measurements were, therefore, obtained primarily using the PWS3 on discrete specimens extracted from the split cores (Table 23). The firm sediment enabled aquisition of good velocity data for most of the cored interval, despite intense natural and drilling-induced fracturing. Attempts were made to measure *P*-wave velocity both on massive crystalline gas hydrate samples and on clathrate-cemented sediment, but these attempts were unsuccessful because of poor coupling of the transducer with the specimen and, probably, attenuation caused by evolving gas.

PWS3 velocities (Fig. 26) increase from 1540 m/s at the surface to ~1650 m/s at 30 mbsf, a trend that is similar to that of the specimen-based bulk densities. A slow increase throughout Subunit A1A to 1730 m/s at 270 mbsf is observed. The velocity gradient becomes larger at this depth, with velocities increasing to ~2000 m/s at 325 mbsf. Velocities at greater depths appear to be constant, although this trend is not well defined because measured scatter also increases below 300 mbsf. The zone of high velocities below 270 mbsf corresponds well to the high-density region observed in the bulk density data sets. These changes may reflect an increase in carbonate cementation. No major change in lithology occurs in this interval, although a larger number of carbonate nodules are observed below 300 mbsf (see "Lithostratigraphy and Structure" section, this chapter).

Magnetic Susceptibility

Magnetic susceptibility (Fig. 1) from the upper cores of Hole 1041A is high, reaching 150 SI units at 5 mbsf. The record below 8 mbsf is relatively featureless, with values of about 25 SI units. This

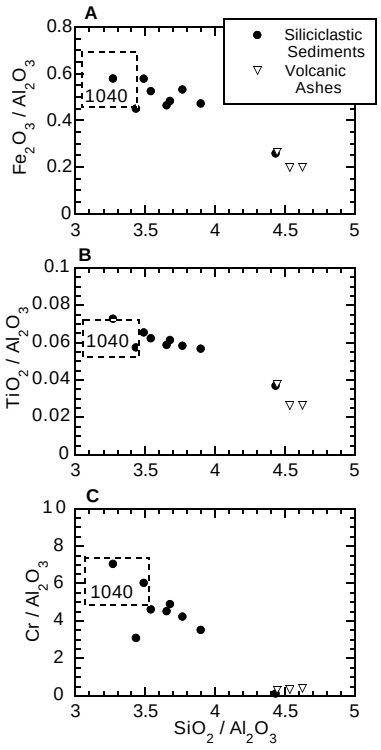

Figure 24. Mixing diagrams showing variations in SiO_2/Al_2O_3 (wt%/wt%) vs. (**A**) Fe_2O_3*/Al_2O_3 (wt%/wt%), (**B**) TiO_2/Al_2O_3 (wt%/wt%), and (**C**) Cr/Al_2O_3 (ppm/wt%). Dashed box labeled "1040" indicates the compositional range shown by the sedimentary wedge above the décollement at Site 1040.

Table 20. Gamma-ray attenuation (GRA) bulk density data for Site 1041.

Leg	Site	Hole	Core	Type	Top (cm)	Bottom (cm)	Depth (mbsf)	GRA density (g/cm^3)
170	1041	A	1	H	4.7	4.7	0.05	1.349
170	1041	A	1	H	6.7	6.7	0.07	1.345
170	1041	A	1	H	8.7	8.7	0.09	1.341
170	1041	A	1	H	10.7	10.7	0.11	1.339
170	1041	A	1	H	12.7	12.7	0.13	1.319
170	1041	A	1	H	14.7	14.7	0.15	1.34
170	1041	A	1	H	16.7	16.7	0.17	1.353
170	1041	A	1	H	18.7	18.7	0.19	1.357
170	1041	A	1	H	20.7	20.7	0.21	1.335
170	1041	A	1	H	22.7	22.7	0.23	1.321

This is a sample of the table that appears on the volume CD-ROM.

uniformity reflects the homogeneity of the sediment encountered, and it is consistent with small changes in grain density (which reflects mineralogy) throughout the cored interval (Table 24). Sharp peaks correlate with ash layers, whereas broader and lower peaks may correspond with sand-rich horizons. Low values of magnetic susceptibility may correspond to intervals rich in biogenic opal and carbonate. From 270 to 340 mbsf, the baseline for magnetic susceptibility values increases by nearly a factor of two. This section corresponds closely with a zone of high densities and high velocities.

Vane Shear Strength

Undrained shear strength measurements were made using the motorized miniature vane shear device on cores from the upper part of Hole 1041A (Table 25). Drilling disturbance and high sediment induration precluded any measurements being made below 16 mbsf. It is not possible to draw statistical conclusions on the small amount of data, and downhole trends cannot be predicted confidently. Figure 27A shows the shear strength data plotted against depth for the upper part of Hole 1041A. The shear strength increases to 200 kPa at 12 mbsf (a value greater than that measured at Sites 1039 and 1040), implying that the sediment is overconsolidated. This is demonstrated in Figure 27B by the plotted ratios of shear strength to effective overburden stress, which are much higher than values typical of normally consolidated sediments (0.25; dashed line).

Thermal Conductivity

Thermal conductivity measurements were taken on sections judged to have intact drilling biscuits or intact pieces large enough for the probe to be inserted and the full-space approximation to be valid (Table 26). These restrictions produced gaps in the recorded data (Fig. 28). Thermal conductivity values range between 0.62 and 0.98 W/(m·K). The average value remains fairly constant at about 0.85 W/(m·K) for the interval of 0–320 mbsf, showing no increase with depth. This constancy could reflect the apparent homogeneity of the sediment recovered at this site.

Heat Flow

Equilibrium temperatures obtained from the DVTP are shown in Table 27 and Figure 29 and as a function of depth in Figure 30A. The error limits were determined subjectively, based on the stability of the equilibration record and tool performance. The average geothermal gradient in the whole interval is 21.6°C/km.

Heat flow is estimated from the in situ equilibrium temperature measurements and the thermal conductivity values measured onboard (Fig. 28). The slope of the temperature vs. cumulative thermal resistance curve (Fig. 30B) yields a direct measure of heat flow. The average heat-flow value in the whole interval is 17.9 mW/m^2, which is more than two times higher than the value at Site 1039 (9.2 mW/m^2; see "Site 1039" chapter, this volume). Estimated heat flow at Site 1041 is significantly lower than the values determined by the precruise heat-flow survey conducted at a nearby location (29.1 ±2.3 mW/m^2; Langseth and Silver, 1996).

Colorimetry

Extreme sediment disturbance and fracturing precluded a satisfactory contact between the spectrophotometer and the material. This situation resulted in a lack of stability of spectrographic measurements, particularly at short wavelengths. As a consequence, the measured values, and particularly the b* values (the denominator in the chromaticity ratio), are erratic, and the measured values are therefore not presented in a graphic plot.

The lightness component (L*) of the sediment retrieved from Site 1041 shows little change throughout the entire section. Values of L* vary only between 38% and 48% and have an average value of ~43%. The only distinctive feature in the lightness curve is a relatively high (nearly 57%) value at 13 mbsf that corresponds with a 1.5-m-thick ash layer (upper part of Subunit A1A). Colorimetric characterization of individual units through red/blue ratio analyses is not meaningful. Mean reflectance vs. wavelength curves for the two subunits at Site 1041 are indistinguishable (Fig. 31). However, photometric measurements are unreliable at wavelengths shorter than 450 nm.

REFERENCES

Bordovskiy, O.K., 1965. Accumulation and transformation of organic substances in marine sediment, 2. Sources of organic matter in marine basins. *Mar. Geol.*, 3:5–31.

Emerson, S., and Hedges, J.I., 1988. Processes controlling the organic carbon content of open ocean sediments. *Paleoceanography,* 3:621–634.

Kahn, L.M., Silver, E.A., Orange, D., Kochevar, R., and McAdoo, B., 1996. Surficial evidence of fluid expulsion from the Costa Rica accretionary prism. *Geophys. Res. Lett.,* 23:887–890.

Kvenvolden, K.A., and McDonald, T.J., 1985. Gas hydrates of the Middle America Trench—Deep Sea Drilling Project Leg 84. *In* von Huene, R., Aubouin, J., et al., *Init. Repts. DSDP,* 84: Washington (U.S. Govt. Printing Office), 667–682.

Langseth, M.G., and Silver, E.A., 1996. The Nicoya convergent margin: a region of exceptionally low heat flow. *Geophys. Res. Lett.,* 23:891–894.

Lowrie, W., 1990. Identification of ferromagnetic minerals in a rock by coercivity and unblocking temperature properties. *Geophys. Res. Lett.,* 17:159–162.

McAdoo, B.G., Orange, D.L., Silver, E.A., McIntosh, D., Abbott, L., Galewsky, J., Kahn, L., and Protti, M., 1996. Seafloor structural observations, Costa Rica accretionary prism. *Geophys. Res. Lett.,* 23:883–886.

McIntosh, K.D., and Silver, E.A., 1996. Using 3D seismic reflection data to find fluid seeps from the Costa Rica accretionary prism. *Geophys. Res. Lett.,* 23:895–898.

Sloan, E.D., 1990. *Clathrate Hydrates of Natural Gases:* New York (Marcel Dekker).

Zuleger, E., Gieskes, J.M., and You, C.-F., 1996. Interstitial water chemistry of sediments of the Costa Rica accretionary complex off the Nicoya Peninsula. *Geophys. Res. Lett.,* 23:899–902.

Ms 170IR-105

NOTE: Core-description forms ("barrel sheets") and core photographs can be found in Section 3, beginning on page 251. Smear-slide data and shore-based processed log data and descriptions can be found on CD-ROM. See Table of Contents for material contained on CD-ROM.

Table 21. Moisture and density data, and calculated phase relationships from discrete core specimens, Site 1041.

Leg	Site	Hole	Core	Type	Section	Top (cm)	Bottom (cm)	Depth (mbsf)	Beaker number	Beaker mass (g)	Beaker volume (g/cm^3)	Wet volume (g/cm^3)	Dry volume (g/cm^3)	Wet mass (g)	Dry mass (g)
170	1041	A	1	H	1	109	111	1.09	2	8.111	3.653604		5.1	16.67	11.8687
170	1041	A	1	H	2	123	125	2.73	5	8.027	3.615766		5.44	16.4324	12.8455
170	1041	A	1	H	2	20	22	1.7	6	7.945	3.578829		5.37	16.9412	12.6214
170	1041	A	1	H	3	40	42	3.4	8	8.022	3.613514		6.52	20.7668	15.8272
170	1041	A	1	H	4	110	112	5.6	9	8.087	3.642793		5.93	18.2956	13.9934
170	1041	A	1	H	4	50	52	5	10	7.887	3.552703		5.5	17.0624	12.8973
170	1041	A	1	H	5	87	89	6.87	12	8.067	3.633784		5.64	17.3049	13.2886
170	1041	A	1	H	5	25	27	6.25	13	7.938	3.575676		5.89	18.3336	13.9206
170	1041	A	2	H	1	130	132	8.7	15	8.224	3.704505		5.95	19.2544	13.9241
170	1041	A	2	H	1	34	36	7.74	14	8.198	3.692793		6.08	19.4688	14.2923

Table 21 (continued).

Leg	Site	Hole	Core	Type	Section	Top (cm)	Bottom (cm)	Depth (mbsf)	Water content (wet)	Water content (dry)	Wet bulk density (g/cm^3)	Dry bulk density (g/cm^3)	Grain density (g/cm^3)	Porosity (%)	Void ratio
170	1041	A	1	H	1	109	111	1.09	0.581	1.39	1.38	0.576	2.62	78.1	3.56
170	1041	A	1	H	2	123	125	2.73	0.442	0.79	1.56	0.869	2.66	67.3	2.06
170	1041	A	1	H	2	20	22	1.7	0.498	0.99	1.48	0.742	2.63	71.8	2.54
170	1041	A	1	H	3	40	42	3.4	0.402	0.67	1.63	0.975	2.7	63.9	1.77
170	1041	A	1	H	4	110	112	5.6	0.437	0.78	1.55	0.875	2.6	66.3	1.97
170	1041	A	1	H	4	50	52	5	0.47	0.89	1.51	0.798	2.59	69.2	2.25
170	1041	A	1	H	5	87	89	6.87	0.451	0.82	1.54	0.846	2.62	67.7	2.1
170	1041	A	1	H	5	25	27	6.25	0.44	0.79	1.55	0.868	2.6	66.6	1.99
170	1041	A	2	H	1	130	132	8.7	0.501	1	1.46	0.729	2.55	71.4	2.5
170	1041	A	2	H	1	34	36	7.74	0.476	0.91	1.5	0.783	2.57	69.5	2.28

This is a sample of the table that appears on the volume CD-ROM.

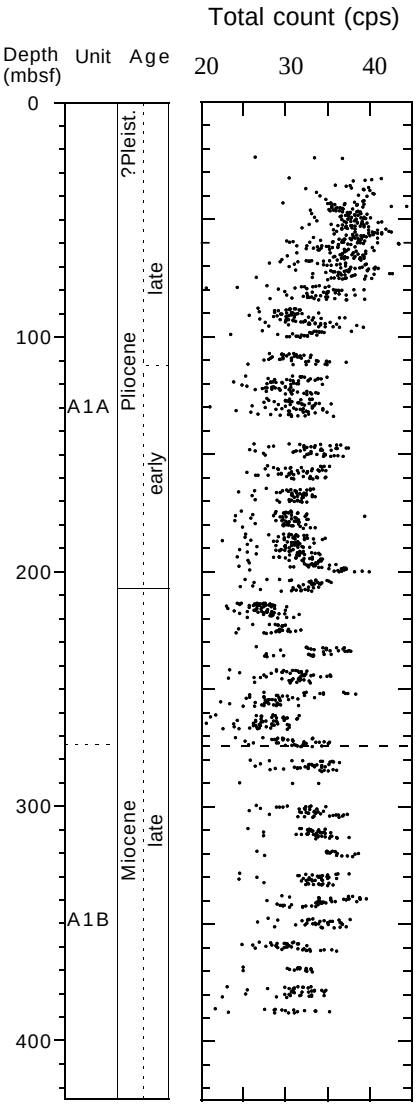

Figure 25. Natural gamma-ray radiation measured with the MST on cores from Holes 1041A and 1041B.

Table 22. Natural gamma-ray data obtained on unsplit core with the MST, Site 1041.

Leg	Site	Hole	Core	Type	Section	Top (cm)	Bottom (cm)	Depth (mbsf)	Total counts/s (cps)	Actual daq period (s)	Core diameter (cm)
170	1041	A	4	X	1	10.4	10.4	23.5	26.4	60	6.7
170	1041	A	4	X	1	40.4	40.4	23.8	33.5	60	6.7
170	1041	A	4	X	1	70.4	70.4	24.1	36.7	60	6.7
170	1041	A	5	X	1	10.4	10.4	32.5	30.4	60	6.7
170	1041	A	5	X	1	40.4	40.4	32.8	41.3	60	6.7
170	1041	A	5	X	1	70.4	70.4	33.1	40.2	60	6.7
170	1041	A	5	X	1	100.4	100.4	33.4	39.4	60	6.7
170	1041	A	5	X	1	130.4	130.4	33.7	38.1	60	6.7
170	1041	A	6	X	1	10.4	10.4	35.5	35.9	60	6.7
170	1041	A	6	X	1	40.4	40.4	35.8	37.7	60	6.7
170	1041	A	6	X	1	70.4	70.4	36.1	37.2	60	6.7
170	1041	A	6	X	1	100.4	100.4	36.4	39.9	60	6.7
170	1041	A	6	X	1	130.4	130.4	36.7	37.8	60	6.7
170	1041	A	6	X	2	10.4	10.4	37	32.4	60	6.7

Note: Daq = data acquisition.

This is a sample of the table that appears on the volume CD-ROM.

Table 23. *P*-wave velocities obtained from the PWS3 on split cores from Site 1041.

Leg	Site	Hole	Core	Type	Section	Top (cm)	Bottom (cm)	Depth (mbsf)	Velocity (m/s)	Distance (mm)	Time (µs)
170	1041	A	1	H	1	75.1	75.1	0.75	1538	37.61	24.98
170	1041	A	1	H	2	122.5	122.5	2.73	1562.9	35.71	23.4
170	1041	A	1	H	2	30.3	30.3	1.8	1535.9	35.72	23.78
170	1041	A	1	H	3	120.1	120.1	4.2	1627.9	35.95	22.7
170	1041	A	1	H	3	64.9	64.9	3.65	1548.7	35.13	23.22
170	1041	A	1	H	4	36.9	36.9	4.87	1586.4	36.97	23.88
170	1041	A	1	H	4	50	50	5	1587	36.7	23.701
170	1041	A	1	H	5	84.9	84.9	6.85	1564.3	37.46	24.5
170	1041	A	1	H	5	19.5	19.5	6.2	1561.5	35.18	23.08
170	1041	A	2	H	1	18	18	7.58	1544		
170	1041	A	2	H	1	67.1	67.1	8.07	1544.4	37.2	24.62
170	1041	A	2	H	1	126	126	15.37	1571		
170	1041	A	2	H	2	138.6	138.6	10.29	1549.1	35.2	23.26
170	1041	A	2	H	3	37.7	37.7	10.78	1552.2	36.88	24.3

This is a sample of the table that appears on the volume CD-ROM.

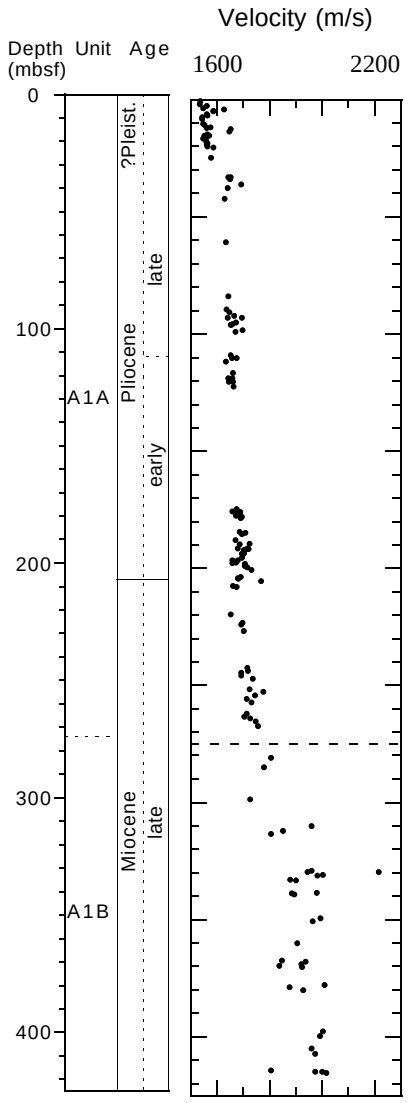

Figure 26. Acoustic *P*-wave velocity, measured by PWS3 transducers on specimens from split cores.

Table 24. Magnetic susceptibility values obtained on unsplit cores using the MST, Site 1041.

Leg	Site	Hole	Core	Type	Section	Top (cm)	Bottom (cm)	Depth (mbsf)	Relative, drift corr. sus.	Relative sus. mean	Actual daq period (s)	Core diameter (cm)	Sample elapsed zero time (s)	Background correction
170	1041	A	1	H	1	4	4	0.04	299	299	2	6.7	10	7.1
170	1041	A	1	H	1	6	6	0.06	274.9	274.8	2	6.7	10	7.1
170	1041	A	1	H	1	8	8	0.08	242.9	242.8	2	6.7	10	7.1
170	1041	A	1	H	1	10	10	0.1	216.5	216.4	2	6.7	10	7.1
170	1041	A	1	H	1	12	12	0.12	187.1	187	2	6.7	10	7.1
170	1041	A	1	H	1	14	14	0.14	134.5	134.4	2	6.7	10	7.1
170	1041	A	1	H	1	16	16	0.16	91	90.8	2	6.7	10	7.1
170	1041	A	1	H	1	18	18	0.18	76	75.8	2	6.7	10	7.1
170	1041	A	1	H	1	20	20	0.2	70.4	70.2	2	6.7	10	7.1
170	1041	A	1	H	1	22	22	0.22	66.4	66.2	2	6.7	10	7.1

Note: Corr. = corrected, sus. = susceptibility, daq = data acquisition.

This is a sample of the table that appears on the volume CD-ROM.

Table 25. Vane shear strength data for Hole 1041A.

Leg	Site	Hole	Core	Type	Section	Top (cm)	Bottom (cm)	Depth (mbsf)	Peak undrained shear strength (kPa)	Overburden (kPa)	S_u/P_0'
170	1041	A	1	H	1	109.6	109.6	1.1	13.5	16.187	0.83403
170	1041	A	1	H	2	123.4	123.4	2.73	20.9	40.172	0.52026
170	1041	A	1	H	3	39.4	39.4	3.39	34.6	49.884	0.69361
170	1041	A	1	H	3	124.6	124.6	4.25	88.4	62.539	1.4135
170	1041	A	1	H	4	109.8	109.8	5.6	114.4	82.404	1.3883
170	1041	A	1	H	5	84.8	84.8	6.85	121.6	100.8	1.2064
170	1041	A	2	H	1	34.5	34.5	7.75	109.1	114.04	0.95667
170	1041	A	2	H	1	130.3	130.3	8.7	81.2	128.02	0.63427
170	1041	A	2	H	2	41.4	41.4	9.31	198.7	137	1.4504
170	1041	A	2	H	2	144.3	144.3	10.34	183.6	152.15	1.2067
170	1041	A	2	H	3	37.6	37.6	10.78	168.6	158.63	1.0629
170	1041	A	2	H	3	130.5	130.5	11.71	192.9	172.31	1.1195
170	1041	A	2	H	4	34.3	34.3	12.24	210.6	180.11	1.1693
170	1041	A	3	X	2	42.7	42.7	16.23	69.9	238.82	0.29268
170	1041	A	3	X	2	70.9	70.9	16.51	83.8	242.94	0.34493

This table also appears on the volume CD-ROM.

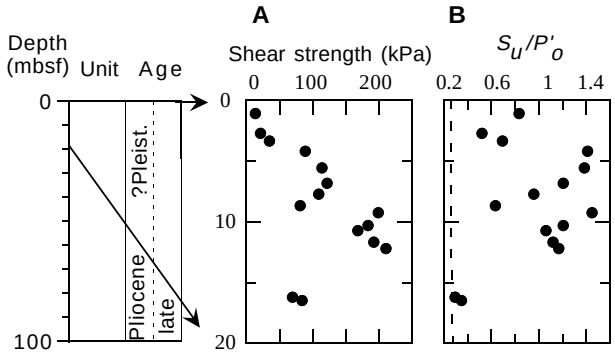

Figure 27. **A.** Undrained shear strength, measured with the automated vane shear device, vs. depth at Site 1041. **B.** Shear strength to effective overburden stress ratio (S_u/P_0') plotted as a function of depth. Typically, normally consolidated sediments have a ratio of about 0.25 (dashed line), suggesting that sediment at Site 1041 is overconsolidated.

Table 26. Thermal conductivity data for Site 1041.

Leg	Site	Hole	Core	Type	Section	Top (cm)	Bottom (cm)	Depth (mbsf)	Thermal conductivity (W/[m·K])
170	1041	A	1	H	1	50	50	0.5	0.791
170	1041	A	1	H	3	50	50	3.5	0.88
170	1041	A	1	H	4	50	50	5	0.911
170	1041	A	1	H	5	50	50	6.5	0.914
170	1041	A	2	H	1	50	50	7.9	0.835
170	1041	A	2	H	2	50	50	9.4	0.799
170	1041	A	2	H	3	50	50	10.9	0.878
170	1041	A	2	H	4	50	50	12.4	0.877
170	1041	A	3	X	1	51	51	14.81	0.827
170	1041	A	3	X	3	50	50	17.8	0.788

This is a sample of the table that appears on the volume CD-ROM.

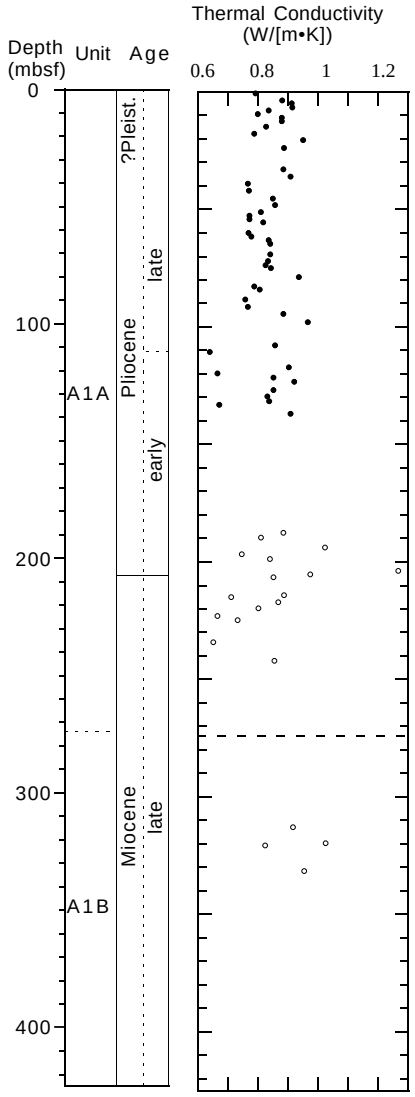

Figure 28. Thermal conductivity vs. depth for Site 1041.

Table 27. Summary of in situ temperature measurements at Site 1041.

Depth (mbsf)	Hole, core	Tool	Equilibrium temp. (°C)	Comments
10 m above mudline	1041A	WSTP	1.99 ± 0.1	
41.5	1041A-7X	DVTP	2.80 ± 0.1	
78.2	1041A-11X	DVTP		Bad data
87.9	1041A-12X	DVTP	3.84 ± 0.1	
126.4	1041A-16X	DVTP	4.69 ± 0.1	
174.2	1041B-3R	DVTP		Bad data
183.8	1041B-4R	DVTP	5.93 ± 0.1	

Note: WSTP = water-sampling temperature probe, DVTP = Davis-Villinger Temperature Probe.

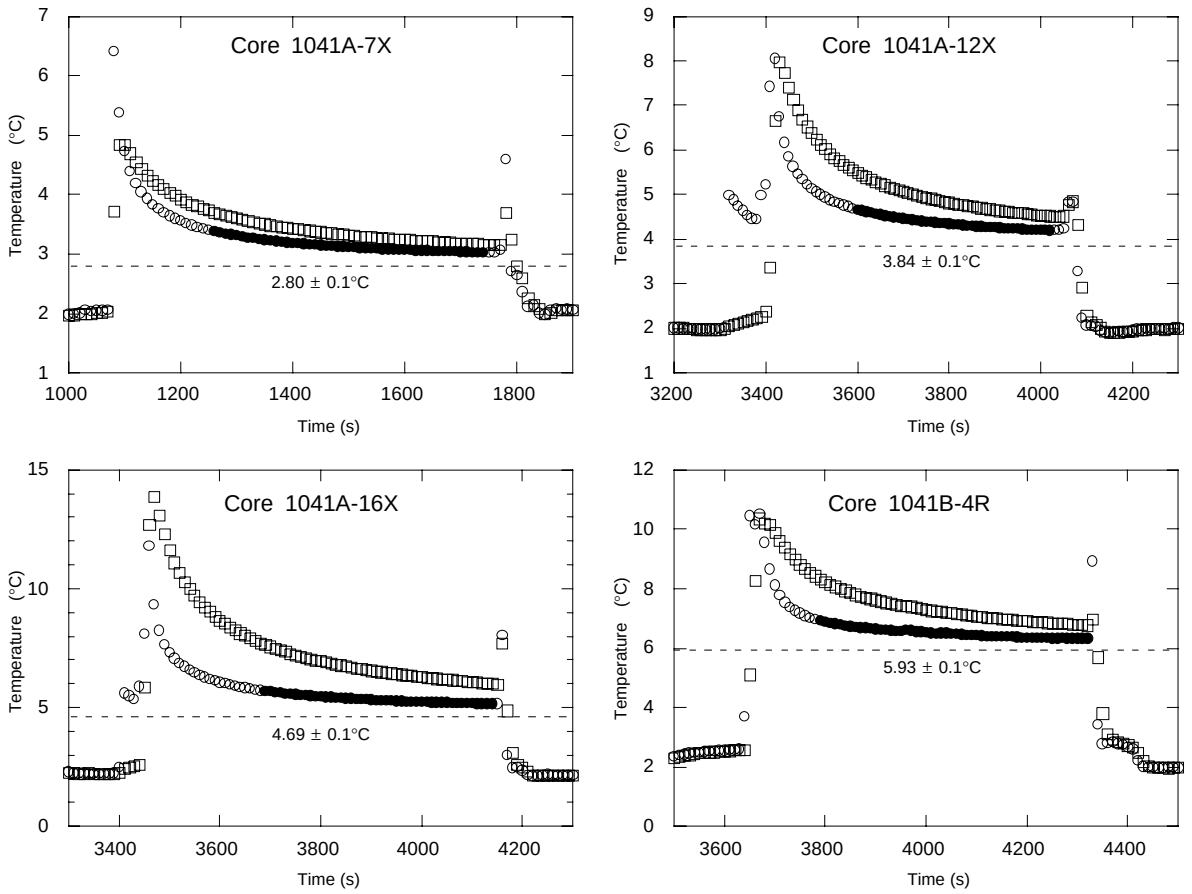

Figure 29. Temperature vs. time data from the DVTP at Holes 1041A and 1041B. The dashed line in each panel indicates the estimated equilibrium temperature determined by fitting a synthetic curve to the equilibration record. Circles and squares for the DVTP indicate temperature data from the upper and lower thermistor, respectively. The part of the equilibrium curve used for curve fitting is indicated with solid circles.

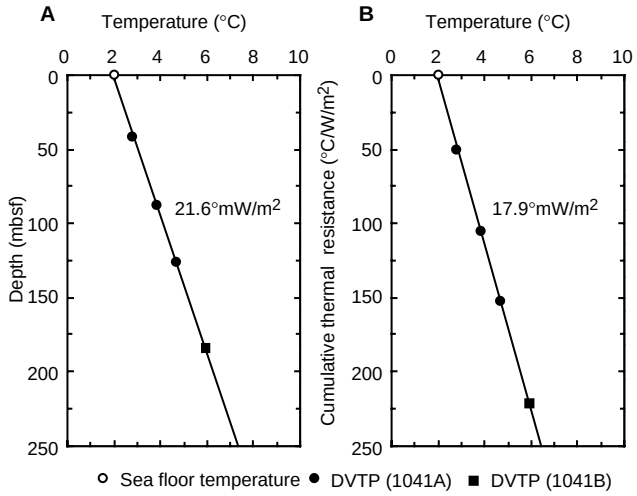

Figure 30. **A.** Temperature vs. depth at Site 1041. Thermal gradient is also indicated. **B.** Temperatures vs. cumulative thermal resistance. Mean heat-flow value is also shown.

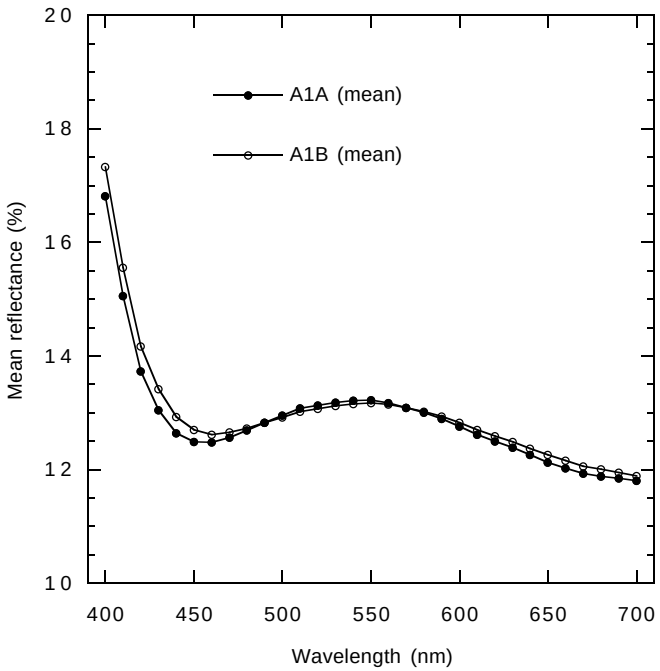

Figure 31. Mean percentage of reflectance vs. wavelength for both subunits cored at Site 1041.

Previous Chapter
Table of Contents
Next Chapter